

ELECTRICAL COMMUNICATION

*Technical Journal of the
International Telephone and Telegraph Corporation
and Associate Companies*

•

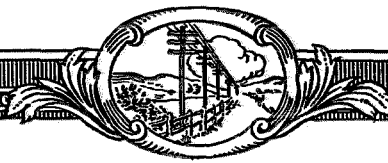
PRODUCTION OF TWO-MOTION-SELECTOR CONTACTS
GRAPHICAL SYMBOLS FOR ELECTRICAL DIAGRAMS
RADAR RECEIVER WITH ELIMINATION OF FIXED-TARGET ECHOES
ELECTRIC SERVOMECHANISMS
MINIMUM NUMBER OF RESONATORS AND MINIMUM Q IN A FILTER
ATTENUATION AND POWER HANDLING OF HELICAL LINES
AVERAGE SPECTRUM OF A DISPLACED AND DISTORTED PULSE SERIES
TELEPHONE STATISTICS OF THE WORLD
UNITED STATES PATENTS ISSUED TO THE INTERNATIONAL SYSTEM



Volume 31

DECEMBER, 1954

Number 4



ELECTRICAL COMMUNICATION

*Technical Journal of the
International Telephone and Telegraph Corporation
and Associate Companies*

H. P. WESTMAN, Editor
J. E. SCHLAIKJER, Assistant Editor

EDITORIAL BOARD

H. G. Busignies H. H. Buttner G. Chevigny E. M. Deloraine W. Hatton B. C. Holding H. L. Hull
J. Kruithof W. P. Maginnis A. W. Montgomery E. D. Phinney G. Rabuteau N. H. Saunders
C. E. Scholz T. R. Scott C. E. Strong A. E. Thompson E. N. Wendell H. B. Wood

Published Quarterly by the
INTERNATIONAL TELEPHONE AND TELEGRAPH CORPORATION

67 BROAD STREET, NEW YORK 4, NEW YORK, U.S.A.

Sosthenes Behn, Chairman William H. Harrison, President
Geoffrey A. Ogilvie, Vice President and Secretary

Subscription, \$2.00 per year; single copies, 50 cents

Copyrighted 1954 by International Telephone and Telegraph Corporation

Volume 31

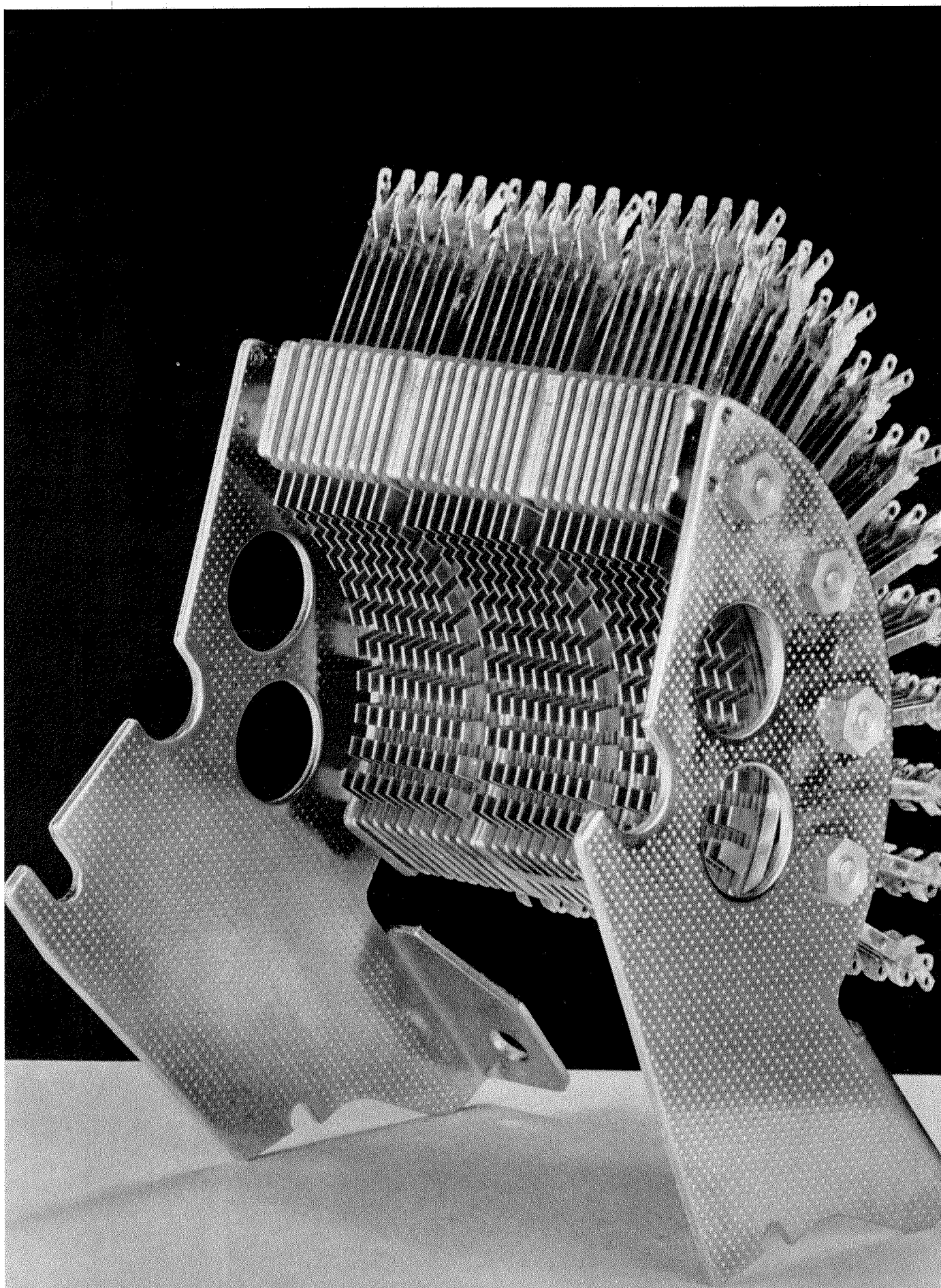
DECEMBER, 1954

Number 4

CONTENTS

PRODUCTION OF TWO-MOTION-SELECTOR CONTACTS	227
GRAPHICAL SYMBOLS FOR ELECTRICAL DIAGRAMS	230
<i>By H. P. Westman</i>	
RADAR RECEIVER WITH ELIMINATION OF FIXED-TARGET ECHOES	235
<i>By Hervé Tanter</i>	
ELECTRIC SERVOMECHANISMS	249
<i>By G. J. Lehmann</i>	
CONCERNING THE MINIMUM NUMBER OF RESONATORS AND THE MINIMUM UNLOADED- RESONATOR Q NEEDED IN A FILTER	257
<i>By Milton Diskal</i>	
ATTENUATION AND POWER-HANDLING CAPABILITY OF HELICAL RADIO- FREQUENCY LINES	278
<i>By J. H. Bryant and E. J. White</i>	
AVERAGE SPECTRUM OF A PERIODIC SERIES OF IDENTICAL PULSES RANDOMLY DISPLACED AND DISTORTED	283
<i>By R. M. Fortet</i>	
TELEPHONE STATISTICS OF THE WORLD	288
UNITED STATES PATENTS ISSUED TO INTERNATIONAL TELEPHONE AND TELEGRAPH SYSTEM; MAY-JULY, 1954	293
IN MEMORIAM—JEAN E. F. ROUSSEL	296
CONTRIBUTORS TO THIS ISSUE	297





Production of Two-Motion-Selector Contacts

BECAUSE of the higher ratio of labor-to-materials costs in the United States than in Europe, production men in the United States normally look first to mechanization when considering means of cutting costs, while Europeans logically concentrate to a greater degree on reducing materials requirements.

Mix and Genest, a Division of Standard Elektrizitäts-Gesellschaft A. G., Stuttgart, Germany, in a recent complete revision of piece-part production and assembly methods for two-motion-selector contact banks, designed and constructed a new machine tool for producing stampings for the banks. The machine, shown on the following pages, turned out to be a two-edged approach to the cost-cutting problem, for it not only reduced by 71 percent the amount of brass required for the stampings, but it also reduced direct labor by an identical 71 percent. Tooling costs are no higher than for the old method.

The area of the brass strip required to produce 5 stampings was reduced from 14 by 42 centimeters (588 square centimeters or 91 square inches) with the old method to 6.2 by 27.6 centimeters (171 square centimeters or 26.4 square inches) with the new design. The illustration at the right shows the five stages in the punching process with the old method, which employed a progressive tool in a normal punch press. Each stroke initiated by the operator produced the 5 stages shown. The soldering holes, although shown punched in the top picture of the completed part, were actually punched in a separate operation on another machine.

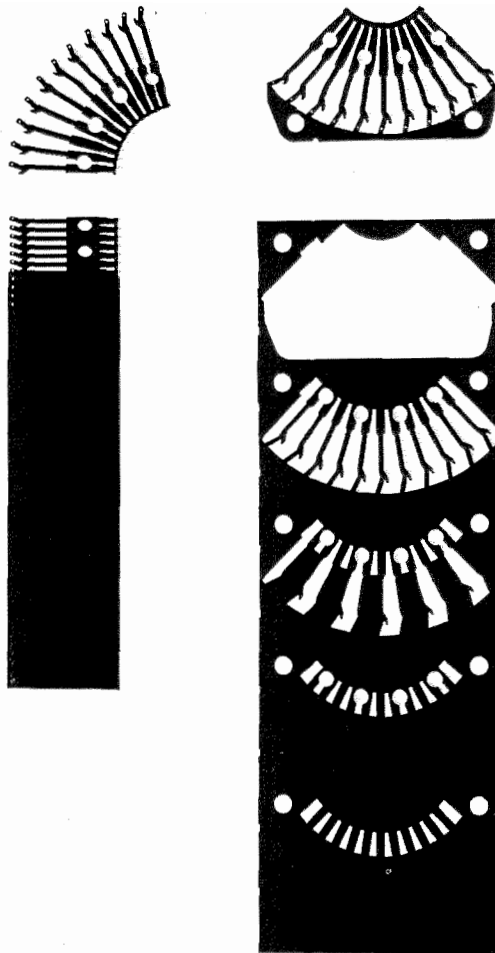
The new machine delivers 11 rapid-fire automatic strokes for each stamping and works continuously, ejecting on every 11th stroke a spread stamping with soldering holes already punched. The machine operates at 220 revolutions per minute, producing 20 completed fans each minute.

When the old machine was in use, the outside scrap of each of the 30 stampings in the bank (see frontispiece) was trimmed off individually

On the facing page is shown a completed contact bank for a two-motion selector switch as used in telephony and other applications. The 330 separate contacts on the bank result from assembling 30 stampings of 11 contacts each.

after assembly with a notching tool. The stampings produced on the new machine require no outside trimming.

A significant factor in the reduction of direct labor achieved by the new machine is the use of spindle feed from a coil of brass strip. The old machine was fed with flat strips 1.5 meters (4.9 feet) long.

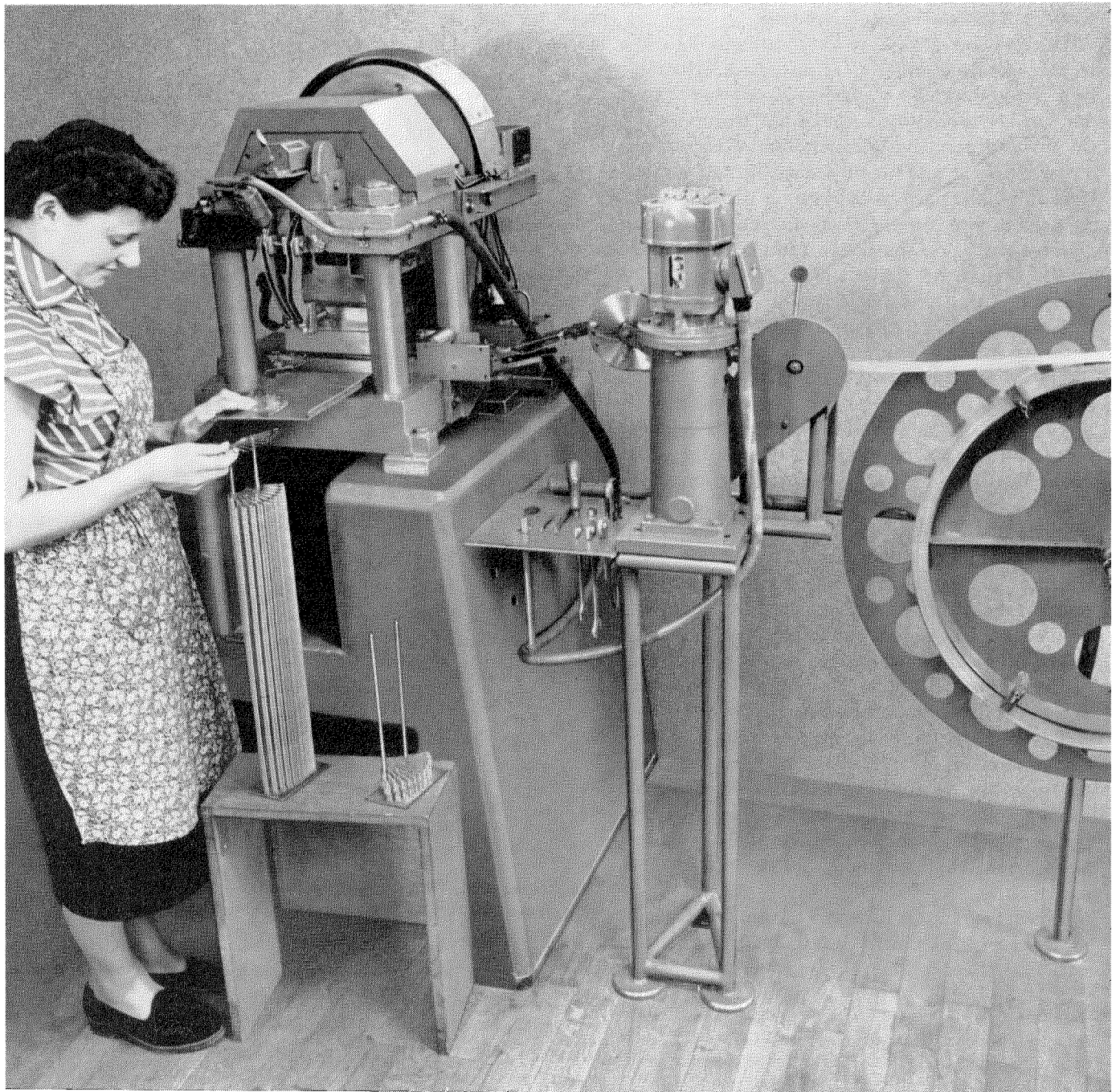


Comparative area of brass strip used to make 5 stampings with the new method (left) and old method (right).

At the same time as the new punch press was put into operation, other piece-part production and assembly methods were simplified so that the contact banks are now produced with 85 percent less direct labor than was required two years ago.

On the opposite page is a detail of the die set of the new machine, showing the spread stampings as they are ejected.

The photograph below gives an over-all view of the new machine in operation.





Graphical Symbols for Electrical Diagrams

By H. P. WESTMAN

International Telephone and Telegraph Corporation; New York, New York

GRAPHICAL symbols are one of the oldest forms of written language known to man. The ancient caveman drew crude pictures of things about him and as he advanced in his desire and need for written communication he simplified and standardized these pictographs to make it easier to draw them and to fix their meanings. As this process continued, some of the pictures lost their resemblance to the original objects and became true symbols; the start of a written language that later blossomed with the invention of the alphabet, which is entirely symbolic.

Today, some of our sciences require descriptions of things that cannot be clearly or simply put into words. An arrangement of apparatus is one such thing. Reverting to the ways of his remote ancestor, the scientist supplemented his alphabetical language with a picture language and found it to be a good tool. Similarly, he started with readily recognizable but coarse pictures of the actual pieces of equipment and then to simplify their drawing and to let them stand for more than one particular design of the device he slowly changed the symbols so that they looked less and less like the apparatus itself.

1. Electrical Symbols

Toward the start of the twentieth century, the economic importance of the industrial utilization of electricity attracted many of the workers in the field away from the signalling applications that had previously occupied most of them. The paths then taken by the heavy-current and by the light-current branches of the electrical industry diverged to an astonishing degree, aided and abetted to a considerable extent by the curious effects that stem from the differences in the frequencies employed in the power and communication domains.

This separation was so complete that the graphical symbols that were developed by one group not only were not identical to those of the other but included direct conflicts among symbols for such fundamental elements as resistance and inductance. That this situation could con-

tinue for several decades without becoming insufferable was clear evidence of how completely the two fields were separated from each other.

During the second world war, relatively large new aircraft were produced for the armed forces and their size combined with a shift from hydraulic actuators to electric motors for the operation of auxiliary equipment and controls called for rather substantial electric-power installations. This meeting of the power and communication industries in a common project brought sharply into focus the conflicts in graphical symbols.

At the request of the armed forces, the War Committee on Radio of the American Standards Association instituted a special project to bring about coordination of the fundamental electrical graphical symbols. By modification of some symbols and the suppression of others for some of the purposes for which they had been used, a coordinated set of symbols was selected. Developed under a special wartime emergency program, they were to be binding only for the duration of the war.

With the advent of peace, our bright brave new world began to slip back into its former habits and the economic pressure of the purchasing power of the armed forces ceased to provide the cement that bound us to the new and strange customs that had been thrust upon us.

Among the good things that may be credited to the warlike activities in Korea should be included the restrengthening of the wartime agreement and another opportunity to convert the war standard into a peacetime standard with its promise of continuing coordination. It is with this promise that we are now concerned.

A special task group was set up by the Sectional Committee on Graphical Symbols of the American Standards Association to draft a standard on graphical symbols for all electrical diagrams. Over a period of several years, this group of about 20 representatives of both the power and communication branches of the electrical field, maintaining constant coordination with the armed forces, produced the new American Standard Graphical Symbols for

Electrical Diagrams.¹ *MIL-STD-15A* issued by the armed forces of the United States is fully coordinated with the American Standard.

1.1 COMPROMISE

The compromise that was brought about during the war concerned four basic elements among which conflicts existed. The objective was to produce with minimum changes in the existing systems, a set of symbols in which each symbol had only one meaning. Alternative symbols for a single element would be permitted where a full compromise could not be obtained.

Figure 1 shows the previous symbols and the compromises that resulted from the project. The major conflicts concerned the communication resistance and the power inductance as well as the communication capacitance and the power open contacts.

It was agreed that the zig-zag symbol would be dropped for power inductance but that it could not be used on power drawings for resistance because of possible confusion. Consequently, both the power and communication symbols for resistance had to be retained as alternatives.

The communication inductance symbol is difficult to draw and the small loops fill with ink when a drawing is reduced to small size. It was agreed, therefore, to dispense with these small loops. A single symbol for inductance was thus

¹ "American Standard Graphical Symbols for Electrical Diagrams, Y32.2-1954," issued by the American Standards Association, 70 East 45th Street, New York 17, New York. (Price \$1.25 postpaid.) Published as "IRE Standards on Graphical Symbols for Electrical Diagrams, 1954," by the Institute of Radio Engineers, *Proceedings of the IRE*, volume 42, pages 965-1020; June, 1954.

possible, although the older (looped) form is still permitted.

It was felt that the communication capacitor and power open contacts were too nearly alike to be used even with strict rules that the capacitor have long lines close together and the contacts be short lines far apart.

The power engineers insisted on a very clear distinction between open and closed contacts, better than that provided by the communication symbol. Unfortunately, their symbols cannot be condensed in size to permit the large number of contacts that are commonly associated with telephone switching relays and it was necessary, therefore, to permit both types as alternatives.

The objections of drafting expense and fill-in between closely spaced lines on reduction in size made the power capacitance unsatisfactory. The smallest modification that could be made in the communication symbol was to curve one of the lines. Although this resulted in an asymmetrical symbol, it was the best single symbol on which a compromise could be obtained.

2. Types of Drawings

There are three basic kinds of drawings. First, there is the type that shows only the major elements of a system. The block diagram of Figure 2 in which rectangles are used to represent complete pieces of equipment or major elements in a system is an example of this.

Second, there is the schematic diagram in which the interconnections among the component parts that make up the system are indicated. This may take either of two forms; a single-line or a complete symbolism.

Single-line or one-line symbolism has developed almost exclusively in the power field. It was adopted for waveguide work by communication engineers because of the obvious difficulties of applying wire symbols to dielectric transmission paths.

In the power field, a 3-phase system may require 3 or 4 wires

Figure 1—Conflicts existing in previous practice and the compromise symbols on which agreement was obtained.

	POWER	COMMUNICATION	COMPROMISE
RESISTANCE			
INDUCTANCE			
CAPACITANCE			
CONTACTS OPEN			
CLOSED			

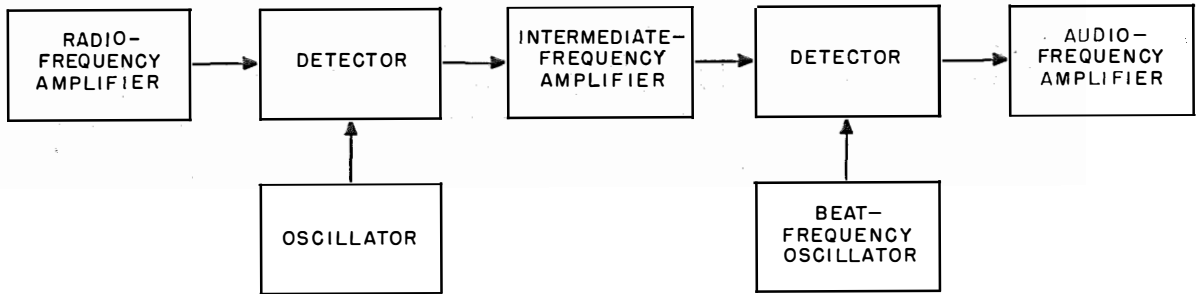


Figure 2—Block diagram of superheterodyne receiver.

for transmitting current and separate transformers for each phase. Figure 3 shows how the single-line method simplifies this type of drawing.

In the single-line system, the regular symbols are frequently used but in some instances certain details of the symbol are omitted. A shunt connection is indicated by bringing the single connecting line to the center of an inductance or resistance and by "hanging" a capacitor off to one side of the connecting line. A series connection is indicated by inserting the symbol in the line. Single-line notation may be considered to be a form of graphical-symbol shorthand.

Figure 4 is a complete and single-line representation of a radio-frequency amplifier coupled to an antenna. Although single-line drawings are not normally used for such things, there are times when they might be quite convenient and we are at liberty to borrow them from the power field.

The third type is the wiring diagram used by the workman in making the connections. For this purpose, Figure 4A would include the numbers of the tube-socket contacts corresponding to the various elements, the designation of the rotor of

the tuning capacitor so it could be connected to the chassis, the colors of leads from transformers, and similar data. Nothing is left to the judgment of the workmen, who need have no knowledge of

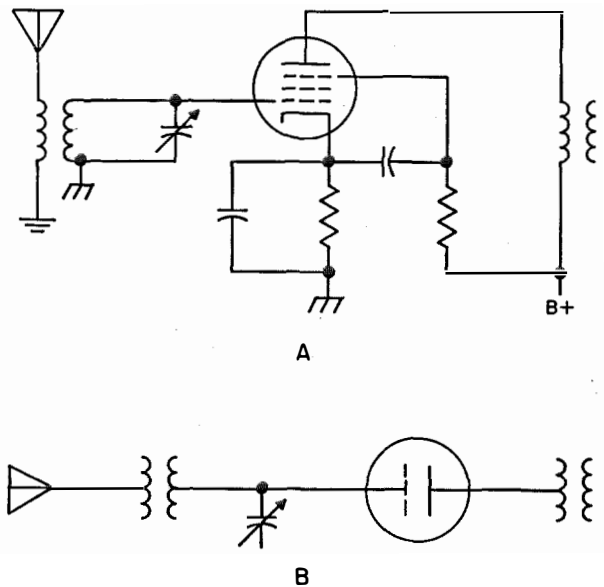


Figure 4—Complete A and single-line B drawings of a radio-frequency amplifier connected to an antenna.

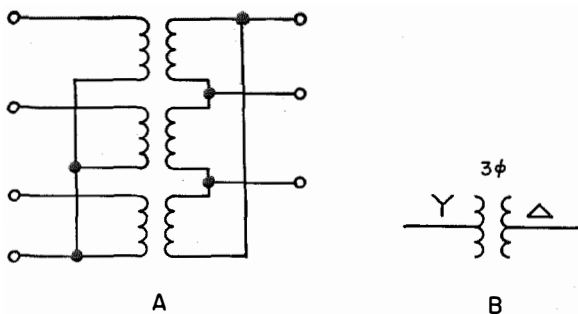


Figure 3—Complete A and single-line B drawing of a 3-phase transformer with wye-connected primary and delta-connected secondary.

how the equipment is to function or even of what it is to do.

In general, the new standard does not include the terminal markings or other designations that are needed on the wiring diagram but will provide for the block and schematic types of presentations.

3. General Rules for Symbols

Once we agree that we are dealing with symbols for functions and not with pictures of specific pieces of equipment, certain general rules may be set up.

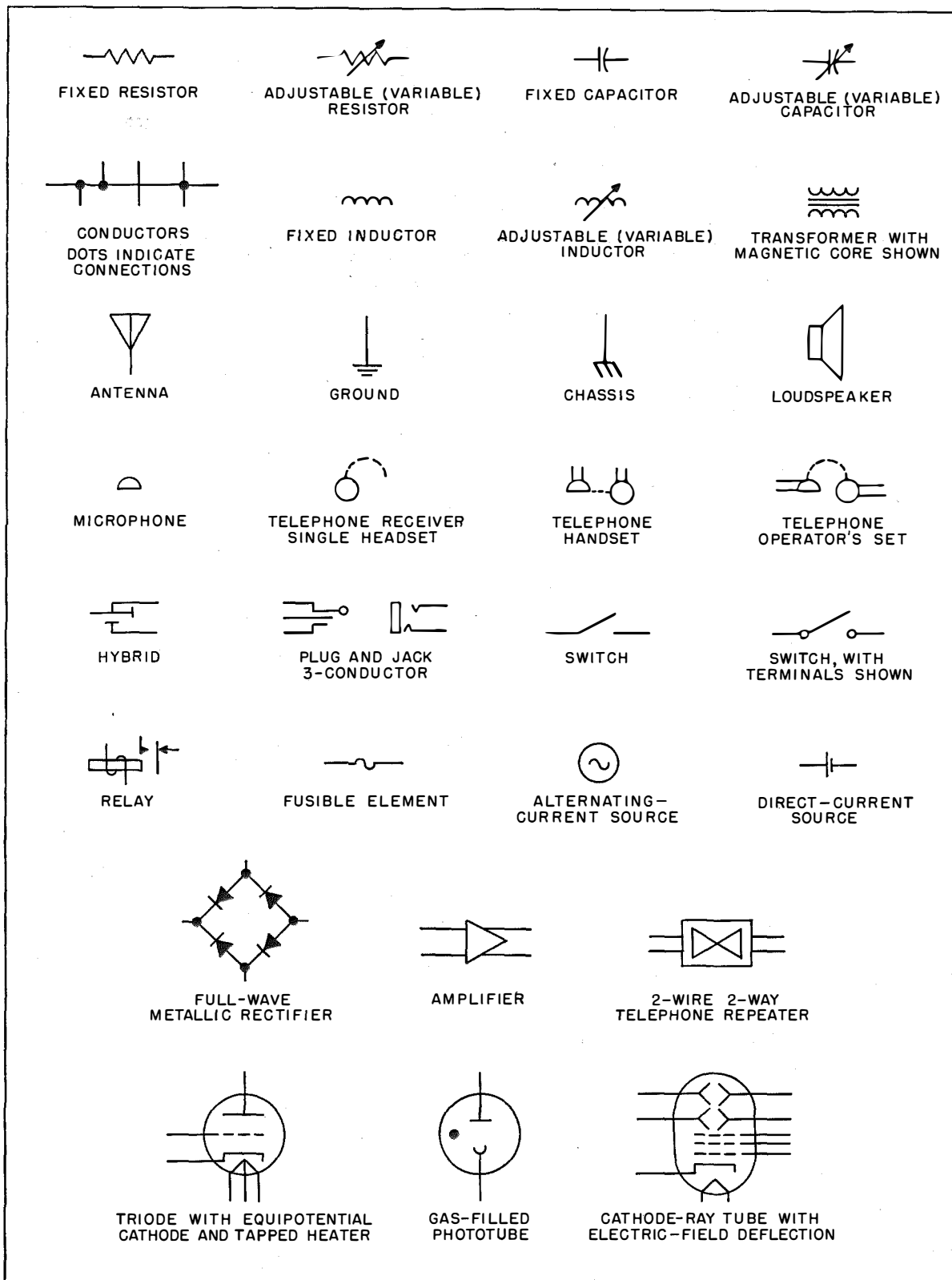


Figure 5—Some of the often-used symbols as they appear in the new standard. Where alternative symbols are permitted, the form nearest to that previously used in communication engineering has been given.

3.1 SIMPLICITY

To increase the speed and accuracy with which symbols may be drawn and to permit them to be reduced by photographic and other means to the smallest possible size, each symbol should be in the simplest form. Additionally, closely spaced lines and small loops should be avoided as they tend to fill with ink when drawings are reduced in size.

All rotating machines in which there are electrical connections to the rotating members use some sort of a brush operating against a commutator or slip ring. It is therefore meaningless to include in the symbol the details of brushes and commutators or slip rings. Similarly, most devices have some sort of terminals to which the wires from other pieces of equipment are connected. Symbols need not show these terminals unless the markings on them are important as in the case of a wiring diagram.

3.2 ORIENTATION AND LEADS

The orientation of a symbol must not change its meaning. A ground symbol is still a ground even if it is pointing upward or to the side. While in general it is best to draw symbols in either a vertical or a horizontal plane, this is a matter of orderliness and is given up at times for clarity as in the case of a bridge circuit, which is invariably arranged in a diamond form.

Similarly, leads may be attached to a symbol from any direction without changing the meaning of the symbol. For instance, a relay contact is a small solid triangle and the lead may come from the center or the end of one side of the triangle as is shown in Figure 5 for a relay.

3.3 TERMINALS

A small circle is used as a terminal to which a connecting wire may be attached. In the case of switches and jacks, it must not be assumed to be the fulcrum on which the movable part pivots. The terminal may be omitted without changing the meaning. This also is shown in Figure 5.

3.4 DETACHED ELEMENTS

There are two cases frequently encountered in which it is inconvenient to assemble all the parts

of a symbol in one place and run the connecting wires to them. Relays having a large number of contacts placed in circuits that are at some distance from each other on the diagram require a confusingly large number of lines. The relay may be identified by a letter followed by a diagonal line (solidus) and a number indicating how many sets of contacts are mounted on it. The contacts may then be inserted wherever they are needed in the drawing and the relay letter added to identify the relay on which they are mounted. If desired, a number may also be assigned to each set of contacts for individual identification.

The second case is the familiar one of two or more electron tubes in a single envelope. In this case, a split envelope may be used and the type number of the tube will identify its multiple character. For emphasis, the notation $\frac{1}{2}$ may precede the type number of the tube.

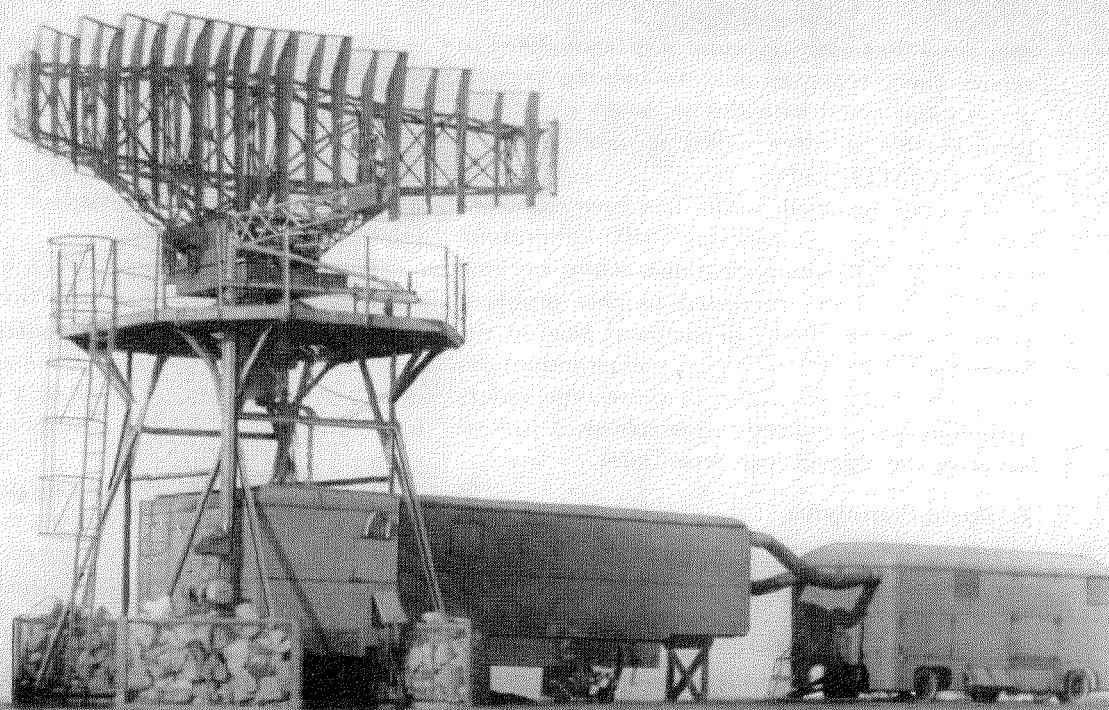
4. *Alternative Symbols*

In a number of cases, two or more alternative forms are permitted. This stems from the hard facts of life that complete agreement between the two major groups could not always be attained. It should be noted, however, that in no case does a symbol represent two different devices and thus confront the reader with a question as to which meaning the writer had in mind.

In general, there will be certain choices made among the alternative forms of symbols depending on whether the user is in the power or communication field. While it would be better if there were a greater tendency to work toward a single symbol in such cases, humans are creatures of habit and much prefer to let the other fellow change his way to bring about a desired coordination.

5. *International Standards*

The International Electrotechnical Commission is in process of revising its standards on graphical symbols. The work already done reflects clearly the contents of the new American standard and we can look forward to a greater degree of coordination in this field throughout the world than ever existed before.



Mobile radar station incorporating the fixed-target-echo-elimination equipment.

Radar Receiver with Elimination of Fixed-Target Echoes*

By HERVÉ TANTER

Laboratoire Central de Télécommunications; Paris, France

SUPERVISION and control of air traffic in the vicinity of airports, long-range detection of enemy aircraft and flying missiles, and coordination of counteraction by friendly fighter aircraft are among the most important applications of radar.

Surveillance radars of the types that perform the above-mentioned functions usually operate on a 10-centimeter wavelength with a pulse-repetition frequency of between 300 and 2000 cycles per second. The antennas used make it possible to obtain radiated beamwidths of the

order of 0.8 to 3 degrees in the horizontal plane; the antennas rotate at speeds of 2 to 30 revolutions per minute.

Generally, surveillance radars now in service are fitted with ordinary indicators that have the disadvantage of showing the operator not only the echoes from the aircraft in which he is interested, but also echoes from various permanent targets such as trees, buildings, hills, mountains, and so forth. The echo of an aircraft flying over one of these obstacles is temporarily lost in that of the fixed target thus greatly reducing the effectiveness of the radar.

The advantage to be gained by eliminating the fixed-target echoes in the radar receiver is thus quite evident. As aircraft are moving, it has been

* Presented before Société Française des Radio Electriciens in Paris, France on November 28, 1953. Reprinted from *L'Onde Electrique*, volume 34, pages 99-109; February, 1954.

suggested that ordinary radar sets be modified to render them sensitive only to moving targets, and a radar fitted with the necessary circuits to perform this is often called a moving-target-indicator (MTI) radar.

The need for such radars has been apparent for a long time. As early as 1940, Laboratoire Central de Télécommunications, while working on radar, became interested in this problem. H. G. Busignies, then a department head at the laboratory, issued a technical memorandum defining the basic principles of pulse-type radars with elimination of fixed-target echoes. A patent¹ covering the subject was issued later.

1. Basic Principles

Discrimination among echoes from fixed and moving targets may be effected by utilizing the Doppler-Fizeau effect. One aspect of this phenomenon is that if a radiating source sends out a fixed-frequency wave that impinges on a target capable of reflecting an electromagnetic wave, the reflected wave as received back at the transmitting site will have the same frequency as the transmitted wave when the distance between transmitter and target is fixed. However, during a period when there is relative motion between the two, the frequency of the reflected wave will be different from that of the transmitted wave. The difference in frequency is directly proportional to the rate of change of distance, being additive when the distance is decreasing and subtractive when the distance is increasing.

This phenomenon can be used in radars by comparing at the receiver the reflected wave with the transmitted wave and then eliminating those echoes that do not differ in frequency from the transmitted frequency.

P. David suggested this method as early as 1928 for an electromagnetic curtain effect wherein a moving airplane causes beat notes to appear in the otherwise silent reception of a non-modulated continuous-wave transmitter; the beat notes cease when the aircraft passes directly between the transmitting and receiving sites, thus indicating its presence but not its location. This same method is also used in continuous-wave (Doppler-type) radars that are sensitive only to moving targets.

¹ H. G. Busignies, French patent 932,930; December 17, 1947; United States patent 2,570,203; application date March 5, 1941, issued October 9, 1951.

The application of this principle to pulse-type radars is more complicated since the transmitter is inoperative when the echoes are received and since the frequency shift caused by the Doppler effect is but a small fraction of the transmitted frequency; frequency comparison is therefore a somewhat difficult matter.

The Doppler frequency f_d has a value of $2v_r/\lambda$, where v_r is the radial velocity of the target and λ is the wavelength of the transmitted wave. For an aircraft flying at 360 kilometers (220 land miles) per hour, directly toward a radar operating on a wavelength of 10 centimeters, $f_d = 2000$ cycles.

A direct comparison between the frequencies of the transmitted wave and the echo would require the generation in the receiver of a local signal preserving the characteristics of the transmitted wave until the last echoes had returned and, if this comparison is to have a meaning, it would be necessary for the transmitter frequency to be defined and stabilized to within better than one part in 10^7 , an exceedingly difficult matter with present pulse-type radars at microwave frequencies.

The difficulty may be obviated by using phase comparison instead of frequency comparison. In fact, it may be considered that the echo has the same frequency as the transmitted wave but that it shifts in phase from one transmitted pulse cycle to the next at a rate corresponding to the Doppler frequency. Or, to put this more simply, the phase angle between each transmitted radio-frequency pulse and each corresponding received echo signal is a function of the distance to the target. If the target is fixed, this phase angle is constant from one transmitting cycle to the next, while if the target is moving, the phase angle changes between pulse cycles.

To effect this phase comparison between the transmitted pulse and the corresponding received echo signal, it is necessary to generate and maintain in the receiver for the entire duration of the echo return time, a signal that preserves a record of the phase of the transmitted pulse.

The phase comparison is performed in a device that converts phase relations into amplitude relations. If the signal resulting from this transformation is applied after demodulation to a type-A cathode-ray-tube indicator (showing amplitude on the ordinate and distance or time on the

abscissa), it will be seen that fixed-target echoes have a constant amplitude, either positive or negative, from one cycle to the next, while the amplitudes of echoes from moving targets vary from one cycle to the next at the Doppler frequency corresponding to the particular radial speed of the target. This fluctuation is called a butterfly effect (Figure 1).

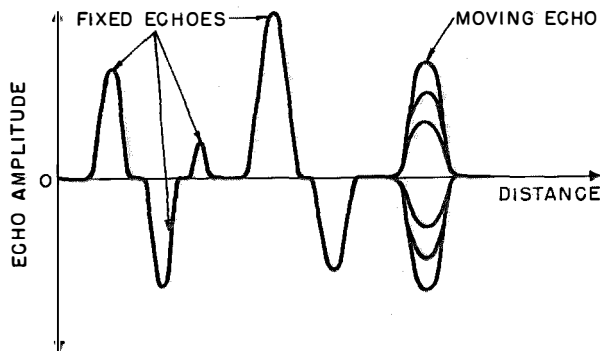


Figure 1—Appearance of echo signals at the output of a coherent-radar phase detector.

It is thus possible to discriminate instantaneously among fixed targets and targets having radial motion with respect to the radar station. Radars embodying the principles just described are called coherent radars.

For the purpose of eliminating from the indicator all motionless targets, all that is necessary is to subtract the echo trains resulting from two successive pulse cycles; that is, two successive cycles from the output of the phase-comparison device as depicted in Figure 1. Echoes from fixed targets, having constant amplitude from one cycle to the next, are then eliminated while echoes from moving targets, having amplitudes that change from one cycle to the next, do not give perfect cancellation, but allow a signal to remain that fluctuates at the Doppler frequency.

To carry out this cancellation, it is necessary to delay one echo pulse train by an interval exactly equal to the time interval between two transmitter pulses; to effect this, a delay or memory device must be incorporated having certain main properties as follows.

A. The delay element should reproduce the signals applied to it with a high degree of fidelity. It should therefore have a sufficiently large inherent bandwidth.

B. The device should have good amplitude linearity so as to preserve small echoes from moving targets both superimposed on and near large fixed echoes and also in all other areas.

C. The delay element and its associated circuits should not introduce noise or stray signals.

The delays required of the device are of the order of several milliseconds. The most suitable delay devices at present available are based on the principle of supersonic propagation in a suitable medium.

2. Coherent Radar Receiver

2.1 GENERAL

Using the basic principles described in the Busignies' memorandum of 1940, Laboratoire Central de Télécommunications undertook the study of the essential elements of radar receivers with elimination of fixed-target echoes. In particular, successful supersonic delay lines using a propagating medium of alcohol and water were developed by Messrs. Biquart and Ahier.²

Wartime conditions interrupted this work in 1944, but it was resumed in 1946 under auspices of the Centre National d'Etudes des Télécommunications with the assistance of the Direction Centrale des Constructions et Armes Navales.

The studies carried out from 1946 to 1948 led the technical service of Service Technique des Télécommunications de l'Air to request in 1949 that Laboratoire Central de Télécommunications build a 10-centimeter radar receiver incorporating fixed-target-echo elimination. This receiver was to be used with a long-range surveillance radar built by Compagnie Générale de Télégraphie Sans Fil. The first model built was accepted in July 1951 and after delivery to the contractor was subjected to numerous field tests at various military experimental stations. Other equipments were supplied to foreign countries.

Two production models are currently available; the first is a single equipment for mobile use and the second is a triple equipment for fixed master stations. The first model delivered to the French administration (Figure 2) is housed in a

² P. Biquard and G. Ahier, "Application des Méthodes d'Impulsion à l'Etude de la Propagation des Ondes Ultrasonores." *Cahiers de Physique*, 3rd year, number 15, pages 21-42; August, 1943.

cabinet 1.7 meters (66 inches) high, 0.66 meter (26 inches) wide, and 0.5 meter (20 inches) deep. On the upper right is an oscilloscope for monitoring purposes, and next to it is a switch panel and low-voltage power supply. The receiver itself and the associated high-voltage power supplies are mounted on the two wide drawers. The receiver controls are on the panel of the uppermost drawer. The delay lines and associated circuits are in the bottom of the cabinet. There are two delay lines, one being the main line that delays the signal and the other a pilot line that accurately sets the pulse-repetition frequency.

The second model of the equipment (Figure 3) was designed for fixed master stations and comprises three receivers and a central synchronizing section. This equipment is contained in a cabinet that can be disassembled into two sections for transportation. The dimensions of the cabinet are 1.7 meters (66 inches) high, 2 meters (78 inches) wide, and 0.5 meter (20 inches) deep. In the upper half of the cabinet are 3 power-supply drawers, 3 drawers containing the 3 coherent receivers, a trigger-signal distribution drawer, a drawer for the monitoring oscilloscope, and a drawer containing the power-supply control circuits. The delay lines and associated circuits (Figure 4) are housed in the bottom half of the cabinet; 3 signal-carrying lines and a pilot line being included.

2.2 CIRCUIT OPERATION

The component units constituting an elementary radar receiver with elimination of fixed-target echoes are shown in Figure 5. The equipment might conveniently be divided into three main portions.

- A. Coherent receiver proper.
- B. Device for eliminating fixed-target echoes.
- C. Trigger circuits.

2.2.1 Coherent Receiver

The manner in which the reference signal used for phase comparison is generated is as follows. A very small portion of the transmitter output pulse is picked up and applied to an auxiliary mixer in the high-frequency head of the transmitter. In the mixer, it is heterodyned with the

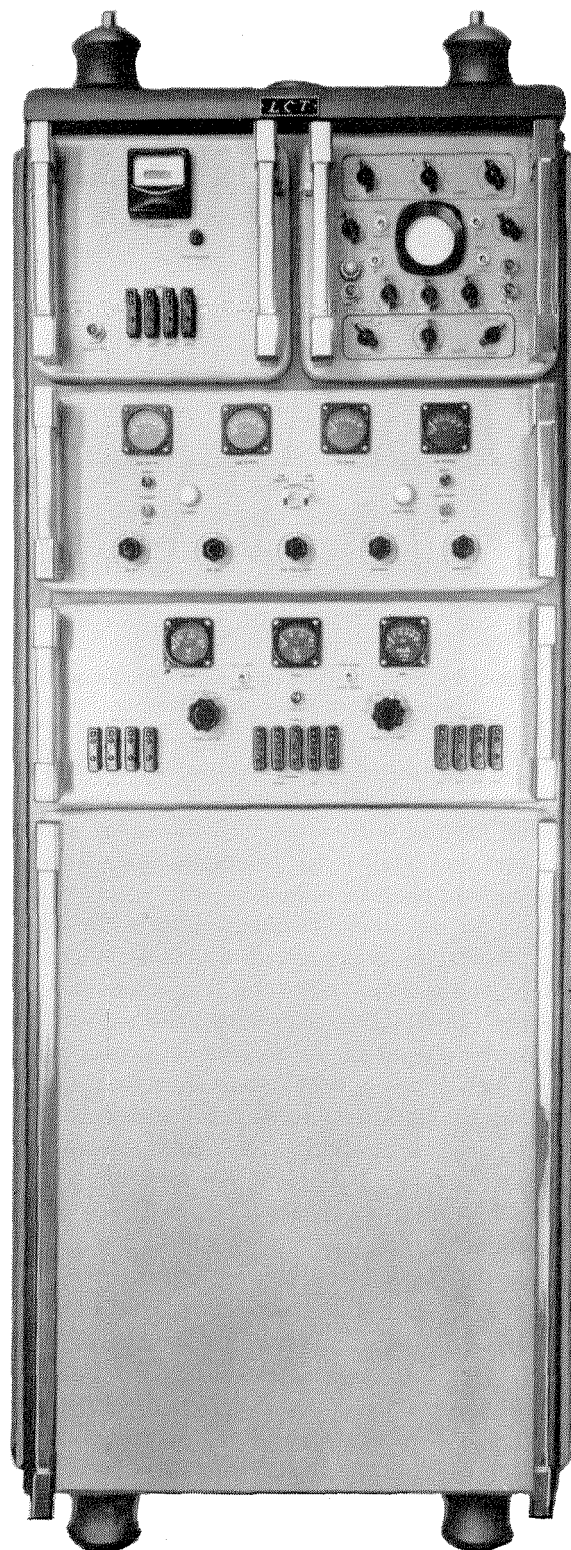


Figure 2—Fixed-echo-elimination receiver for mobile radars.

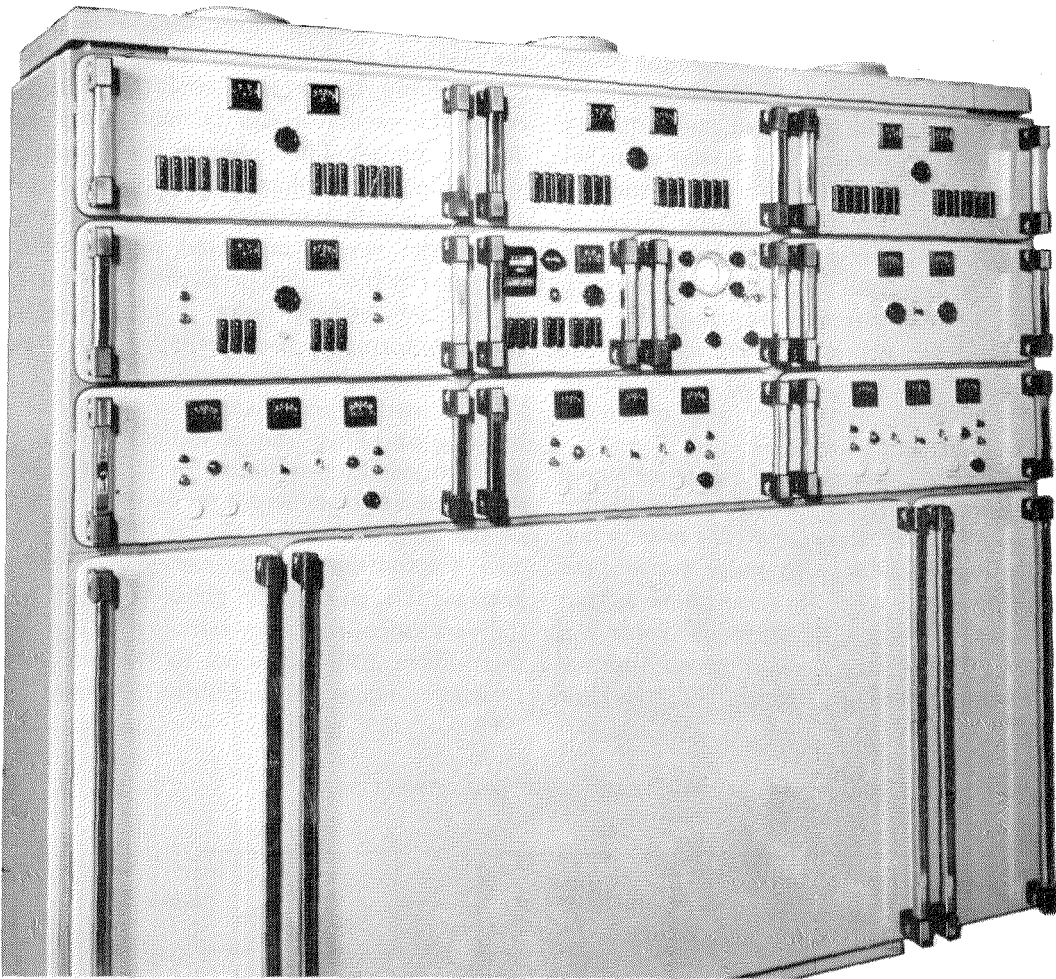


Figure 3—Above, triple fixed-echo-elimination receiver equipment for large master radar installations.

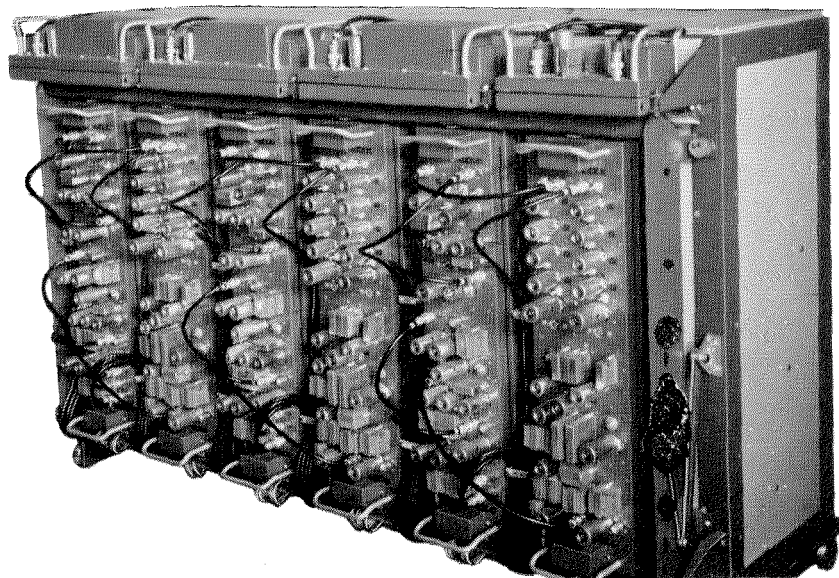


Figure 4—At right, triple fixed-echo-elimination equipment. The 4 delay lines are mounted behind the chassis comprising the associated circuits.

signal from the normal local oscillator. Provided the local oscillator is sufficiently stable, the phase relations between the intermediate-frequency reference signal and the intermediate-frequency echo signals are the same as those that exist between the microwave transmitter pulse and the microwave echoes returning from the target.

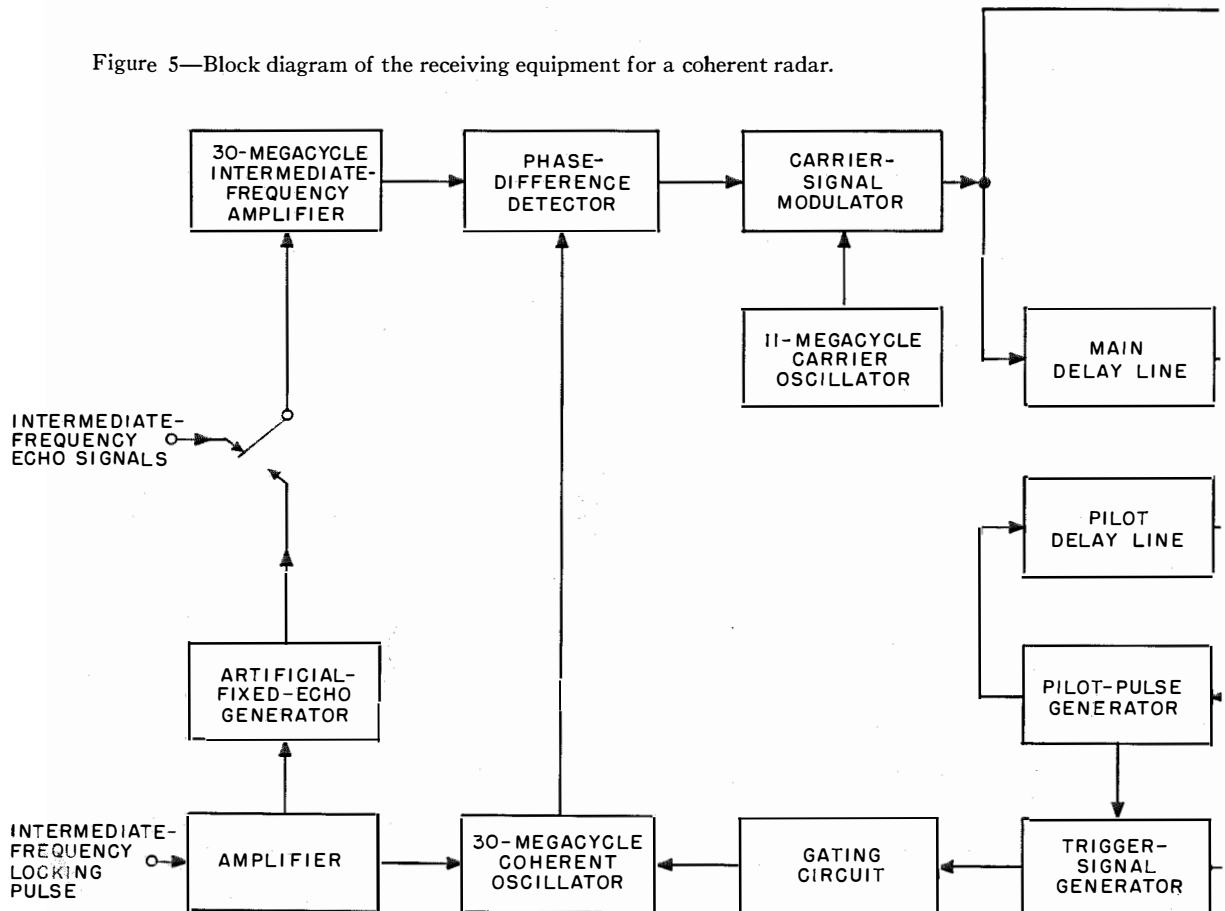
Available at the input of our receiver, then, are two signals; the low-level intermediate-frequency echo signals and the intermediate-frequency reference signal from the transmitter, called the locking pulse. These are indicated at the left of Figure 5. The echo signals are applied to an intermediate-frequency amplifier.

In the meantime, the pulse of reference signal is amplified and applied to the coherent oscillator. This is a 30-megacycle oscillator that is switched on at the moment the locking pulse arrives; the oscillator thus starts with the same phase as that signal. As is well known, a normal oscillator will start in random phase, depending on thermal fluctuations in the resonant circuit. If, at the time

of starting of the oscillator, there is injected into the resonant circuit a signal having an amplitude considerably larger than the thermal fluctuations, the oscillator can be made to start in a definite phase. The coherent oscillator having started in correct phase, it continues to generate a 30-megacycle reference-wave signal until just before the next transmitted pulse, when it is temporarily blocked in preparation for the arrival of this new locking pulse. The local oscillation then, conforms to the particular phase of each transmitted pulse.

The intermediate-frequency amplifier is a limiting amplifier and is followed by a phase-sensitive detector actuated by the reference wave delivered by the coherent oscillator. The purpose of the amplitude limitation is to remove amplitude fluctuations of the intermediate-frequency echo signals, so that the phase-sensitive detector delivers video-frequency signals whose amplitude fluctuation is proportional to the intermediate-frequency phase fluctuation of the echoes.

Figure 5—Block diagram of the receiving equipment for a coherent radar.



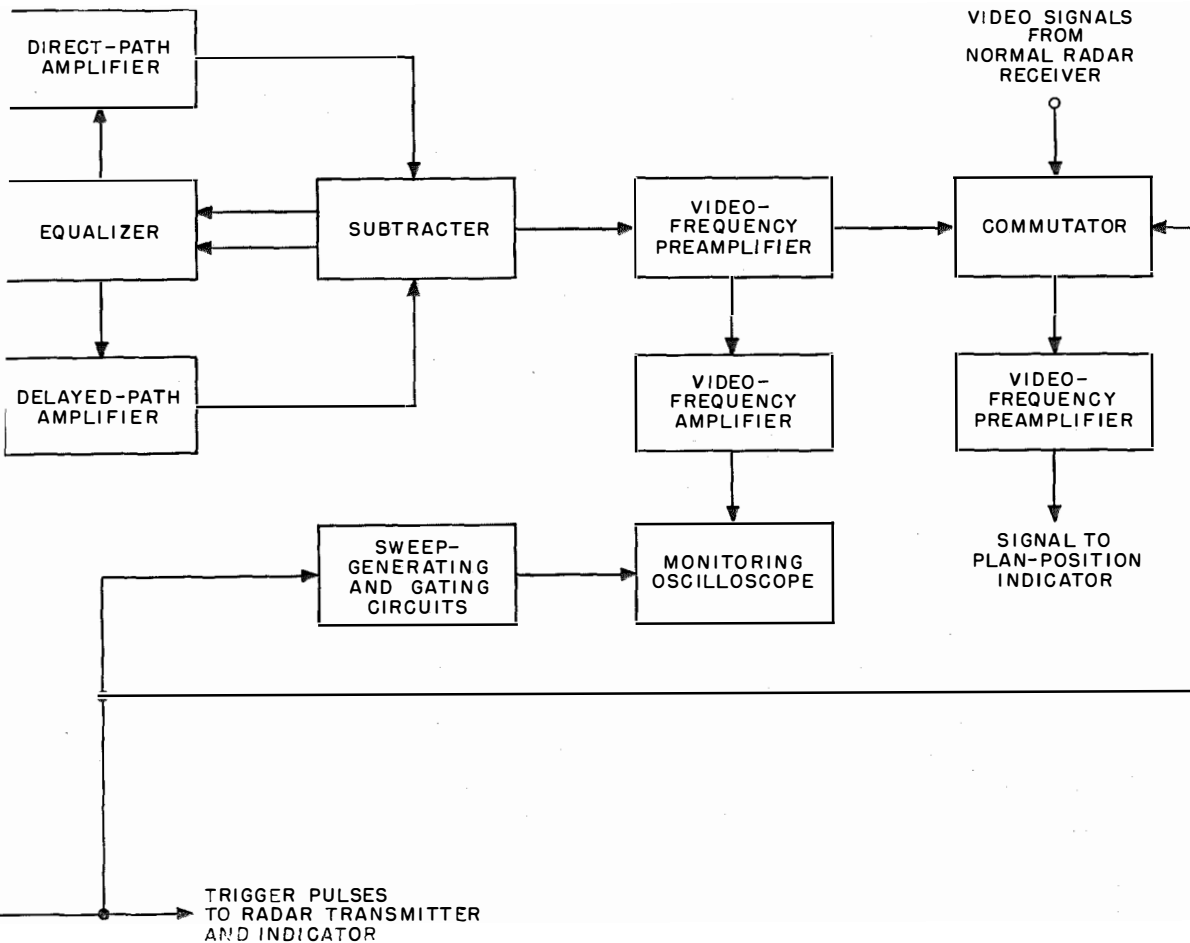
2.2.2. Fixed-Target-Echo Elimination

Comparison in the phase-difference detector of the amplified and limited echo signals and the output from the coherent oscillator results in a carrier-wave signal having amplitude modulation similar to that shown in Figure 1. After demodulation, this signal is applied to the circuits that eliminate the fixed-target echoes.

The essential element of these circuits is the supersonic delay line. In these devices, the electric oscillations corresponding to the echo signals to be delayed are applied to a quartz crystal at the input end of the line. The crystal vibrates mechanically at a rate corresponding to the frequency of the signals, and these vibrations are transferred to the propagating medium in contact with the crystal. At the other end of the column of propagating medium is another crystal that picks up the supersonic vibrations from the medium and reconverts them to electric signals.

The propagating medium may be either liquid or solid; in the present case, mercury was chosen for two reasons. It has a high acoustic impedance that permits proper damping of the crystals, thus providing a large bandwidth that will carry short pulses without distortion; and it also offers a relatively low attenuation to the passage of supersonic waves. This attenuation is of the order of 4.4 decibels per meter (1.3 decibels per foot) at 10 megacycles; the attenuation is proportional to the square of the frequency.

For quartz crystals having a given resonant frequency, the acoustic bandwidth is of the order of half of this frequency. Transmission is zero, however, at zero frequency, which may lead to distortion in the video-frequency signals if they are applied directly to the line. Thus, to take full advantage of the large bandwidth of the line, the video signals are modulated onto a carrier wave and it is this amplitude-modulated wave that is propagated down the delay line. The quartz



crystals are resonant at the frequency of the carrier wave, which in the present case is 11 megacycles.

Figure 5 shows how the signals from the phase-difference detector are applied to the carrier-frequency modulator, which consists of a balanced modulator followed by a wideband amplifier that drives the transmitting crystal in the main delay line and also drives the input of the direct-path amplifier through an attenuator. The oscillator associated with the modulator is quartz-crystal stabilized.

The delay line is followed by an amplifier that compensates for the attenuation introduced by the line. This attenuation is due to the relatively low efficiency of the end-cell transducers and to the propagation of supersonic waves through the medium. The amplifier defines the over-all bandwidth of the delayed-signal channel and corrects for the frequency-dependent losses in the line, thus giving a flat over-all pass band.

The gain of the delayed channel is about 1, so the gain of the direct-path amplifier is made the same; the purpose of this latter amplifier is to assure that signals passing through each channel will undergo identical deformations, if any.

Each of the two amplifiers is followed by a detector; the detectors deliver signals of opposite polarity so that subtraction may be done in a resistance common to the two circuits. For successful subtraction, and thus successful cancellation of the fixed-target echoes, it is necessary that the over-all delay time of the delayed-signal channel be exactly equal to the repetition period of the transmitter and that the gains of the direct and delayed channels be identical. The equalization of gains of the channels is done by a circuit that compares the carrier-wave levels at the detection points and acts differentially on the amplifiers to maintain equal carrier-wave amplitudes.

2.2.3 Trigger Circuits

The delay time in the delayed channel may vary as a result of temperature effects that change the propagation time in the mercury columns. To prevent differences in delay time and transmitter repetition rate from causing imperfect cancellation, the delay line (pilot line) that controls the repetition rate of the transmitter is placed in the same enclosure as the main delay

line and thus experiences identical temperature effects.

The trigger circuits associated with the pilot line supply trigger pulses to the transmitter, indicators, monitoring oscilloscope, coherent-oscillator gating circuits, and to the commutator. This latter circuit enables an operator to observe on an indicator from zero distance to an arbitrary distance the signals from the cancellation equipment and beyond this distance, the signals from a normal receiver. This can be of advantage in some instances, as masses of fixed targets (so-called ground clutter) tend to appear at short ranges on the indicator, while being less bothersome at longer ranges.

2.3 CONSTRUCTION OF DELAY LINES

The two delay lines for the mobile equipment are mounted on both sides of a light-alloy frame (Figure 6). Since the repetition frequency of the radar is 500 cycles, the delay time of the main line must be 2000 microseconds; the propagation speed of sound in mercury is about 1500 meters

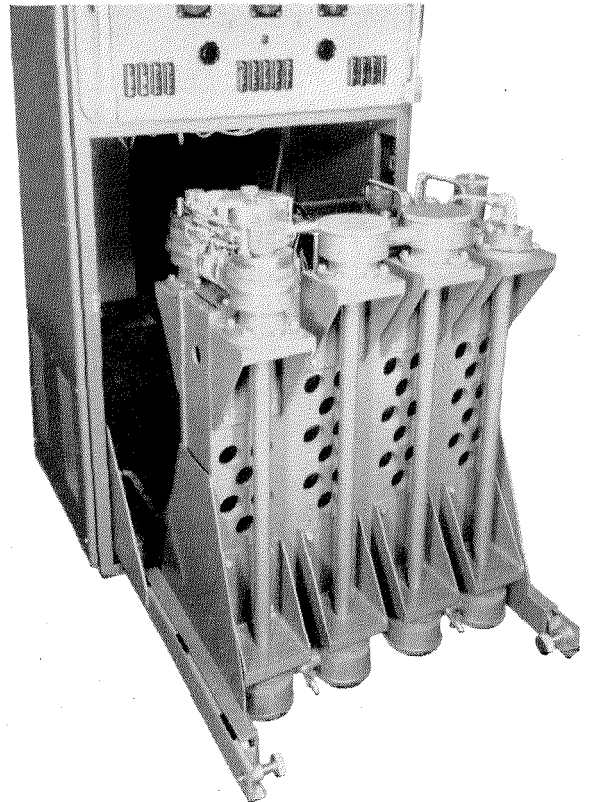


Figure 6—Delay lines for the mobile equipment. The frame mounts two folded lines.

(4900 feet) per second and the line must therefore be 2.88 meters (9 feet, 6 inches) long.

The line is folded; it consists of 4 vertical steel tubes filled with mercury. The tubes are interconnected by 6 adjustable reflector blocks that

The X-cut quartz crystals vibrate longitudinally, one face being in contact with the mercury and the other excited by a steel electrode. A thin layer of air between the crystal face and the electrode ensures optimum efficiency of the

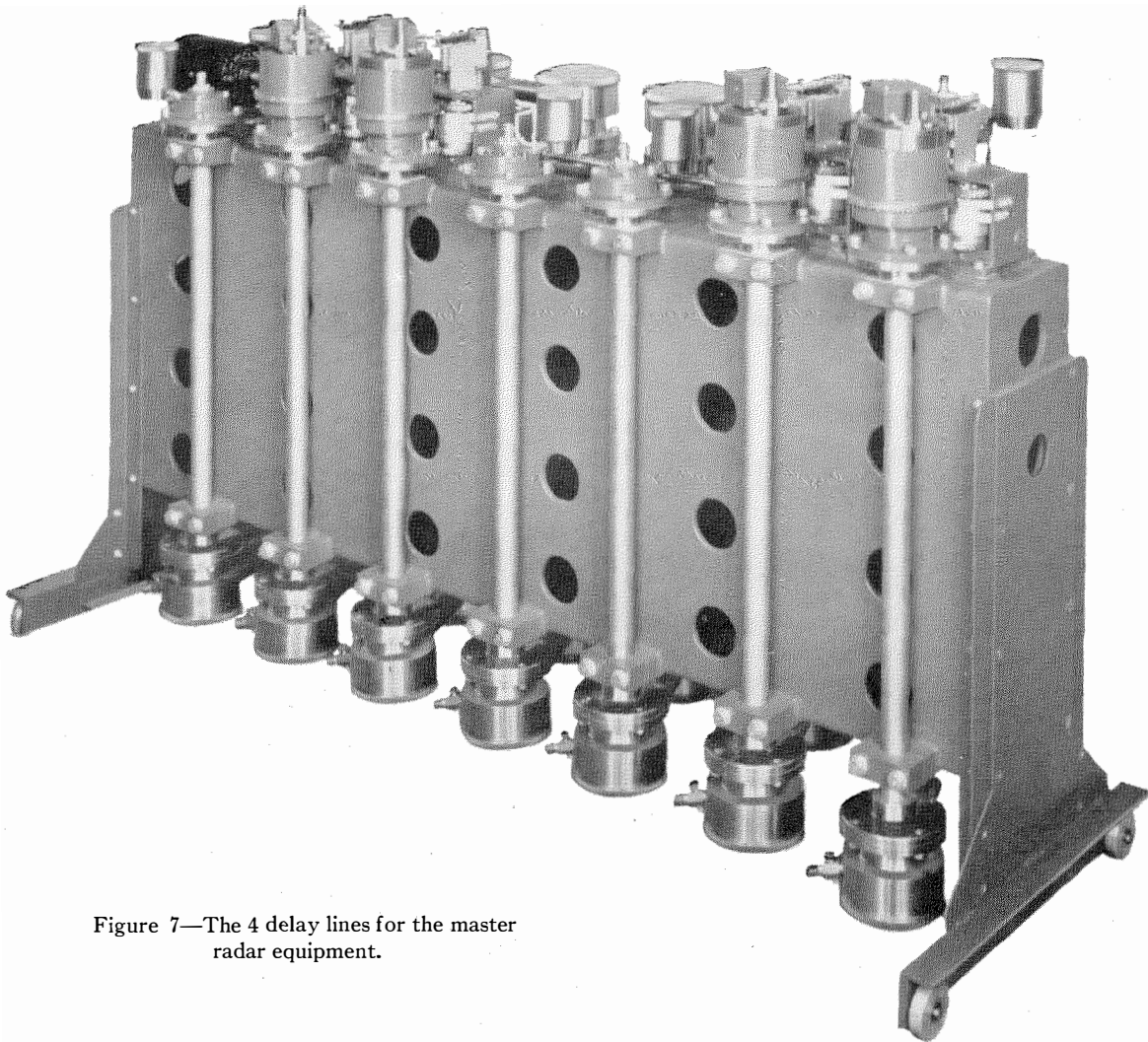


Figure 7—The 4 delay lines for the master radar equipment.

introduce 90-degree bends in the path of the supersonic wave. Mechanical alignment of the system is performed by optical methods.

The receiving crystal is mounted on a fixed support, while the transmitting crystal can be moved to provide for a precise adjustment of the length of the line. The crystal supports are placed at the top of the columns, which allows for easy removal of the air that might remain between the face of the crystal and the mercury. Expansion containers are used as mercury reserves and ensure a certain pressure within the line.

transducers by creating a certain amount of reflective acoustic mismatching.

The construction of the pilot line is identical with that of the main line, but it is only half as long. It therefore defines a repetition frequency of twice the desired value, which is obtained by frequency division. The pilot line contains only two reflector blocks; it is adjustable in length to enable matching the delay of the main line and operates on a carrier frequency of 17 megacycles.

The line assembly for the triple equipment (Figure 7) comprises 3 main lines and a pilot

line. Each of these line assemblies are contained in a thermal enclosure made of Klégécel plates covered by two thin metallic sheets.

3. Theoretical Performance and Experimental Results

The following are the essential criteria that determine the performance of a radar with fixed-target-echo elimination.

A. Visibility of a target outside of fixed-echo areas; that is, the maximum range of the radar.

B. Degree of elimination of fixed-target echoes.

C. Visibility of echoes from moving targets in the vicinity of fixed echoes.

3.1 RANGE OF THE RADAR

In the absence of fixed echoes, the amplitude of a moving echo given by a coherent radar at time t is expressed by

$$y_1 = y_0 \cos 2 \pi f_d t, \quad (1)$$

y_0 being the amplitude of the echo from a normal radar. It may be seen that the signal is amplitude modulated at the Doppler frequency f_d . At the time $t + T$ corresponding to the next pulse, the amplitude becomes

$$y_2 = y_0 \cos 2 \pi f_d (t + T), \quad (2)$$

which gives, after subtraction,

$$y = y_1 - y_2 = 2 y_0 \sin (\pi f_d T) \sin 2 \pi f_d (t + T/2). \quad (3)$$

The amplitude of the echo after subtraction is still modulated at the Doppler frequency.

The echo amplitude is zero when $\sin \pi f_d T = 0$, that is, when $f_d T = f_d / f_r = k$, where k is an integer. Therefore, radial speeds at which the Doppler frequency is a multiple of the pulse-repetition frequency f_r are *blind speeds*. For a wavelength of 10 centimeters and $f_r = 500$ cycles, the blind speeds are multiples of 25 meters per second (90 kilometers or 56 land miles per hour).

On the other hand, the maximum amplitude of the echo is twice the amplitude of the normal radar echo when $\sin \pi f_d T = 1$, or when $f_d = (2k + 1) f_r / 2$. The corresponding speeds are *optimum speeds*.

The sensitivity of the radar, therefore, is function of the speed of the target. The curve representing this sensitivity as a function of radial speed is a succession of sinusoidal arcs (Figure 8).

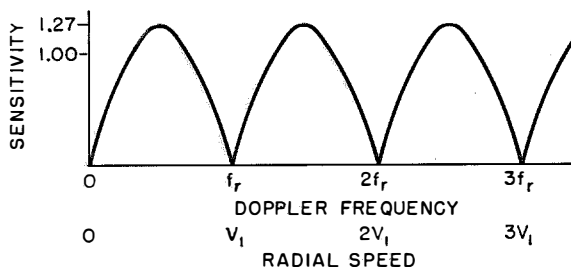


Figure 8—A coherent radar is more sensitive to target moving at certain speeds than at others. The variation is plotted above.

The signal represented by (3) is a fluctuating bipolar signal that must be rectified in a full wave circuit before application to the plan-position indicator. To calculate how this new fluctuating signal will affect the indicator, it is necessary to find its mean value.

$$|\bar{y}| = \frac{4}{\pi} y_0 (\sin \pi f_d T) \quad (4)$$

with $4/\pi = 1.27$.

The noise amplitude is the same as in a normal radar. The phase detector delivers signals in which the amplitude is a function of both the amplitude and phase of the intermediate-frequency signals. The amount of signal information relative to noise is therefore multiplied by a factor of $2^{1/2}$. But on the other hand, since the noises in the direct channel and the delayed channel are independent, their powers add in the subtraction circuit, and the relative amount of noise is increased by a factor of $2^{1/2}$ at that point.

Thus the ultimate sensitivity of the coherent radar is always a function of the speed of the target. For optimum speeds, the sensitivity is slightly higher than that of a normal radar. If it is assumed, however, that all speeds are equally possible, it may be said that on the average, the fixed-echo-eliminating radar shows no loss of sensitivity compared with a normal radar. Experience confirms these theoretical results.

Numerous tests were made with various types of 4-engined, 2-engined, and jet aircraft and

helicopters. In these tests, two plan-position indicators were observed, making it possible to see simultaneously the signals from the coherent radar and from a normal radar. It was found that the ranges of the radars were substantially the same. Many of the tests gave identical ranges, but some showed a decrease in range for the coherent radar of 5 to 10 kilometers (3 to 6 land miles) at 150-kilometer (90-land-mile) ranges.

It should be noted that the echo from an aircraft is the result of a very complex reflection; for propeller aircraft, in addition, modulation of the echo by rotation of the propeller makes the aircraft visible even if it has a radial motion corresponding to one of the blind speeds, or even if it has no radial component of motion.

3.2 DEGREE OF FIXED-ECHO CANCELLATION

The quality of fixed-target-echo elimination is primarily a function of the performance of the subtraction device in the receiver. In the present receiver, the delay and subtraction devices reduce fixed echoes by 40 decibels, or to 1-percent of the original amplitude.

In the truest sense, it might be said that there is no such thing as an ideal fixed echo; in fact, intermediate-frequency signals corresponding to "fixed" echoes fluctuate both in amplitude and phase. A first reason for this is the effect of the wind, which causes, for instance, motion of branches and leaves on trees. A second cause is the rotation of the radar antenna that causes amplitude modulation of the echoes from isolated targets as the antenna polar diagram is swept across the target. Also, rotation of the antenna modifies, from one pulse cycle to the next, the ground area whose scattering elements contribute to the constitution of the echo received from a given range. Another cause is the influence of instabilities in the transmitting and local oscillators of the equipment.

Fixed echoes are made up of the vector sum of the contributions of a large number of elemental reflecting targets. The phases of the elemental echoes are distributed at random, so that the fluctuations of the fixed echoes are of the same nature as the receiver random noise. These fluctuations are not eliminated and it is desirable that the corresponding residues have the same amplitude as the receiver noise so that they will

not appear as a ghost echo on the plan-position indicator.

Analysis of the fluctuation of fixed echoes shows that the root-mean-square fluctuation in amplitude is proportional to the root-mean-square value of the amplitude of the echo, while the root-mean-square fluctuation in phase is independent of the echo amplitude. The use of an amplitude-limiting intermediate-frequency amplifier followed by a phase-sensitive detector makes it possible to eliminate the amplitude fluctuations of the intermediate-frequency echoes and results in video-frequency signals in which the amplitude fluctuation is only a function of the phase fluctuations of the intermediate-frequency echoes, and consequently is independent of their amplitude.

To adjust a coherent receiver properly, it is necessary to understand thoroughly its operation; let us therefore study the relevant vector diagrams shown in Figure 9.

The left portion of the figure shows the vector **OA** representing the coherent-oscillator signal applied to the phase-sensitive detector. Vector **AB** shows a signal of variable phase with respect to the reference signal. This signal may be the intermediate-frequency noise of the receiver or the signal resulting from the intermediate-frequency vector composition of the noise and a moving target.

The reference signal and the aforementioned signal are combined in the phase detector to give a resultant intermediate-frequency signal **OB**, and the video-frequency signal after demodulation of **OB** would have an amplitude proportional to $|OB|$. Consequently, the amplitude of the phase-detector output is the result of fluctuations of vector **OB** from one transmitter pulse to the next, around its mean value $|OA|$. If we assume that **AB** rotates erratically in time around point *A* (pure noise) or in an almost regular manner (combination of a moving echo with noise) with a maximum amplitude $|AB|$, it will be seen that the peak-to-peak amplitude of the phase-detector output is proportional to $2|AB|$.

If the gain of the receiver is increased gradually, the magnitude of the output increases linearly until it reaches the limiting level *L*. For intermediate values of gain, the vector representing the signal becomes **AB'** or **AB''** and the

peak-to-peak output is then proportional to $2 |AB'|$ or $2 |AB''|$, increasing linearly with gain.

Consequently, so long as the gain of the receiver does not raise the signal above the limiting level L , the ratio of the moving-target echo to the receiver noise at the phase-detector output is constant. Therefore, it may be said that the visibility of a moving echo not superimposed on a fixed echo is independent of the gain of the intermediate-frequency amplifier.

Let us now assume that there is a fixed echo at the distance considered. In the right part of Figure 9, the reference signal is represented by vector OA . Vector AD is the intermediate-frequency fixed echo. Its phase θ is fixed with respect to OA . Vector DB is a variable-phase signal superimposed on the fixed echo.

The vector combination of DB on AD causes a fluctuation in amplitude of $2 |DB|$ and a fluctuation in phase of $2\Delta\theta$ of the resultant vector AB . At the output of the detector, the amplitude fluctuation of OB is observed. It will be seen that when the gain is such that the amplitude of AB is less than the limiting level L , the peak-to-peak amplitude fluctuation at the phase-detector output is proportional to $2 |DB|$. With this in view, it is possible to draw certain conclusions.

A. If DB represents the receiver noise superimposed on an ideal fixed echo represented by AD , then at the output of the detector the noise superimposed on the fixed echo has the same amplitude as the noise appearing at points outside the fixed echo.

B. If DB represents the combination of a moving echo and noise, then at the output of the detector the visibility of the moving echo superimposed on the fixed echo is the same as in the absence of the fixed echo.

C. If DB represents the fluctuations of the fixed echo, then at the detector output, the amplitude of the fluctuation is proportional to the amplitude of the echo at the input of the detector.

Let us now assume that the gain of the intermediate-frequency amplifier is gradually increased so that the amplitude of AB becomes greater than the limiting level L (vectors AB' and AB'' in Figure 9). It will be seen that in the case of AB'' , the fluctuation in amplitude of the signal applied to the detector is zero ($AC = AC'$). The phase fluctuation $2\Delta\theta$ remains constant, irrespective of the gain. At the detector output, the amplitude fluctuation of the echo is proportional to the amplitude fluctuation of the vector OC when point C moves along an arc having A as a center and L as a radius (between C and C' within an angle $2\Delta\theta$).

If the gain is further increased, this fluctuation remains constant. Consequently, when the gain is such that the corresponding amplitude of the fixed echo is higher than the limiting level, certain statements may be made.

A. If the receiver noise is superimposed on an ideal fixed echo, then at the detector output the amplitude of the echo fluctuation due to the noise is definitely smaller than the amplitude of the noise outside the fixed echo.

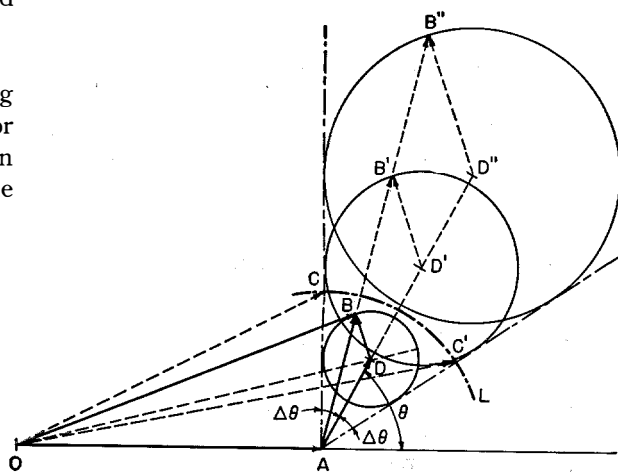
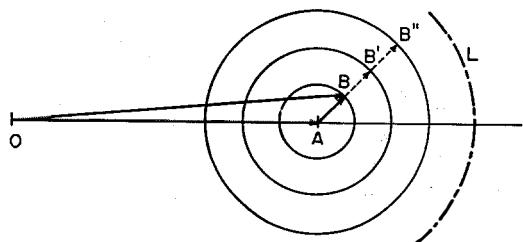


Figure 9—Vector diagrams illustrating the operation of the limiting amplifier and of the phase-detector circuit.

B. If a moving echo is superimposed on an ideal fixed echo, then at the output of the detector the amplitude of the fixed-echo fluctuation due to the moving echo is less than the amplitude of the moving echo when it is away from the fixed echo. When the gain is increased, the amplitude of the fluctuation remains constant while the noise outside of the fixed echo increases.

C. If the fixed echo is not ideally fixed, then the amplitude of the fluctuation of this echo remains constant when the gain is increased, while the noise outside the echo increases.

The fixed-echo-cancellation circuits allow only the fluctuating parts of the video-frequency signals to appear on the indicator. It is possible, by observing the video signals, to effect a correct adjustment of the gain of the intermediate-frequency amplifier. This alignment consists of adjusting the noise level outside of the fixed echoes to the same value as the fixed-echo residues. This is easily effected by observation of the receiver output on a type-*A* oscilloscope.

If the gain is too low, the residues are higher than the rest of the noise and consequently appear on the plan-position indicator. If the gain is too high, the residues are lower than the noise and black spots will appear on the indicator at the location of fixed echoes. Visibility of small moving targets superimposed on the fixed echoes is thus decreased.

At the limit, if the quality of fixed-target-echo elimination is poor (due perhaps to very unstable transmitting and local oscillators), which leads to large residues from the fixed echoes, it is possible to mask the inefficient performance of the radar by considerably increasing the gain of the receiver. The fixed echoes do not then appear on the indicator, the moving echoes outside of the area of fixed echoes are visible, but the visibility of moving echoes superimposed on fixed echoes is markedly deteriorated.

3.3 VISIBILITY FACTOR

The above considerations lead to a definition of the visibility factor. By visibility factor is meant the ratio of the amplitude of a given fixed echo to that of the moving echo that would be just detectable when superimposed on it.

If a moving echo with an amplitude y_0 is superimposed on a fixed echo having a root-mean-

square amplitude R_0 , the maximum amplitude variation of R_0 due to the moving echo from one repetition cycle to the next is

$$y = 2 y_0 \sin \pi f_d T.$$

Taking the arithmetic mean value for all speeds,

$$\bar{y} = \frac{4}{\pi} y_0.$$

Assuming that in order to be visible, the moving echo should have an amplitude equal to 3 times that of the root-mean-square value r_0 of the fluctuation of the fixed echo R_0 , there should be obtained

$$y_0 = \frac{3\pi}{4} r_0 = 2.4 r_0,$$

or 8 decibels. r_0 is the square root of the sum of the squares of the root-mean-square values of the elementary fluctuations due to the effect of the wind, to the rotation of the antenna, and to the instabilities of the radar oscillators.

If the ratio R_0/r_0 has a certain value k , it is possible to derive from it the value of the visibility factor.

$$\frac{R_0}{y_0} = \frac{4}{3\pi} \frac{R_0}{r_0} = \frac{4}{3\pi} k.$$

This means that the visibility factor depends essentially on the characteristics of the radar. The fluctuations of the actual fixed echoes become more important as the number of pulses striking a given target during one revolution of the antenna decreases. This number of pulses is a function of the repetition frequency of the radar, of the horizontal aperture of the beam, and of the speed of rotation of the antenna.

In the case of a repetition frequency of 500 cycles with a beamwidth of 3 degrees and a rotational speed of 3 revolutions per minute, the number of pulses striking the target is 84, corresponding to $R_0/r_0 = 34$ decibels. Under these conditions, provided that perfect operation of the equipment is assumed, the visibility factor would be 26 decibels.

Measurements on actual targets are difficult to perform, but some were made at Trappes, France. For the echo from the Eiffel tower at a distance of 30 kilometers (19 land miles), the results varied between 20 and 24 decibels. The visibility factor of the receiver alone using artificial fixed and moving echoes is more than 30 decibels.

If the beamwidth were 0.8 degree and the speed of rotation 6 revolutions per minute, the number of pulses striking a target would be 11, and theoretical considerations then show that the visibility factor would drop to 12 decibels maximum.

3.4 OTHER EXPERIMENTAL RESULTS

Numerous observations showed that with fixed-echo elimination it is possible to follow aircraft in as close as 2 kilometers (6500 feet) from the radar. This performance stands out extremely favorably when compared to that of an ordinary radar where aircraft are invisible as soon as they enter the area of dense ground clutter existing out to ranges of 10 to 15 kilometers (6 to 9 land miles).

When the gain of the coherent receiver is adjusted to give maximum sensitivity for moving echoes superimposed on fixed echoes, examination of the indicator shows that out to 5 kilometers (3 land miles), luminous dots that are obviously not aircraft appear. Careful inspection and photographs taken after several revolutions of the antenna show that some of these dots are moving. Also, inspection of the output of the phase detector makes it possible to identify extraneous echoes of two categories.

A. Echoes having the shape of Doppler beats with well-defined frequencies. It seems reasonable to assume that these are echoes from moving objects on the ground, as automobiles or bicycles, or from birds.

B. Echoes having the shape of Doppler beats with erratic frequencies. These might correspond to falling leaves or smoke.

It is not intended to imply that all of these extraneous echoes—which are not echoes from aircraft and which might be identified by in-

experienced operators as fixed-echo residues—can be classified in the above groups. Their study is difficult since they are fugitive and their identification requires long patient work.

Experience shows, however, that a skilled operator who follows an aircraft echo from one revolution of the antenna to the next, cannot confuse that echo with echoes from indiscriminate moving targets since the aircraft echo is substantially larger.

Moreover, it is possible at a site sufficiently clear of large fixed targets (such as an airport) to cut down the sensitivity of the radar so as to cause the disappearance of these indiscriminate moving echoes while not causing any considerable loss in sensitivity to aircraft echoes. Aircraft may then be tracked to the immediate vicinity of the radar.

3. Acknowledgments

The author acknowledges his debt to the French governmental agencies that have made the present development possible, and especially to the Service Technique des Télécommunications de l'Air, the Centre National d'Etudes des Télécommunications, and the Direction Centrale des Constructions et Armes Navales. Thanks are also due to Compagnie Générale de Télégraphie Sans Fil, with whom the development of the radar was carried out in a spirit of friendly cooperation.

The various studies concerning the elimination of fixed-target echoes were done in Lyons during the German occupation and in Paris after the war under the technical direction of Mr. G. Lehmann. His invaluable assistance is gratefully acknowledged. Space limitations prevent mentioning here the names of all of the engineers, technicians, and draftsmen of Laboratoire Central de Télécommunications whose team work made this development possible.

Electric Servomechanisms*

By G. J. LEHMANN

Laboratoire Central de Télécommunications and Société des Servomécanismes Electroniques; Paris, France

ELECTRIC servomechanisms intended for the automatic aiming of weapons will be the subject of this paper. This is a field in which a large number of servomechanisms have been designed and built in a great many variations. Most of them are used to impart to a weapon (naval or anti-aircraft gun, radar antenna, submarine microphone, et cetera) predetermined angular motions. They are usually position-control devices and they must always offer an extreme precision. Their high accuracy is frequently the very reason for their use.

These military instruments are generally representative of present techniques in the field of electric servomechanisms; the studies leading to their development have formed the basis of most of the literature in the field of servomechanisms for the last ten years.

1. Electric Motors for Servomechanisms

Special requirements are imposed on the motors because of the nature of their functions—the control of weapon-aiming motions.

This service is characterized by low permanent torques and violent transient torques of short duration. The speeds of rotation are low on the average, with high speeds during short but infrequent periods. The permanent torques are due to frictional stresses in the aiming and pivoting mechanisms, but these torques are always low, due to the high quality of mechanical construction required to permit precision aiming.

Other quasi-permanent torques exist in naval and tank weapons due to unbalances of the rotating masses during tilting of the platform (ship rolling at sea or tank moving on a slope). Generally speaking, these torques are low when compared to those due to the inertia of the weapons during periods of acceleration or to those due to the effect of firing.

A mitigating factor is that the acceleration

stresses do not last for long, the maximum speed being limited; they are at a maximum during a search period or when changing the target. Similarly, stresses due to firing are never continued for a very long time, due to the necessity of allowing the weapon to cool.

The situation is similar as regards speeds; in normal operation the aiming speeds are low and high speeds are required only during search periods or target changes.

It appears from the above remarks that the average power supplied by a weapon servomotor is low in general, but that transient high powers are required at intervals. For example, the maximum output of a motor is seldom required for a duration exceeding one second, followed by a long period of very low output.

These conditions result in a fundamental difference between the operating requirements of weapon servocontrol motors and those of industrial motors. In the latter, the power is limited by the losses resulting in a temperature rise that must not exceed the value that is dangerous to the insulating materials used in the construction of the motor. Heating is not the limiting factor in servomotors, since the amount of heat evolved during short periods of full output is stored by the thermal inertia of the motor with no great temperature rise and is then dissipated during the long low-output periods.

This mode of operation, with no restrictive effect due to heating, is comparable to that found in pulse-type radar transmitters. Just as the development of radars using pulses modified the construction technique of transmitter tubes by making possible the generation of enormous peak powers using very small tubes, the pulse-type operation of motors for servomechanisms very substantially modified the conditions of use and the performance obtainable from electric machines and motors.

Heating no longer being a limitation to the power generated by an electric machine, it then becomes interesting to examine the other fundamental phenomena that now limit the

* Reprinted from *Mécanique Industrielle*, number 1, pages 28-36; January, 1954. Presented on June 8, 1953 at the Institut Supérieur des Matériaux et de la Construction Mécanique; Paris, France. Section 4 and Figure 3 did not appear in the original publication of the paper.

momentary peak powers obtainable. This question has been the subject of an interesting analysis¹ by G. Darrieus; a brief account of his discussion follows.

Heating due to losses being disregarded, the power of an electric machine is subject to a limitation of fundamental nature due to the use of ferromagnetic materials for carrying the magnetic fields that are the source of the mechanical forces generated by such machines. The limitation is due to saturation, which limits inexorably to about 18 000 gausses the magnetic fields obtainable at present regardless of the exact type of metal or machine.

Let us evaluate the maximum power obtainable taking this limitation into account. Any rotary electric machine consists of one fixed and one moving part, each of them incorporating a magnetically permeable metallic ring. These two rings, stator and rotor, are separated by a cylindrical air gap as shown in Figure 1.

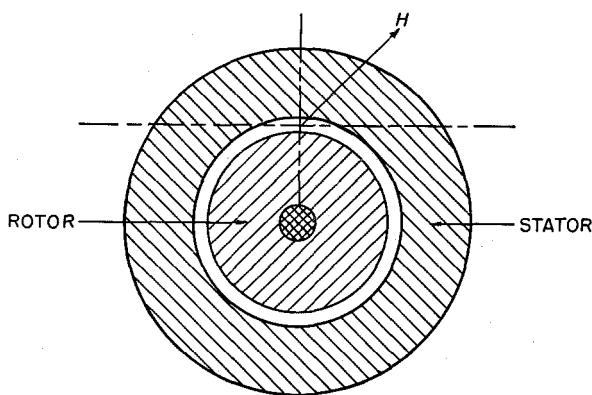


Figure 1—Construction of a rotary electric machine.

In the free space constituting the air gap, there is a magnetic field that is the origin of the mechanical stress exerted between rotor and stator and consequently of the effective torque of the machine. The laws that relate a magnetic-field intensity to the stress exerted on the surface limiting this field are well known. They show the existence of stress proportional to the area normal to the field; the relevant equation is

$$P ds = \frac{H^2}{8\pi} ds,$$

where P has the dimensions of a pressure and is

¹G. Darrieus, "La Mécanique et l'Electrotechnique," *Memoires de la Société des Ingénieurs Civils de France*, number 1, page 1; 1952.

known as Maxwell's tension, ds is an area element normal to the field, and H is the magnetic-field intensity. Two statements may now be made.

A. If the field exists in an annular air gap limited by two parallel surfaces (as is the case in rotary machines), the *tangential* stress that is exerted between the two surfaces is maximum when the field in the air gap makes a 45-degree angle with the perpendicular to the air gap.

B. The maximum value of the field is limited by saturation effects in the iron.

Introducing the maximum value of the field (18 000 gausses) in the above expression for Maxwell's tension gives for the latter a value of 12 kilograms per square centimeter (172 pounds per square inch). This maximum-possible pull is normal to the direction of the field.

From this value, simple calculations give the maximum value of the tangential stress exerted by the field on each square centimeter of the periphery of the air gap; this is 6 kilograms per square centimeter (86 pounds per square inch) of air gap as a maximum tangential stress corresponding to a field inclined at 45 degrees.

In an actual machine, the magnetic field cannot be constant all along the air gap since the total flux going through the gap should be zero. In fact, the field intensity in all machines has a sinusoidal distribution along the periphery and the mean square of the field must be taken for H^2 , which leads to dividing the above result by 2; hence the mean value of the tangential stress for the whole rotor is 3 kilograms per square centimeter (43 pounds per square inch) of air gap. Thus the presence of iron limits to this figure the mean tangential stress to which the rotor is subject at the periphery of the air gap.

It can be shown easily that this stress requires the existence of a surface current density of 5000 amperes per centimeter (12 500 amperes per inch) of rotor circumference. The construction of machines meeting these values requires special precautions that are beyond the scope of the present discussion. The resistivity of copper makes it impossible to approach this current requirement for small machines a few centimeters or tens of centimeters in diameter; however, it is at present approached in large machines where the rotor diameter reaches 1 meter (3.28 feet).

Table 1 shows a few characteristic values for an electric motor and a hydraulic motor, the powers of which are nearly the same; both are commonly used in servocontrols for weapons. For this particular electric motor are shown the theoretical limiting values calculated as indicated above and the values obtained in an actual motor.

In most actual cases, such rapid rates of acceleration cannot be used advantageously and it is preferable to design instead for mechanical sturdiness of the motor and economy in its manufacture. Is it necessary, or even mechanically possible, to accelerate a weapon to its full speed in 0.05 second? Is it feasible in practice to

TABLE I
SERVOCONTROL MOTORS

Characteristic	Servodyne MU7X-130 Electric Motor		Vickers Hydraulic Motor
	Theoretical Maximum Value	Actual Value	
Maximum Torque C in Centimeters \times Dynes	7.8×10^9	5×10^8	5×10^8
Moment of Inertia I in Centimeter-Gram-Second Units	187 000	187 000	16 600
C/I in Radians per Second per Second	40 000	2 670	30 000
Acceleration Time in Seconds from 0 to 2500 Revolutions per Minute	0.006	0.093	0.0082
Peak Power in Kilowatts	230 at 3000 revolutions per minute	15 at 3000 revolutions per minute	10.5 at 2500 revolutions per minute
Weight in Kilograms	40	40	21
Weight in Kilograms per Peak Kilowatt	0.17	2.7	2
Steady-State Power in Kilowatts	—	2.75	10.5

The electric motor chosen as an example in Table 1 is of the same type as that shown in operation before the Société des Radioélectriciens and described in a recent paper².

Certain conclusions may be derived from Table 1.

A. The weight of the actual electric motor is close to that of the hydraulic motor having the same power. However, weight comparisons can be useful only if they bear on a servocontrol assembly, taking into account the possibility of moving the electric motor away from its associated amplifier.

B. Whereas the acceleration times of the hydraulic motor and theoretical electric motor are close to each other, the acceleration time of the actual electric motor is 15 times longer.

However, in practical use this is no drawback. Electric motors of the so-called low-inertia type may be built having shorter acceleration times; for instance, 0.02 second instead of 0.1 or 0.15 second.

²G. J. Lehmann, "Les Dynamos Amplificatrices, leur emploi dans les Servomécanismes," *L'Onde Electrique*, volume 32, pages 78-88; March 1952; also, *Bulletin de la Société Française des Electriciens*, volume 2, pages 198-209; April, 1952; also (in English), *Electrical Communication*, volume 30, pages 12-25; March, 1953.

utilize the full capability of the hydraulic motor of accelerating in 0.008 second, taking into account the limitations imposed by oil and pumps?

Simple and sturdy motors should be preferred; a motor must be selected that does not limit the accuracy and acceleration demanded of the entire equipment.

1.1 CHOICE OF ELECTRIC MOTOR

Two conflicting conditions must be recognized in selecting a motor.

A. High rotational speed permits minimum weight per kilowatt rating.

B. Low rotational speed permits a short acceleration time.

How can the optimum compromise be found? In general, in a problem of this type the following data are available.

J = moment of inertia of the weapon

Ω = maximum rotational speed

τ = total acceleration time desired.

From these data, the maximum peak power is

$$W = J\Omega^2/\tau.$$

It will be shown that the most favorable

electric motor is the one that fulfills the following requirements.

- A. Capable of delivering the required peak power.
- B. Has a moment of inertia equal to that of the weapon (referred to the same axis of rotation).

This double condition determines the size of the motor, its maximum speed, and the value of the reduction-gear ratio.

For lightness and economy, the motor should be of small size and rotate rapidly. A limitation in this respect is the acceleration time required by the combination of the motor, reduction gear, and inert load.

Assume for the motor that

- I = moment of inertia
- C = peak torque
- N = reduction-gear ratio.

The fundamental equation of the motor-gun system, referred to the rotating shaft of the load may be written

$$(N^2I + J) (d\Omega/dt) = NC, \quad (1)$$

this equation expressing the equality between the inertia torque of the assembly and the driving torque.

The torque C being assumed constant, the system must accelerate uniformly from rest to a speed Ω in a time τ and the above equation may be written

$$\frac{\Omega}{\tau} = \frac{NC}{N^2I + J}. \quad (2)$$

Let us assume that for the different motors of a given type the ratio C/I has a constant value

$$\frac{NI}{N^2I + J} = A. \quad (3)$$

A is a constant depending only on Ω , τ , and the ratio C/I characterizing the type of motor considered. The gear ratio N should be chosen to correspond to the minimum values for I and C , hence to accommodate the smallest motor suited to the problem.

In (3), I is made minimum by letting

$$N^2I = J, \quad (4)$$

which means that the gear ratio and the weight of the motor are so chosen that the moment of

inertia of the later, referred to the axis of the load, is equal to the moment of inertia of the load.

Thus the motor selected is the lightest one meeting the desired conditions.

Under such conditions, the acceleration of the motor will be half of its unloaded acceleration. With the motors illustrated in Table 1, the zero-load acceleration is 450 revolutions per second per second; under load the acceleration of motors of this class would reach 225 revolutions per second per second.

By limiting the speed of the motor to 50 revolutions per second (3000 revolutions per minute), the weapon will be accelerated to its full speed in

$$50/225 = 0.22 \text{ second.}$$

Few weapons are mechanically capable of withstanding such a rapid start. Experience shows that with such motors, the gearing must be reinforced to prevent breakdown.

In the same manner, to use to best advantage a hydraulic motor that could accelerate a weapon in 0.2 second, the motor would have to rotate at a maximum speed of 500 revolutions per second, or 30 000 revolutions per minute, which is impossible. This clearly illustrates the fact that the present acceleration time of electric motors is perfectly suited to the control of weapons, without risking other characteristics in designing especially for acceleration.

Along this same line of thinking, it may be recalled that 10 000-horsepower motors capable under load of accelerating from zero to their nominal speed in 0.5 second are used in reversible hot-rolling mills.

2. Output Amplifiers for Electric Servomechanisms

Rotary amplifiers and gas tubes (particularly thyratrons) are widely used at the present time for driving servomotors. It may be predicted that magnetic amplifiers, already used for low powers, will be extended to this field of operation.

The control device for the motor—the output stage of the amplifier—should possess two qualities that are fundamental to the accuracy of the servomechanism.

- A. It must amplify correctly currents of progressively higher frequencies as the desired accuracy is increased.

B. It should have a perfectly continuous relation between its output amplitude and input amplitude.

Any discontinuity in the characteristic mentioned in B destroys the obtainable accuracy; particularly, jolts will appear in the motion of the motor and the stabilization of the servomechanism will be very difficult.

The main two-fold advantages of the currently available electric systems are as follows:

A. The cutoff frequency of the amplifier is high.

B. The mathematical continuity of the electric amplifiers, which do not show any effect comparable with backlash or friction. This is a considerable advantage in comparison with hydraulic amplifiers that often have a 1-percent area of zero sensitivity.

2.1 ROTARY AMPLIFIERS

The main characteristics of rotary amplifiers have been discussed previously,² but will be reviewed briefly.

Use of these machines is practical up to frequencies of 15 to 30 cycles per second; at the latter frequency they can still give their full output with an amplification factor of 10. Their use is quite general for the control of weapons. The cutoff frequency of the servomechanism (the frequency at which the gain with the main loop open falls to unity) varies from 4 to 12 cycles per second.

The performance of rotary amplifiers is in accordance with the fundamental considerations pointed out in connection with servomotors; rotary amplifiers can also generate short-duration powers of from 5 to 10 times their nominal steady-state ratings and they therefore lend themselves particularly well to the control of

TABLE 2
ROTARY AMPLIFIERS

Characteristic	Type DU7X-130	Type RR-334
Steady-State Power in Kilowatts	3	10
Peak Power in Kilowatts	20	70
Weight in Kilograms	40	200
Weight in Kilograms per Peak Kilowatt	2	2.85

direct-current servomechanism motors. Table 2 indicates the main characteristics of two types of rotary amplifiers.

With the machines mentioned in this table, the output voltage of the generator can rise from 0 to its maximum value in 0.03 second.

2.2 THYRATRON AMPLIFIERS

In application to precision-type servomechanisms, thyatron amplifiers should be designed to enable the direction of rotation of the motor to be reversed in addition to controlling its torque. This leads to more-complicated circuits than if only speed variations are required.

Nevertheless, the absence of any mechanical or magnetic inertia gives thyatrons extreme rapidity of response, especially if they are energized by a high-frequency current (400 cycles per second, for instance). When power is supplied from industrial 50-cycle mains, thyatrons make it possible to obtain cutoff frequencies similar to those of good rotary amplifiers, with the advantage, however, of simpler correcting networks. A description of equipment of this type has been published.³ The preferred field of use is in the range of peak-power values of 50 watts to 20 kilowatts.

When energized at 400 cycles, thyatron amplifiers can transmit frequencies up to 100 cycles with high uniformity, thus allowing the construction of servomechanisms having very high accuracy.

As a consequence of the advances made recently in the technique of magnetic amplifiers, they tend more and more to compete with thyatron devices.

3. Considerations Concerning Servomechanisms—Comparison of Systems

From a purely practical standpoint, electric devices have several advantageous characteristics, among which the following may be stressed particularly.

A. It is possible to separate completely the amplifier from the motor; connection is by electric

³ R. Aubry, H. Le Boiteux, and G. J. Lehmann, "Etude et Réalisation d'une Télécommande Electronique d'Artillerie," *L'Onde Electrique*, volume 29, pages 311-328; August/September, 1949.

conductors. Rotary slip-ring-and-brush-type contacts allow the installation of a motor on a rotating frame (movable turret), the amplifier being mounted on a fixed part of the weapon or even installed at a distance from it. Due to this, the rotary amplifier may be driven by direct coupling to a thermal motor, possibly a single motor for an entire battery of guns.

On the other hand, it is generally necessary to place the pump and motor of hydraulic systems as near together as possible.

Figure 2 shows that an electrical installation may be limited to three machines; thermal motor, rotary amplifier, and servomotor. The corresponding hydraulic installation generally consists

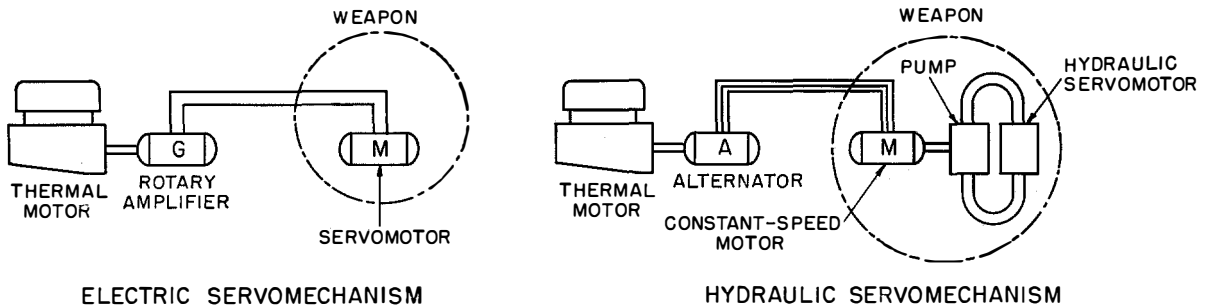


Figure 2—The electric servomechanism consists of a thermal motor, rotary amplifier, and servomotor driving the weapon. The hydraulic servomechanism includes a thermal motor, alternator, constant-speed motor, pump, and hydraulic servomotor driving the weapon.

of five machines; thermal motor, alternator, electric motor, pump, and hydraulic motor; the three latter units are mounted on the movable turret.

B. The effects of temperature variations are negligible on electric systems, which can operate without any adjustment between -40 and $+70$ degrees centigrade.

C. The maintenance of electric systems is a minor matter concerning mainly brushes that must be checked and replaced at infrequent intervals.

D. The stability of electric systems with time is excellent. Service for years is possible without any change in characteristics and performance.

3.2 ACCURACY

As already mentioned, accuracy depends mainly on the

A. Cutoff frequency.

B. Linearity of the characteristic.

Consider for example the problem of fire control for naval anti-aircraft weapons, one of the most difficult applications due to the required accuracy of 0.001 radian or 3 minutes of angle despite the roll of the ship carrying the weapon.

A few facts presented in a previous paper⁴ should be recalled. For a typical rolling motion

$$\alpha = \alpha_0 \cos \omega t$$

with $\omega = 1$ radian per second and $\alpha_0 = 20$ degrees. Now the maximum dynamic angular

error tolerated in the presence of this rolling is 3 minutes.

It will be found that the gain of the open loop at an angular frequency $\omega = 1$ radian per second should be equal to or greater than 400; in practice, the gains used are of the order of 800 to 1000, leading to errors of the order of 1.5 minutes of angle as shown by the recordings illustrating the above-mentioned paper.

The main loop of the servomechanism should satisfy the relationship

$$G = (\omega_c/\omega)^2,$$

where G = gain along the loop, ω = angular frequency, and ω_c = angular cutoff frequency.

It is seen that if $G = 900$ for $\omega = 1$, then $\omega_c = 30$, or system cutoff frequency $F_c = 4.8$ cycles per second.

In practice, the joint considerations of accuracy and stability lead to adopting an actual cutoff frequency of $F_c = 8$ cycles per second for the equipment studied, which is representative

of the problems frequently encountered in this field.

The above example shows that, in general, between the acceptable error ϵ of a servomechanism and its angular cutoff frequency ω_c , there is a relation

$$\epsilon = K/\omega_c^2.$$

Thus if the cutoff frequency of a hydraulic servomechanism is limited to about 4 cycles, electric systems reaching cutoff frequencies of 8 to 10 cycles have an accuracy that is from 4 to 6 times better.

What are the reasons for such differences? Electric amplifiers can be built to reproduce very exactly the analytic relations on which their dynamic operations are based.

In hydraulic amplifiers, parasitic phenomena inevitably complicate the situation; the main problems involve backlash and friction in the controlling elements for the oil circuit, particularly the valves and mechanisms of variable-flow pumps—there exists a dilemma between backlash and friction that has no counterpart in electric amplifiers. The unavoidable backlashes and frictions that depend also on wear and on temperature variations combine to deteriorate the response of hydraulic systems at very low speeds and during changes in speed.

To avoid any misunderstanding, it should be emphasized here that this discussion does not include backlash and friction in the gearing chain connecting the servomotor to the weapon; this chain has its own defects, whether the servomotor is hydraulic or electric. Consideration is limited here to the mechanical defects of the oil-controlling mechanism, which are without any equivalent counterpart in electric systems; this difference is very important.

In addition, the mass inertia of the oil-controlling mechanism also has no electrical counterpart and increases the difficulties experienced with hydraulic systems. There must be added to it the effects of elasticity of oil and pipes, of wear, and of temperature variations.

The ease with which electric systems can satisfy high-precision requirements was shown by experimental servomechanisms built at the Laboratoire Central de Télécommunications; by driving a direct-current servomotor by thyristors operating at 200 cycles per second, cutoff

frequencies higher than 40 cycles were obtained, ensuring an accuracy 100 times higher than that of a system with a cutoff frequency limited to 4 cycles.

In such servomechanisms, the accuracy obtainable reaches a few seconds of angle; the angular position of the shaft of the servomotor is fixed by the servomechanism with a rigidity almost as if it were welded in place. Even large torques exerted on the motor shaft can rotate this shaft only by very small angles.

Such accurate servomechanisms cannot economically be used for the control of conventional weapons due to mechanical defects in gun carriages and turrets (gear backlash and lack of rigidity in the various elements). In fact, an electric remote-control system with a cutoff frequency of 40 cycles has dynamic errors smaller than those of a high-quality gearing since it is devoid of elastic flexures in shafts and of backlash in gears transmitting stress.

The construction in the laboratory of servomechanisms giving only very small errors compared to errors from external causes has an important consequence; it proves that by the use of a suitable electrical technique, difficulties of a theoretical nature can be entirely overcome with a large safety coefficient.

There is no longer any dynamic difficulty inherent to electric servomechanisms. Difficulties still do exist in the construction of precision mechanical equipments and a technological and economic problem has to be solved with each new application—that of choosing the safest and least-costly solution. This problem cannot be solved entirely by calculation.

4. Application

An electrically controlled antiaircraft gun, described⁴ in *Interavia*, was built by Hispano Suiza Company in Geneva and is shown in Figure 3. It employs two 34-millimeter barrels, each 74 calibers long. The elevating speed is 50 degrees per second and the traversing speed is 100 degrees per second. The weight in travelling position is 3800 kilograms (8000 pounds). Firing rate is 500 shots per minute per barrel at a muzzle velocity of 1000 meters (3200 feet) per second.

Elevating and traversing movements are by two electric motors controlled by a computer

⁴ "New Look in Weapons Planning, Part 8," *Interavia*, volume 9, number 8, pages 542-543; 1954.

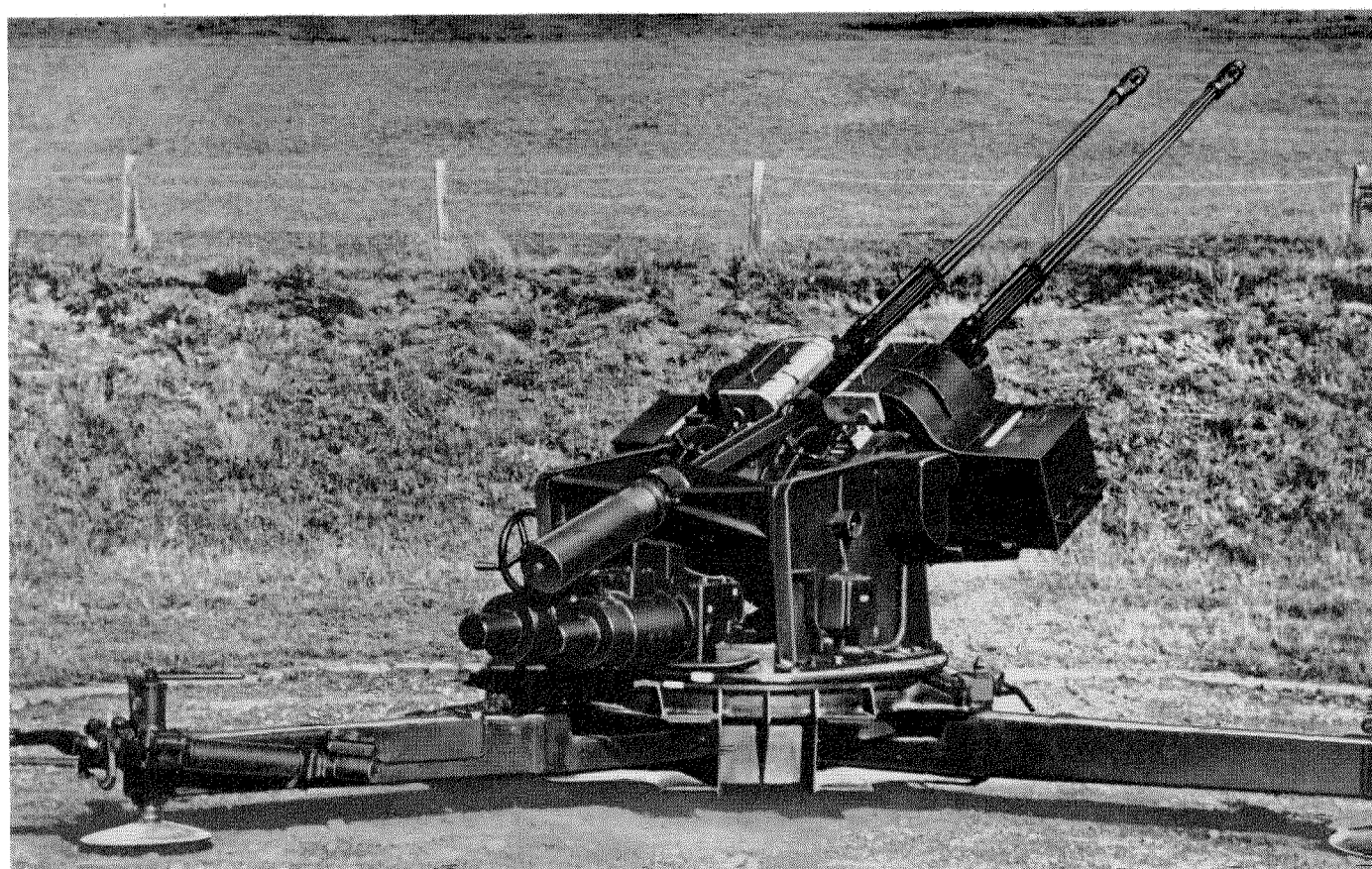


Figure 3—Firing position of an electrically controlled twin-barrelled anti-aircraft gun. The motors for elevating and traversing are clearly discernible. Photograph courtesy of *Interavia*.

through electronic and short-time-constant rotary amplifiers. The relatively small weight of the gun, despite its high firing power, flexibility, and accuracy of laying, is in part attributable to mechanical simplifications resulting from electrical control.

The electrical control was developed by the Swiss army in cooperation with Standard Telephone et Radio S. A. in Zurich and the servomechanism was built by Société des Servomécanismes Electroniques in Paris.

5. Conclusions

Following the technological advances effected during the last twenty years in electric systems, we are now witnessing a large extension of the use of electric servomechanisms.

Nearly all automatic controls for radar antennas and for naval weapons are electrical.

Guns of ground anti-aircraft artillery increasingly use electric servomechanisms, particularly because of their capability of giving the weapons motions that are slow, accurate, very uniform, and free of jolts. This evolution in ground artillery has been speeded up by the ease of installation of servomechanisms having elements that

can be remote from one another without damage to operation.

Tank turrets, traditionally turned by hydraulic systems, are also adopting electric systems in the latest models, affording new possibilities, particularly as regards stabilization to permit firing while moving; this is the case for the American *M-48* and the British Centurion tanks.

The most accurate servomechanisms are often also the most powerful: this is the case of the automatic electric controls for modern continuous-rolling mills using rotary amplifiers or mercury-vapor rectifiers with direct-current motors; they involve powers of thousands of kilowatts and precisions that are sometimes higher than those required for aiming weapons.

Finally, electric regulators having a still higher accuracy fulfill essential functions in a large number of installations for nuclear-physics research.

It is clearly evident that the union of mechanics and electricity grows closer day by day and will continue to do so unless other methods are developed that perform the required tasks more effectively.

Concerning the Minimum Number of Resonators and the Minimum Unloaded-Resonator Q Needed in a Filter*

By MILTON DISHAL

Federal Telecommunication Laboratories, a division of International Telephone and Telegraph Corporation; Nutley, New Jersey

GIVEN a selective-circuit or filter specification, two important questions that arise are: what is the minimum number of elements that can be used to satisfy the specification and what is the minimum unloaded Q that these elements must have?

These questions are answered by means of three pairs of design equations, (6) and (11), (7) and (12), and (8) and (13) for filter networks supplying only attenuation zeros (that is, filters equivalent to the constant- K type) and the corresponding three pairs of equations, (22) and (32), (23) and (33), and (24) and (34), for filters supplying both attenuation zeros and attenuation poles (that is, filters equivalent to the m -derived type).

• • •

1. Introduction

Because simple classical image-parameter filter theory does not provide accurate information, this paper is written to supply the engineer with some of the detailed mathematics that will enable him to deal more accurately with filter problems. The following example illustrates the type of problem to be considered. Suppose selective circuits for a receiver are required that will produce a 6-decibel-down "accept bandwidth" that is no less than some number of cycles per second that will be called BW_a ; and a 100-decibel-down "reject bandwidth" no greater than some number of cycles that will be called BW_r . Inside the 6-decibel-down points, that is, the accept band, ripples with a peak-to-valley ratio as large as some number V_p/V_v are allowable; and outside the 100-decibel-down points, that is, in the reject band, any type of response

is allowable so long as the attenuation is never less than 100 decibels over a frequency range of at least 10 reject bandwidths. Figure 1 illustrates the problem. Symbols are defined in section 5.

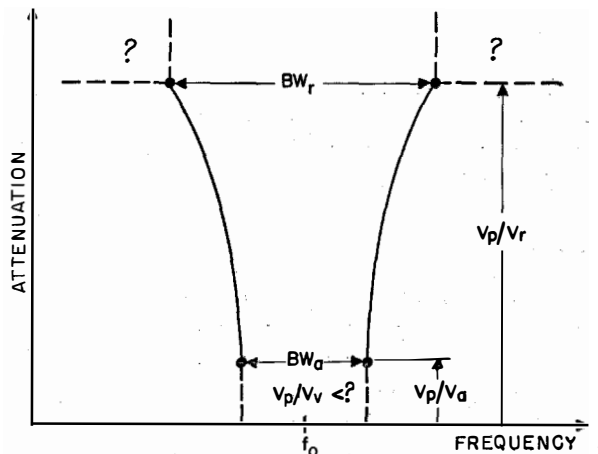


Figure 1—The band-pass-selectivity specification considered in this paper. The question marks outside the reject bandwidth indicate that in general the shape in this region may be of any form so long as the minimum attenuation is always greater than V_p/V_v for a frequency range at least 10, say, reject bandwidths wide.

As is usually the case, there are size, weight, economic, and other limitations that make it mandatory that the engineer satisfy the selectivity specification with as few resonators as possible, and furthermore the resonators must have unloaded Q 's that most certainly are not infinite. This paper will deal in detail with just two parts of the over-all problem, that of the exact number of elements required and the lowest unloaded Q 's that the resonators may have.

For the sake of brevity, only band-pass filters producing symmetrical response shapes will be considered, but the reader should realize that the discussion applies equally well to low-pass circuits when the analogous frequency variables and circuit constants are used. Also, only node-type circuits will be shown in the figures; the

* Presented before Institute of Radio Engineers Professional Group on Vehicular Communication in Washington, District of Columbia, on December 3, 1952. Reprinted from *Transactions of the IRE Professional Group on Vehicular Communication*, volume PGVC-3, pages 85-117; June, 1953. Section 4.3 and Figure 11 did not appear in the original publication of the paper.

reader should realize that the discussion applies equally to the corresponding mesh circuits, which can be obtained simply from the node circuits by the principle of duality.

quired, it is almost mandatory to use the coupled-resonant-circuit configuration, because then the element values required for the inverse-arm configuration become physically impracticable.

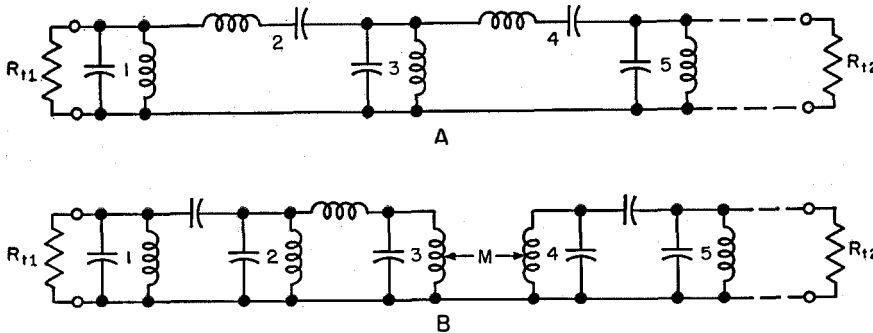


Figure 2—The basic inverse-arm or constant- K configuration and its small-percentage-bandwidth node-network equivalent. The correct element values are not the same as those obtained from classical filter theory; only the configuration is the same. All discussions apply of course to the dual mesh networks, which are not shown.

With respect to the relation between the number of *arms* n in the basic inverse-arm ladder of Figure 2A and the number of *physical resonators* that must be supplied, simple examination of Figure 2 shows that the number of resonators required is identically equal to n for the networks of both Figure 2A and 2B.

1.1 CIRCUITS THAT ARE USED

To meet a given selectivity requirement, the first step is usually that of deciding what network configuration should be used. In most practical situations, a ladder-type network will be used. For the last three decades, it has been realized that the basic ladder-type *configurations* are those described by the words "constant K " and " m derived." The former is an inverse-arm configuration and the latter is one in which either, but not both, of the arms is modified to produce infinite attenuation at finite frequencies near the edges of the reject band rather than at frequencies infinitely far from the edges of the reject band.

It is important to note that when the percentage bandwidth required is small, then by the use of simple straightforward equivalences, the configuration of the basic inverse-arm band-pass ladder of Figure 2A can be transformed into a chain of coupled resonant circuits as shown in Figure 2B wherein any or all of the well-known methods of coupling two resonators can be used; that is mutual inductance, high-side capacitance, low-side capacitance, low-side inductance, et cetera. The number of resonators that must be used is exactly the same as the number of resonators appearing in the inverse-arm configuration. When small-percentage bandwidths are re-

quired, the configuration of the basic m -derived band-pass ladder, Figure 3A, can be transformed to the three configurations shown in Figure 3B, 3C, and 3D, which require more easily obtainable element values. It should be realized that all the resonant circuits shown in Figure 3 are true resonators, tuned either to the midband frequency or to one of the frequencies of infinite rejection.¹ Thus, the number of resonators that must be physically constructed includes every one of the resonators shown in that circuit of Figure 3 that is to be used.

With respect to the relation between the number of *arms* n in the basic m -derived-configuration ladder of Figure 3A and the number of *physical resonators* that must be supplied, simple examination of Figure 3 shows that for circuits A, B, and C,

$$\begin{aligned} \text{Number of resonators} &= n + \frac{n-1}{2} \text{ for } n \text{ odd,} \\ &= n + \frac{n}{2} \text{ for } n \text{ even,} \end{aligned}$$

and for circuit D,

$$\begin{aligned} \text{Number of resonators} &= 2n - 1 \text{ for } n \text{ odd,} \\ &= 2n \text{ for } n \text{ even.} \end{aligned}$$

¹ In Figures 3A, 3C, and 3D, the inductance of the null-producing resonators (a , b , et cetera) can be supplied by using magnetic coupling between the two resonators to which this inductor is connected. The proper value of coupling coefficient is so large however (0.2 and up) that it seems proper to call these circuits (a , b , et cetera) true resonators even if their inductances are supplied by magnetic coupling.

1.2 ELECTRICAL, MECHANICAL, AND QUARTZ-CRYSTAL RESONATORS

In recent years, there has been an increasing use of mechanical resonators (made of Ni-Span C alloy) in filters.

For small-percentage bandwidths (10 percent or less), it is important to realize that insofar as filtering is concerned, there is no fundamental difference whatsoever between a mechanical resonator and an electrical resonator; the unloaded Q of each resonator, the loaded Q of the end resonators, and the coefficient of coupling between adjacent resonators has exactly the same meaning for both mechanical and electrical filters.

As soon as a required rate of cutoff BW_r/BW_a and ripple in the pass band V_p/V_v is specified, two filter constants are immediately fixed; first,

the minimum required number of resonators and, second, the highest allowable ratio of fractional midfrequency f_0/BW_a to unloaded-resonator Q (Q_0) that can be used. Therefore, the high unloaded Q that is available when mechanical resonators are used is advantageous because it enables a required rate of cutoff BW_r/BW_a and an allowable V_p/V_v to be obtained at a *higher midfrequency* than do lower- Q elements.

Conversely, when the designer may choose the midfrequency, high unloaded Q 's do not, as is so-often implied, enable better rates of cutoff to be obtained; with both high or low unloaded Q 's, exactly the same number of resonators will be required to satisfy a specified BW_r/BW_a and V_p/V_v . To satisfy the maximum allowable $(f_0/BW_a)/Q_0$ ratio, it is simply necessary to use a

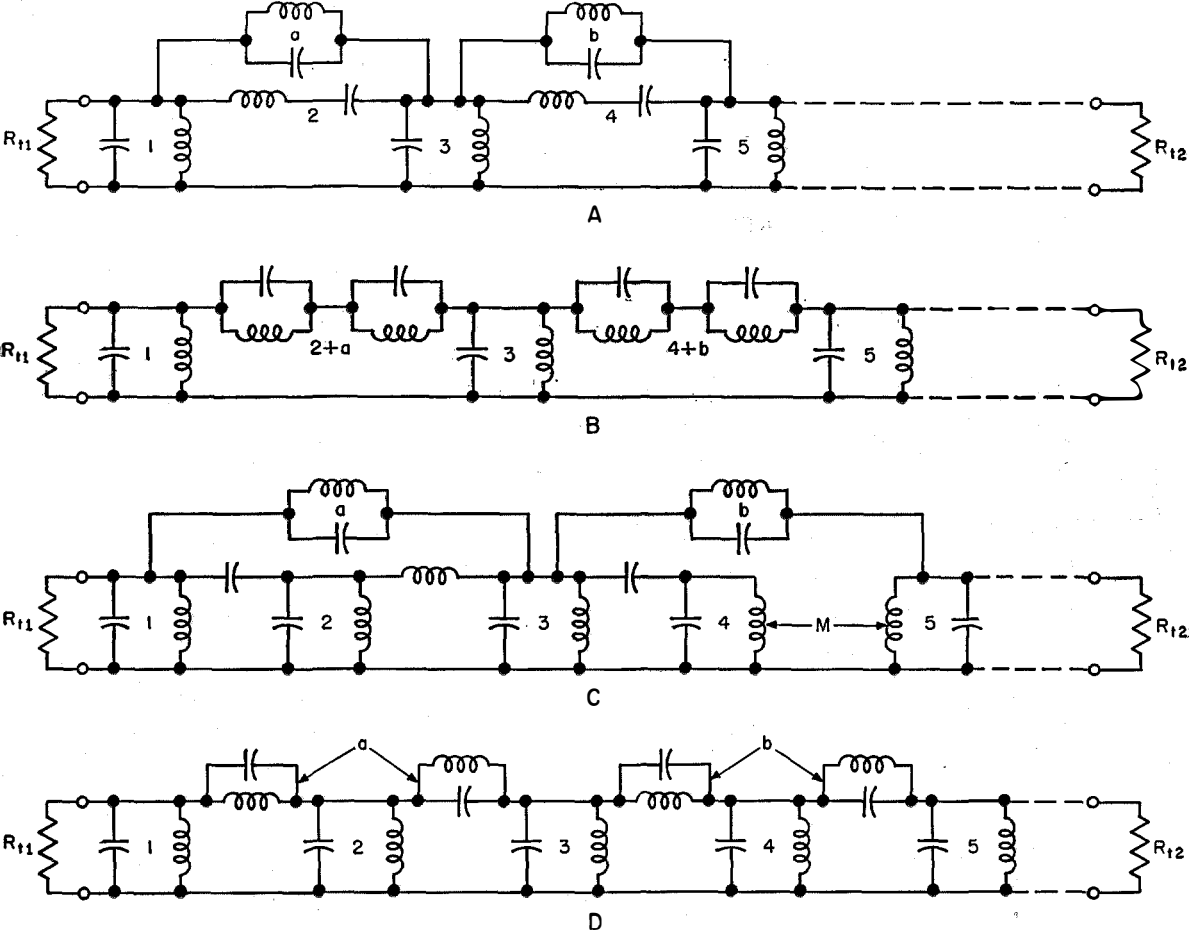


Figure 3—The basic m -derived configuration and its node-type equivalents. The correct values of the elements are not the same as those obtained from classical filter theory; only the configuration is the same. All discussions apply, of course, to the dual mesh networks, which are not shown.

lower midfrequency with the lower Q_0 resonators. And there are many practical situations wherein the designer does have some freedom to choose the midfrequency, for example, the intermediate frequencies in superheterodyne receivers or, in general, in the many cases where it is permissible to develop a required selectivity at one midfrequency and then make this selectivity appear at a higher midfrequency by the use of a local oscillator and mixer tube. It is of course understood that whenever frequency conversion is used, the accompanying problems of spurious responses, cross modulation, intermodulation, and desensitization must always be considered.

To stress the similarity between mechanical-resonator filters and electrical-resonator filters, Figure 4 shows the equivalent electrical circuit of a triple-tuned (for example) mechanical filter of the half-wave-resonator quarter-wave-coupling type. The equivalent electrical circuit is the node network of Figure 4D if voltage is made equivalent to velocity and current is made equivalent to force. If current is made equivalent to velocity and voltage is made equivalent to force,

the dual mesh network shown in Figure 4E is obtained. Patently, the design information for any one of the networks of Figures 2 and 4 is sufficient to permit the design of all the other networks.

With reference to the use of quartz-crystal resonators in ladder-network filters, the configuration of Figure 3A is the only one specifically considered in this paper. Here the crystal supplies the series-resonant circuits of the series arms, and the crystal holder capacitance is absorbed in the parallel-resonant circuit that is across the series-resonant circuit. The reader should realize, however, that the attenuation shapes to be described apply also to the lattice and half-lattice crystal filters in common use.

1.3 SPECIFIC QUESTION CONSIDERED IN THIS PAPER

Having decided on the circuit to be used, the next question is the one with which this paper deals. It has the following two parts. A) *With a specified V_p/V_s ratio in the pass band, exactly how many physical resonators must be used to*

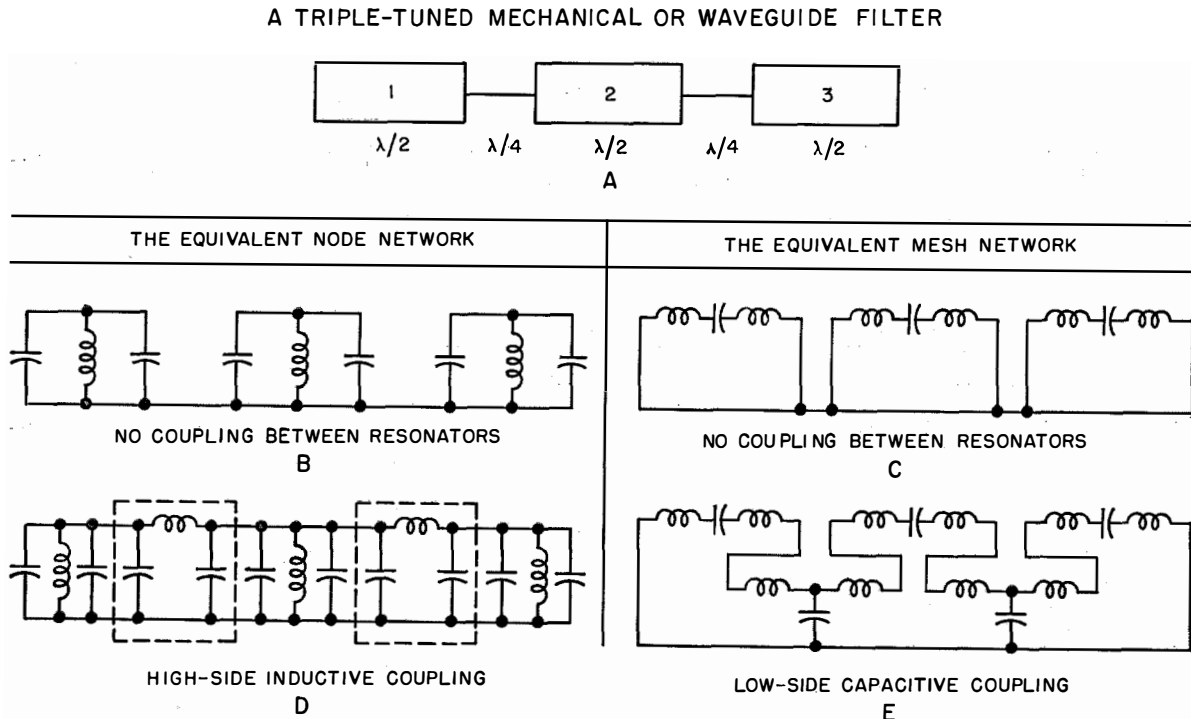


Figure 4—Filters employing mechanical resonators are fundamentally the same as those employing electrical resonators. The node-network equivalent is obtained if voltage is made equivalent to velocity and current to force; and the mesh-network equivalent is obtained if current is made equivalent to velocity and voltage to force.

satisfy a selectivity requirement of the type given in the introduction? and B) for a given midfrequency, what is the minimum unloaded Q that these resonators must possess?

The material that follows is divided into three parts: section 2 uses the results of the derivation of sections 3 and 4 to give the reader a numerical example of the use of the derived design equations; section 3 gives the derivation of the design equations for the inverse-arm configuration or coupled-resonant-circuit filters; and section 4 gives the equivalent derivation for the m -derived-configuration and equivalent filters.

2. Numerical Examples

2.1 INVERSE-ARM-CONFIGURATION AND EQUIVALENT FILTERS OF FIGURE 2

For these filters, which supply n attenuation zeros and no attenuation poles, the three pairs of design equations are (6) and (11), (7) and (12), and (8) and (13).

As a numerical example of the use of these design equations, consider a practical case that arises in radio communication in the vehicular field. The number of actual and potential users is starting to overcrowd the available channels. There is therefore a desire to increase greatly the number of available channels. An obvious procedure is to use receivers having the smallest possible acceptance bandwidth consistent with the information bandwidth and signal-to-noise ratio required and with the conditions of temperature, shock, vibration, humidity, et cetera to which the oscillators, resonators, and other components will be subjected and then have the highest practicable rate of cutoff outside of this accept bandwidth so that adjacent channels can be placed as near as possible to each other.

Since superheterodyne receivers are used, the above selectivity would be developed in the intermediate-frequency amplifier and consideration must be given to the well-known abrogating phenomena of spurious responses, cross modulation, intermodulation, desensitization, et cetera. However, it is still true that the intermediate-frequency selectivity is the major receiver characteristic that defines the possible adjacent-channel spacing. One suggestion for the desired

selectivity of the intermediate-frequency amplifier of these so-called split-channel receivers is as follows: a total bandwidth at 6 decibels down of 17.5 kilocycles per second and a total bandwidth at 100 decibels down of 30 kilocycles; that is $BW_a = BW_{6db} = 17.5$ kilocycles and $BW_r = BW_{100db} = 30$ kilocycles.

Given the above requirement, accurate answers must be obtained for the following two questions: A) with a specified pass-band peak-to-valley ratio how many resonators must be used; and B) for a given pass-band midfrequency, what is the lowest unloaded Q that these resonators may have. This last question can of course be stated in its inverted form: for a given available unloaded-resonator Q , what is the highest pass-band midfrequency that can be used?

The answers to these questions are obtained as follows: first substituting in (6) that $BW_{100db}/BW_{6db} = 1.71$, that $V_p/V_a = 2$, and $V_p/V_r = 10^5$, it is found that the minimum number of resonators that can be used when the limiting case of complete (6-decibel) rippling is allowed in the pass band is 9.75 resonators. (Of course, 10 resonators would be used in the physical filter.) Substituting $n_c = 9.75$ and $V_p/V_a = 2$ in (11), it is found that the resonators must have unloaded Q 's greater than 109 times the "fractional midfrequency" f_0/BW_{6db} .

Next, substitution in (7) shows that the minimum number of resonators for the other limiting case of 0-decibel ripples in the pass band is 20.4 resonators. Substituting $n_b = 20.4$ and $V_p/V_a = 2$ in (12), it will be seen that these resonators must have unloaded Q 's greater than 13.4 times the fractional midfrequency f_0/BW_{6db} .

A graph of the type shown in Figure 5 helps to show the relation between the four important variables considered in this paper, and the above two pairs of values give the 6-decibel and 0-decibel ripple points on the curve marked 1 STAGE.

The intermediate points on this curve are obtained by inserting a specific V_p/V_v ratio in (8), substituting values of n between 9.75 and 20.4 in (8), and constructing an auxiliary graph of the resulting BW_{100db}/BW_{6db} versus n . Where this curve crosses the desired $BW_{100db}/BW_{6db} = 1.71$ line, the required value of n_{ic} for this V_p/V_v

must have unloaded Q 's greater than 64.3 times the fractional midfrequency $f_0/BW_{6\text{db}}$.

Next, for the other limiting case of no ripples in the accept band, that is, Taylor-accept-band Chebishev-reject-band behavior, substitution in (23) produces $n_{tc} = 9.75$; a minimum of 9.75 arms or 15 resonators will be required with this response shape. Using $n_{tc} = 9.75$ for (33) so that $A_1^t = 0.161$ and $B_t = 1.255$, it is found that the resonators must have an unloaded Q higher than 8.2 times the fractional midfrequency $f_0/BW_{6\text{db}}$.

The above two pairs of values give the 6-decibel and 0-decibel ripple points on that curve of Figure 6 marked 1 *STAGE*.

The intermediate points on this curve are obtained by solving (24) for n_{icc} by the method given immediately below (24); and then using these values of n_{icc} and the values of f, f', K_f, v, v' , and K_v obtained from (24) to solve (34) for the corresponding required value of unloaded Q . Thus, for example, if we use a response shape having a 0.1-decibel ripple in the pass band to supply our required $BW_{100\text{db}}/BW_{6\text{db}} = 1.71$, it is found that 7.76 arms are needed and the unloaded Q of the resonators must be greater than 19.4 times the fractional midfrequency.

The discussion in section 2.2 concerning the cascading of like stages to reduce the required unloaded Q , of course, also applies to m -derived configurations. On the basis of the procedure discussed there, the 2- and 3-stage curves in Figure 6 were calculated and plotted.

3. Constant- K Configuration

3.1 OPTIMUM RESPONSE SHAPE

It has long been realized that if, by straightforward application of Kirchhoff's laws, one solves for the transfer function of the inverse-arm configuration of Figure 2A, that is, the ratio output/input; one obtains a numerator that is a constant (it is not a function of the frequency variable) and a denominator that is a simple polynomial in consecutive descending powers of the complex-frequency variable

$$j\left(\frac{\omega}{\omega_0} - \frac{\omega_0}{\omega}\right) \equiv j\left(\frac{BW}{f_0}\right);$$

the highest power n of $j(BW/f_0)$ will be the number of arms used in the configuration of Figure

2A; and the coefficients of the polynomial will be real, independent of frequency, and formed from various combinations of the circuit constants. The above is true not only when lossless resonators are used, but also for finite- Q resonators^{2,3}. The peak response will of course be obtained when the above polynomial has its minimum value and so the *relative* attenuation, that is, the ratio of peak V to complex V at any frequency will be in the form

$$\frac{V_p}{V} = \frac{1}{\Delta_{\text{min}}} \left\{ \left(j\frac{BW}{f_0} \right)^n + U_{n-1} \left(j\frac{BW}{f_0} \right)^{n-1} + U_{n-2} \left(j\frac{BW}{f_0} \right)^{n-2} + \dots \right\}, \quad (1)$$

where Δ_{min} stands for the minimum value of the magnitude of the bracketed complex polynomial.

It is now well known that even with dissipation present it is possible to adjust the coefficients of (1) so that the shape of the magnitude squared of (1) is as shown in Figure 7 for the case of odd n , that is, $n = 5$ and is given analytically by (2).

$$\left| \frac{V_p}{V} \right|^2 = 1 + \left[\left(\frac{V_p}{V_v} \right)^2 - 1 \right] \times \cosh^2 \left(n \cosh^{-1} \frac{BW}{BW_v} \right). \quad (2)$$

When the configurations of Figure 2 are used for filtering purposes, the important reason why it is desirable to adjust them so that their relative-attenuation magnitude is given by (2) is as follows: for a given number of resonators n and a given ripple V_p/V_v in the accept band, (2) gives the sharpest rate of cutoff between the accept band and the reject band that can be produced physically by the circuits⁴ of Figure 2. Thus through the medium of (2), the filter designer is in the wonderful position of knowing that when inverse-arm-type networks are used it is physically impossible to produce a higher rate of cutoff than that given by (2), and a design based on this equation will call for the smallest number of resonators it is possible to

² E. L. Norton, United States Patent 1,788,538; January, 1931.

³ M. Dshal, "Design of Dissipative Band-Pass Filters Producing Desired Exact Amplitude-Frequency Characteristics," *Proceedings of the IRE*, volume 37, pages 1050-1069; September, 1949; and *Electrical Communication*, volume 27, pages 56-81; March, 1950.

⁴ P. I. Richards, "Universal Optimum-Resonance Curves for Arbitrarily Coupled Resonators," *Proceedings of the IRE*, volume 34, pages 624-629; September, 1946.

use in the configuration⁵ of Figure 2. The normalizing bandwidth BW_v in (2) is that skirt bandwidth where the relative attenuation is equal to the V_p/V_v ratio, and in general this "valley bandwidth" is not equal to the required accept

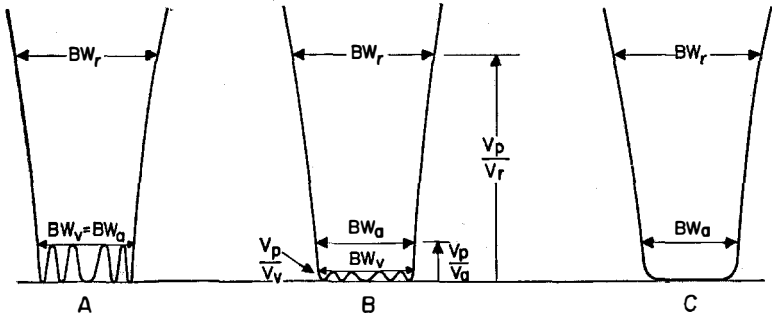


Figure 7—The optimum relative-attenuation shapes of (2) that can be produced by the constant- K -type networks of Figure 2. See section 3.1.1. A—Complete Chebyshev, B—incomplete Chebyshev, and C—Butterworth behavior. This specific example is for the case of n odd ($n = 5$). When n is even, there are also n points of zero-decibel relative attenuation, with a "response valley" at the midfrequency.

bandwidth given in the selectivity specifications. It is therefore necessary to modify (2) so that the attenuation shape is expressed in terms of the V_p/V_v and BW_a of the selectivity requirement. This modification is performed in the next section.

3.1.1 Complete Chebyshev, Incomplete Chebyshev, and Butterworth Behaviors

It is important to realize that, as shown in Figure 7B, BW_v in (2) is the bandwidth between the points on the skirts that are that number of decibels down equal to the peak-to-valley ratio. Now only for the limiting case, which will be called the complete Chebyshev behavior as shown in Figure 7A, is this BW_v identical with the accept bandwidth BW_a specified in filter requirements. In many practical cases, the edge of the accept bandwidth may be specified for example as the 6-decibel-down points whereas the allowable ripple in the passband may be limited to 0.1 decibel. This type of attenuation, shown in Figure 7B, will be called the incomplete Chebyshev behavior. Finally there is the other limiting case where for a required accept bandwidth the peak-to-valley ratio is made just to

⁵ It is assumed that the reader realizes that the magnitude equations given by classical filter theory are approximations that cannot be produced by physical networks.

reach 0 decibels. This type of attenuation, shown in Figure 7C, will be called the Butterworth relative-attenuation shape.

Even when there is no limitation on the V_p/V_v ratio inside the accept bandwidth BW_a , there is a very important practical reason why an incomplete Chebyshev response may have to be used. This reason, which will be considered in detail in the next section, is as follows: for a required rate of cutoff, the unloaded Q required for the resonators of Figure 2 will become smaller when the desired V_p/V_v is made smaller. Correspondingly, the required number of resonators will unfortunately become greater; the exact number will be obtained from (8).

To obtain the shape of the complete Chebyshev response in terms of the specified bandwidth BW_a , simply make the valley bandwidth BW_v in (2) equal to the required accept bandwidth BW_a . Solving for the bandwidth ratio, (3) is obtained.

$$\frac{BW}{BW_a} = \cosh \left\{ \frac{1}{n_c} \cosh^{-1} \left[\frac{(V_p/V)^2 - 1}{(V_p/V_a)^2 - 1} \right]^{1/2} \right\}. \quad (3)$$

In order to get the shape of the attenuation curve in terms of the accept bandwidth BW_a for the incomplete Chebyshev response, use must be made of (2) twice, first at BW_a and then at any other BW on the skirt. Dividing the resulting two equations, (4) is obtained for the bandwidth ratio.

$$\frac{BW}{BW_a} = \frac{\cosh \left\{ \frac{1}{n_{ic}} \cosh^{-1} \left[\frac{(V_p/V)^2 - 1}{(V_p/V_v)^2 - 1} \right]^{1/2} \right\}}{\cosh \left\{ \frac{1}{n_{ic}} \cosh^{-1} \left[\frac{(V_p/V_a)^2 - 1}{(V_p/V_v)^2 - 1} \right]^{1/2} \right\}}. \quad (4)$$

Finally, as we make the peak-to-valley ratio inside the accept band approach zero, so that $1/[(V_p/V_v)^2 - 1]^{1/2}$ approaches infinity, (4) becomes (5) in the limit.⁶

$$\frac{BW}{BW_a} = \left[\frac{(V_p/V)^2 - 1}{(V_p/V_a)^2 - 1} \right]^{1/2 n_b} \quad (5)$$

⁶ Equation (5) is obtained from (4) by using the facts that

$$\begin{aligned} \cosh^{-1} x &= \ln 2x, & (x > 10), \\ \cosh y &= \frac{1}{2} e^y, & (y > 3). \end{aligned}$$

Solving (5) for V_p/V_v , (5A) is obtained and will be recognized as the well-known Butterworth or maximally flat relative-attenuation shape.

$$\left| \frac{V_p}{V_v} \right|^2 = 1 + \left[\left(\frac{V_p}{V_a} \right)^2 - 1 \right] \left(\frac{BW}{BW_a} \right)^{2n_b}. \quad (5A)$$

Thus, it is evident that when the edge of the accept band is defined by points outside the valley-decibels-down points, the limiting case of the Chebyshev shape is the Butterworth shape.

3.1.2 Number of Resonators Required

It is now possible to obtain the desired design equations for inverse-arm configurations. Solving (3) for the number of arms (and therefore resonators) required to produce the desired rate of cutoff when the limiting case of complete Chebyshev behavior can be used, results in (6).

$$n_c = \frac{\cosh^{-1} \left[\frac{(V_p/V_r)^2 - 1}{(V_p/V_a)^2 - 1} \right]^{1/2}}{\cosh^{-1}(BW_r/BW_a)}. \quad (6)$$

Equation (6) is the first of the desired design equations for constant- K -type networks. When complete Chebyshev behavior is allowed, the n_c obtained from (6) is the smallest n that can be used to obtain the required rate of cutoff.

Next desired is the number of arms (and therefore resonators) required to produce the desired rate of cutoff when the other limiting case of Butterworth behavior is used. Solving (5) for n gives (7).

$$n_b = \frac{\log \left[\frac{(V_p/V_r)^2 - 1}{(V_p/V_a)^2 - 1} \right]^{1/2}}{\log(BW_r/BW_a)}. \quad (7)$$

This is the second of the desired design equations for constant- K -type networks. The required number of arms n_b (and therefore resonators) obtained from it will be appreciably greater than would be specified by (6), but remember that, as will be shown in the next section, the unloaded Q that the resonators must possess will be appreciably less than required with (6).

Equations (6) and (7) give, respectively, the smallest and largest numbers of resonators that can be used to produce a required selectivity with the optimum Chebyshev type of relative attenuation described by (2).

To find the pass-band ripple that must be accepted when the number of resonators used is between n_c and n_b , use is made of (4) to solve for n_{ic} with a specific value of peak-to-valley ratio inserted in (4); or solve for the resulting peak-to-valley ratio with a specific number of arms n_{ic} —greater than n_{cc} but fewer than n_b —inserted in (4). Unfortunately, it does not seem possible to solve (4) and obtain an explicit equation for n or V_p/V_v . A procedure that is not very elegant

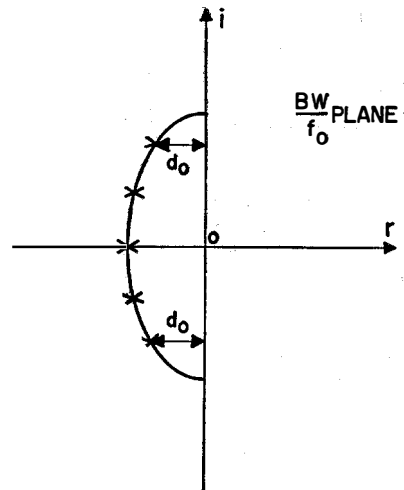


Figure 8—The networks of Figure 2 must be adjusted so that their attenuation zeros are in the positions given by (9) and (10). The perpendicular distance d_0 of that attenuation zero nearest the $j(BW/f_0)$ axis sets the lowest allowable resonator unloaded Q that can be used. See section 3.2.

but is actually not too time consuming is merely to rewrite (4) as (8).

$$\frac{BW_r}{BW_a} = \frac{\cosh \left\{ \frac{1}{n_{ic}} \cosh^{-1} \left[\frac{(V_p/V_r)^2 - 1}{(V_p/V_v)^2 - 1} \right]^{1/2} \right\}}{\cosh \left\{ \frac{1}{n_{ic}} \cosh^{-1} \left[\frac{(V_p/V_a)^2 - 1}{(V_p/V_v)^2 - 1} \right]^{1/2} \right\}}. \quad (8)$$

Then, first insert a specific value of V_p/V_v in this equation; second, insert values of n between n_c and n_b and construct an auxiliary graph of the resulting BW_r/BW_a versus n ; third, where this curve crosses the required value of BW_r/BW_a , the corresponding necessary value of n_{ic} will be found.

Equation (8) is the third of the desired design equations for constant- K -type networks and together with (6) and (7) gives answers to the first question stated in section 1.3 for the constant- K configurations of Figure 2.

3.2 LOWEST UNLOADED-RESONATOR Q

The answer to the very important second question, "For a given midfrequency, what is the minimum unloaded Q that these resonators must possess?" is obtained from the following reasoning.

As is well known, a desired complex relative-attenuation expression (together with the generator-load resistance ratio) specifies a *lossless* network that will produce the desired relative attenuation magnitude. To obtain this complex expression, a solution must be found for the $2n$ roots of the desired magnitude equation. Those n of the $2n$ roots that are in the left half-plane are then used to form the required complex polynomial. Figure 8 shows a typical root-position pattern for constant- K -type filters for the case of $n = 5$.

However, the desired attenuation shape must be produced with resonators having finite Q . It is therefore necessary to make the attenuation zeros of the *dissipative* network coincide with those of the desired attenuation shape.

Darlington⁷ and Bode⁸ have shown that if all the resonators of Figure 2 have the same unloaded Q , then by a simple procedure it is possible to obtain a complex polynomial that (together with the ratio of generator resistance to load resistance) *specifies only the reactances* of the required dissipative network.

The procedure is simply to *move the attenuation zeros of the desired attenuation shape closer to the real-frequency axis by an amount equal to the inverse of the unloaded Q possessed by the resonators*; then when these newly positioned left-half-plane zeros are used, they will define the reactances of a network that will produce the desired attenuation shape when the reactive elements used have the assumed finite unloaded Q .

This procedure and the well-known requirement that attenuation zeros of a physically realizable network cannot appear in the right half-plane immediately fixes the lowest allowable resonator Q 's that can be used to obtain a desired attenuation shape. Referring to Figure 8, it

⁷ S. Darlington, "Synthesis of Reactance Four-Poles Which Produce a Prescribed Insertion Loss Characteristic," *Journal of Mathematics and Physics*, volume 18, pages 257-353; September, 1939.

⁸ H. W. Bode, "Network Analysis and Feedback Amplifier Design," D. Van Nostrand and Company, New York, New York; first edition, 1945; pages 216-218.

will be seen that *the smallest allowable resonator unloaded Q that can be used to produce the attenuation defined by this root plot is equal to the inverse of the perpendicular distance between the $j(BW/f_0)$ axis and that attenuation zero that is closest to this axis*. The next section applies this principle to find the design equations giving the minimum unloaded-resonator Q 's that can be used when the optimum Chebyshev attenuation shape is desired.

3.2.1 Lowest Unloaded-Resonator Q 's for Complete Chebyshev, Incomplete Chebyshev, and Butterworth Shapes

As outlined in the previous section, a solution must first be obtained for the $2n$ roots, that is, attenuation zeros of the desired attenuation magnitude equation.

The roots of the general Chebyshev shape of (2) are given by (9), which gives the real r and imaginary i coordinates of these attenuation zeros on the complex-frequency plane whose axes have the dimensions of BW/f_0 .

$$\frac{r_m}{BW_v/f_0} = S_n \sin (2m - 1) \frac{90^\circ}{n}, \quad (9A)$$

$$\frac{i_m}{BW_v/f_0} = C_n \cos (2m - 1) \frac{90^\circ}{n}, \quad (9B)$$

where

$$\left. \begin{aligned} S_n &= \sinh \left\{ \frac{1}{n} \sinh^{-1} \frac{1}{[(V_p/V_v)^2 - 1]^{1/2}} \right\} \\ C_n &= (1 + S_n^2)^{1/2}. \end{aligned} \right\} \quad (9C)$$

By solving (5A) directly for its zeros (or by substituting for BW_v in (9), its value in terms of BW_a as given by (2) and then letting the V_p/V_v ratio approach unity) (10) is obtained giving the required root locations for the Butterworth attenuation shape.

$$\frac{r_m}{BW_a/f_0} = \frac{1}{[(V_p/V_a)^2 - 1]^{1/2n}} \sin (2m - 1) \frac{90^\circ}{n}, \quad (10A)$$

$$\frac{i_m}{BW_a/f_0} = \frac{1}{[(V_p/V_a)^2 - 1]^{1/2n}} \cos (2m - 1) \frac{90^\circ}{n}. \quad (10B)$$

The elliptical pattern formed by plotting the zero positions as given by (9) is now well known and is shown in Figure 8 for the case of $n = 5$.

Equation (10) gives the limiting case, which is a circular pattern.

From Figure 8 and (9) and (10), it is found that setting m equal to unity gives the root nearest the jF axis and therefore, in accord with the principle of section 3.2, (9A) and (10A) with m set equal to unity will give directly the inverse of the lowest unloaded-resonator Q that can be used to produce the optimum Chebyshev attenuation shape.

For the limiting case of the complete Chebyshev response, wherein the valley bandwidth BW_v is identical with the required accept bandwidth BW_a , (11) is directly obtained from (9A).

$$\frac{Q_{0 \min}^{ic}}{f_0/BW_a} = \frac{1}{\sinh \left\{ \frac{1}{n_c} \sinh^{-1} \frac{1}{[(V_p/V_a)^2 - 1]^{1/2}} \right\} \sin \left(\frac{90^\circ}{n_c} \right)}, \quad (11)$$

where n_c is obtained from (6). This is the fourth of the desired design equations for constant- K -type networks and it gives the lowest unloaded resonator Q that can be used to produce the complete Chebyshev attenuation shape.

For the other limiting case of the Butterworth response, wherein the V_p/V_v ratio is unity, (12) is obtained directly from (10A).

$$\frac{Q_{0 \min}^b}{f_0/BW_a} = \frac{[(V_p/V_a)^2 - 1]^{1/2n}}{\sin(90^\circ/n_b)}, \quad (12)$$

when n_b is obtained from (7). This is the fifth of the desired design equations for constant- K -type networks.

Finally for the incomplete Chebyshev attenuation shape, where the accept bandwidth BW_a is outside the valley bandwidth BW_v , there must be substituted for BW_v in the root-location equations (9) its value in terms of BW_a ; this relation is of course given by (2) and when substitution is made, (13) is obtained, the sixth and last of the constant- K -type-network design equations.

$$\frac{Q_{0 \min}^{ic}}{f_0/BW_a} = \frac{\cosh \left\{ \frac{1}{n_{ic}} \cosh^{-1} \left[\frac{(V_p/V_a)^2 - 1}{(V_p/V_v)^2 - 1} \right]^{1/2} \right\}}{\sinh \left\{ \frac{1}{n_{ic}} \sinh^{-1} \frac{1}{[(V_p/V_v)^2 - 1]^{1/2}} \right\} \sin \left(\frac{90^\circ}{n_{ic}} \right)}, \quad (13)$$

where n_{ic} and $1/[(V_p/V_v)^2 - 1]^{1/2}$ are not independent of each other, but are obtained from the solution of (8).

These three pairs of equations, (6) and (11) for the limiting complete Chebyshev shape, (7) and (12) for the other limiting case of the Butterworth response, and (8) and (13) for the general case of the incomplete Chebyshev response, permit complete and exact answers to the two questions stated in section 1.3. The numerical example given in section 2.1 illustrates the use of these three pairs of equations.

4. m -Derived Configurations

4.1 OPTIMUM ATTENUATION SHAPE

By the straightforward application of Kirchhoff's laws to the basic m -derived configuration of Figure 3A, it will be found that with lossless

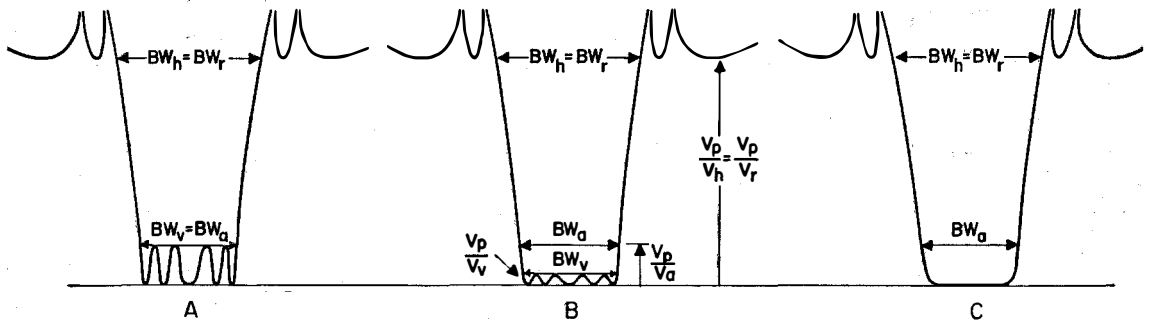


Figure 9—The optimum attenuation shapes of (15) that can be produced by the m -derived-type networks of Figure 3. See section 4.1.1. This specific example is for the case of n odd ($n = 5$), for which (15) produces $(n - 1)$ infinite-attenuation points with infinite attenuation at infinite frequency. When n is even, there are in the pass band n points of zero-decibel relative attenuation with a response valley at the midfrequency; and in the reject band there are n points of infinite attenuation with finite attenuation at infinite frequency.

elements the ratio of the peak output voltage to the complex output voltage at any frequency, that is, the relative attenuation, is given by the ratio of two polynomials as in (14).

$$\frac{V_p}{V} = \frac{1}{\Delta_{\min}} \left\{ \frac{(jF)^n + U_{n-1}(jF)^{n-1} + U_{n-2}(jF)^{n-2} + \dots}{(jF - jF_{\infty 1})(jF + jF_{\infty 1})(jF - jF_{\infty 2})(jF + jF_{\infty 2}) \dots} \right\}, \quad (14)$$

where Δ_{\min} is the minimum value of the magnitude of the bracketed expression; F stands for the band-pass frequency variable BW/f_0 ; and coefficients U of the numerator polynomial are real, independent of frequency, and formed from various combinations of the circuit constants; and the specific fractional bandwidths $F_{\infty 1}$, $F_{\infty 2}$, et cetera are the fractional bandwidths at which infinite attenuation is produced.

It is important for the reader to realize that n in (14) is *not* the number of resonators being used, but is the number of arms in the basic ladder of Figure 3A. To find the number of resonators required, use is made of the relations given at the end of section 1.1.

If the number of arms n being used is *odd*, then there will be $(n - 1)$ denominator factors; if n is even, there will be n denominator factors.

In Darlington's classic paper⁷ published in 1939, it is pointed out that it is possible to adjust the coefficients and infinite-attenuation frequencies of (14) so that the shape of the magnitude squared of (14) is as shown in Figure 9 for the case of an odd n , that is, $n = 5$, and is given analytically⁹ by (15).

$$\left| \frac{V_p}{V} \right|^2 = 1 + \left[\left(\frac{V_p}{V_v} \right)^2 - 1 \right] cd_v^2 \left[n \frac{K_v}{K_f} cd_f^{-1} \frac{BW}{BW_v} \right], \quad (15A)$$

where

$$v = \left[\frac{(V_p/V_v)^2 - 1}{(V_p/V_h)^2 - 1} \right]^{1/2}, \quad (16)$$

$$f = BW_v/BW_h. \quad (17)$$

The number of arms n and the moduli v and f that must be used in (15) cannot be picked inde-

⁹The writer has used the cn/dn rather than the sn elliptic function because with the former one equation (15) can be written for both n odd and n even. Similarly, the important zero- and pole-location equations, (26) and (28), will apply to both n odd and even. Insofar as numerical work is concerned, the fact that $(cn/dn)u = sn(K - u)$ enables the cn/dn values to be obtained from the more-common sn tables.

pendently of each other but must always satisfy the relation between the three quantities given by (18).

$$\log q_v = n \log q_f, \quad (18)$$

where q is the so-called modular constant of the modulus given by the subscript. The function $(\log q_k)$ is tabulated on pages 49 through 51 of the 1945 edition of Jahnke and Emde; and the Smithsonian Elliptic Function Tables compiled by G. W. and R. M. Spenceley contains a very useful short appendix dealing with the numerical computation of the various elliptic functions. It will be noted that for modulus values k less than 0.1, say, the corresponding modular constant is simply $q_k = (k/4)^2$. In (15), the symbol cd stands for the ratio of the two elliptic functions cn over dn , where the subscript v or f is the modulus of the function; and K_v and K_f are the complete elliptic integrals of the first kind, evaluated for the modulus value given by the subscript.

It is evident that the modulus v in (16) is immediately set by *two voltage ratios*; the maximum allowable ripple in the pass band V_p/V_v and the minimum required attenuation in the reject band V_p/V_h . Similarly, the modulus f in (17) is immediately set by *the ratio of two bandwidths*; the ripple bandwidth (which except for complete Chebyshev pass-band behavior will not be the required accept bandwidth) and the hill bandwidth (which will be the required reject bandwidth only if complete Chebyshev reject-band behavior is used).

When the attenuation requirements are as stated in the introduction and the configurations of Figure 3 are used to satisfy this type of attenuation requirement, the reason for adjusting the network so that the amplitude response of Figure 9 and (15) is obtained is exactly similar to that given for using (2); that is, for a given number of arms n and a given allowable peak-to-valley ratio V_p/V_v in the accept band, and a given required minimum attenuation or peak-to-hill ratio V_p/V_h in the reject band, (15) gives the sharpest rate of cutoff that can be produced physically by the circuits of Figure 3.

Equation (15A) has two different forms depending on the part of the attenuation characteristic of interest. From the middle of the pass band out to the valley bandwidth, that is, when BW/BW_v is less than unity, (15A) stays as given. In the cutoff region between the edge of the valley bandwidth and the edge of the hill bandwidth, that is, where BW/BW_v varies between unity and $1/f$, (15A) turns into (15B).

$$\left| \frac{V_p}{V} \right|^2 = 1 + \frac{(V_p/V_v)^2 - 1}{dn_{v'}^2 \left[n \frac{K_v}{K_f} dn_{f'}^{-1} \left(\frac{BW_v}{BW} \right) \right]}, \quad (15B)$$

where the prime indicates the complementary modulus, that is, $v' = (1 - v^2)^{1/2}$ and $f' = (1 - f^2)^{1/2}$. (Note also the inversion of the bandwidth ratio in the bracketed expression of the denominator.) Making use of the definitions of (16) and (17), (15B) can be changed immediately to (15C), which gives attenuation in terms of the hill bandwidth BW_h and the peak-to-hill ratio V_p/V_h .

$$\left| \frac{V_p}{V} \right|^2 = 1 + \frac{\{v[(V_p/V_h)^2 - 1]^{1/2}\}^2}{dn_{v'}^2 \left[n \frac{K_v}{K_f} dn_{f'}^{-1} \left(f \frac{BW_h}{BW} \right) \right]}. \quad (15C)$$

Finally outside the hill bandwidth or where BW/BW_v is greater than $1/f$, (15A) turns into (15D).

$$\left| \frac{V_p}{V} \right|^2 = 1 + \frac{(V_p/V_h)^2 - 1}{cd_{v'}^2 \left[n \frac{K_v}{K_f} cd_{f'}^{-1} \frac{BW_h}{BW} \right]}, \quad (15D)$$

and of course the relations of (16), (17), and (18) apply to (15A), (15B), (15C), and (15D).

It is important to realize that the two normalizing bandwidths BW_v and BW_h in the above equations are the two bandwidths on the skirts of the response where the attenuation is equal to the V_p/V_v ratio and V_p/V_h ratio, respectively. In general, these normalizing bandwidths will not equal the accept and reject bandwidths specified in a selectivity requirement and it is therefore necessary to modify (15) so that the attenuation shape is expressed in terms of the V_p/V_a and V_p/V_r and of the BW_a and BW_r of the selectivity requirement. This modification is performed in the next section.

4.1.1 Complete Chebyshev Accept-Band and Reject-Band Behavior; Incomplete Chebyshev Accept-Band and Reject-Band Behavior; and Taylor Accept-Band and Complete Chebyshev Reject-Band Behavior

As shown in Figure 3B, BW_v in (15) is the bandwidth between the points on the skirt where the attenuation is equal to the peak-to-valley ratio V_p/V_v ; and BW_h in (15) is the bandwidth between the points on the skirt where the attenuation is equal to the peak-to-hill ratio V_p/V_h . Now only for the case shown in Figure 9A, which will be called the complete Chebyshev accept- and reject-band behavior does the valley bandwidth BW_v equal the required accept bandwidth BW_a ; and the hill bandwidth BW_h equal the required reject bandwidth BW_r . For this limiting case, the shape equation is obtained in terms of the specified bandwidths by simply setting BW_v in (15B) equal to the required accept bandwidth BW_a , or by setting BW_h in (15C) equal to the required reject bandwidth BW_r . Solving for the bandwidth ratio, (19A) or (19B) is obtained.

$$\frac{BW}{BW_a} = \frac{1}{dn_{f'} \left[\frac{1}{n_{cc}} \frac{K_f}{K_v} dn_{v'}^{-1} \left\{ \frac{(V_p/V_v)^2 - 1}{(V_p/V)^2 - 1} \right\}^{1/2} \right]} \quad (19A)$$

$$\frac{BW}{BW_r} = \frac{f}{dn_{f'} \left\{ \frac{1}{n_{cc}} \frac{K_f}{K_v} dn_{v'}^{-1} \left\{ v \left[\frac{(V_p/V_r)^2 - 1}{(V_p/V)^2 - 1} \right]^{1/2} \right\} \right\}} \quad (19B)$$

where v , f , and n are obtained from (16), (17), and (18), with $V_p/V_v \equiv V_p/V_a$ and $V_p/V_h \equiv V_p/V_r$.

The next type of response considered is that shown in Figure 9B, where the peak-to-valley ratio is less than the number of decibels down defining the edge of the accept band; but the hill bandwidth is still the same as the required reject bandwidth. Incomplete Chebyshev reject-band behavior will not be considered because in most cases it is practical to demand complete Chebyshev reject-band behavior, with its attendant higher rate of cutoff.

To obtain the shape of the attenuation curve in terms of the specified accept bandwidth BW_a for this case of incomplete Chebyshev pass-band and complete Chebyshev reject-band behavior, it is

necessary to use (15) twice, first at BW_a and then at any point on the curve BW . Dividing the resulting two equations will give an equation equivalent to Figure 7 for the constant- K configuration. However, because complete Chebishev reject-band behavior is being considered, a simpler equation results if the attenuation shape is expressed in terms of the required reject bandwidth rather than in terms of the required accept bandwidth. Setting BW_h in (15C) equal to the required reject bandwidth BW_r , (20) is obtained.

$$\frac{BW}{BW_r} = \frac{f}{dn_{f'} \left\{ \frac{1}{n_{icc} K_v} dn_{v'}^{-1} \left[\frac{(V_p/V_v)^2 - 1}{(V_p/V)^2 - 1} \right]^{1/2} \right\}}, \quad (20)$$

where n , v , and f will have numerical values obtained from (16), (17) and (18) with $V_p/V_h = V_p/V_r$ but V_p/V_v not equal to V_p/V_a .

The final type of m -derived-configuration attenuation considered is that obtained when, while still keeping the hill bandwidth equal to the required reject bandwidth, the peak-to-valley ratio in the accept band approaches and just reaches zero decibels. For this case, v approaches zero and therefore, no matter how many arms n are used, f must approach zero due to the required relation of (18). Therefore f' and v' approach unity and (20) becomes¹⁰ in the limit (21).

$$\frac{BW}{BW_h} = \frac{1}{\cosh \left\{ \frac{1}{n} \cosh^{-1} \left[\frac{(V_p/V_h)^2 - 1}{(V_p/V)^2 - 1} \right]^{1/2} \right\}}. \quad (21)$$

Solving (21) for V_p/V results in (21A), which is the attenuation equation for the limiting case of 0-decibel ripple in the pass band, an attenuation shape that may be said to have Taylor accept-band and complete Chebishev reject-band behavior.

$$\left| \frac{V_p}{V} \right|^2 = 1 + \frac{(V_p/V_h)^2 - 1}{\cosh^2 \left[n \cosh^{-1} (BW_h/BW) \right]}. \quad (21A)$$

As a matter of academic interest, it should be noted that if (21) is applied to two points on the

¹⁰ Equation (21) is obtained from (20) by realizing that when the angle involved is very close to $1K_k$ and k is very close to unity, then

$$dn_k^{-1}x = K_v - \cosh^{-1}(x/k')$$

and

$$dn_k u = k' \cosh (K_k - u).$$

It is also necessary to realize that when f and v both approach zero, then $K_f = K_v/n$.

skirt and then the V_p/V_h ratio is allowed to become infinite, the Butterworth equation (5A) results. Similarly, (15) would turn into the Chebishev (2) if the V_p/V_h ratio is correctly made to approach infinity.

4.1.2 Number of Arms

We are now ready to obtain our desired design equations for m -derived-configuration filters.

For the limiting case of complete Chebishev accept-band and reject-band behavior, (19A) and (19B) apply with the number of required arms n obtained directly from (18), (16), and (17). These equations are rewritten below with the proper subscripts as (22).

$$\left. \begin{aligned} n_{cc} &= \frac{\log q_v}{\log q_f} = \frac{\log (v/4)^2}{\log q_f}, \\ \text{where} \quad v &= \left[\frac{(V_p/V_a)^2 - 1}{(V_p/V_r)^2 - 1} \right]^{1/2} \\ \text{and} \quad f &= BW_a/BW_r. \end{aligned} \right\} \quad (22)$$

As previously noted, $\log q_f$ can be directly read from pages 49 through 51 of Jahnke and Emde. Equation (22) is the first of the desired design equations for m -derived configurations.

Next, let us find the number of arms required to produce the desired selectivity for the other limiting case of Taylor pass-band behavior and complete Chebishev reject-band behavior, as shown in Figure 9C. Here, (21) or (21A) applies, and solving for n , the number of arms, (23) is obtained.

$$n_{ic} = \frac{\cosh^{-1} \left[\frac{(V_p/V_r)^2 - 1}{(V_p/V_a)^2 - 1} \right]^{1/2}}{\cosh^{-1} (BW_r/BW_a)}. \quad (23)$$

This is the second of the desired design equations for m -derived configurations. The required number of arms obtained from it will be greater than that called for by (22), but as will be shown in the next section the unloaded Q that the resonators must possess will be smaller than for the resonators of (22).

Equations (22) and (23) give, respectively, the smallest number and the largest number of arms in Figure 3A that can be used to produce a required selectivity with the optimum attenuation shape of (15).

Finally, to find the number of arms n required for the intermediate case of Figure 9B wherein

the V_p/V_v in the pass band is less than the number of decibels down defining the edge of the pass band but greater than zero, use is made of (20) with (16), (17), and (18).

Equation (20) applied to the edge of the accept band gives (24).

$$\frac{BW_r}{BW_a} = \frac{dn_{f'} \left\{ \frac{1}{n_{icc}} \frac{K_f}{K_v} dn_{v'} \left[\frac{(V_p/V_v)^2 - 1}{(V_p/V_a)^2 - 1} \right]^{1/2} \right\}}{f} \quad (24)$$

$$\frac{V_p}{V_v} = \frac{1}{\Delta_{\min}} \left\{ \frac{(jF)^n + U_{n-1}(jF)^{n-1} + U_{n-2}(jF)^{n-2} + \dots}{[jF - (-d + jF_{\infty 1})][jF - (-d - jF_{\infty 1})] \dots} \right\} \quad (25)$$

The reader should realize that (24) is meaningless without (16), (17), and (18). Unfortunately, it does not seem possible to obtain from these equations an explicit equation for n_{icc} , but the following procedure can be used in a straightforward manner.

Pick a specific V_p/V_v ratio. Solve (16) for v . Then $v' = (1 - v^2)^{1/2}$ is immediately known and K_v is obtained from tables. Now for this v , prepare an auxiliary graph of n versus the resulting BW_r/BW_a . The points for the curve are obtained as follows. First, pick an n larger than n_{cc} but smaller than n_{io} , and use (18) to solve for f . Then $f' = (1 - f^2)^{1/2}$ is immediately known and K_f is obtained from tables. Second, use these values of n , v' , K_v , K_f , and f' in (24) to obtain the resulting BW_r/BW_a . Three points are usually sufficient, and the correct required value of n_{icc} for the V_p/V_v ratio chosen is found where this curve crosses the desired value of BW_r/BW_a .

Equation (24), with (16), (17), and (18) is the third of the desired design equations for m -derived configurations and together with (22) and (23) will provide the answer to the first question stated in section 1.3 (for the m -derived configurations of Figure 3).

4.2 APPROXIMATION INVOLVED WHEN FINITE- Q RESONATORS ARE USED

When the constant- K configurations of Figure 2 are used, the optimum attenuation shape of Figure 7 and (2) can be exactly produced when finite- Q resonators are used, so long as the unloaded Q 's are higher than the limiting values given by (11), (12), and (13). Unfortunately,

when the m -derived configurations of Figure 3 are used, the optimum attenuation shape of (15) cannot be exactly produced when finite- Q resonators are used.

The transfer-impedance equation (25) for the finite- Q network shows why this is unfortunately the case; the numerator of the resulting transfer impedance is still in exactly the form shown in (14), but the denominator of the transfer impedance will now contain both even and odd powers of the frequency variable.

Another way of stating this latter point is that the conjugate pairs of roots of the denominator can never be placed on the real-frequency axis when finite- Q resonators are used in the configurations of Figure 3, but will always appear to the left of the real-frequency axis by a distance exactly equal to the unloaded decrement of the resonators for as can be seen, the root locations of the denominator of (25) are $-d \pm jF_{\infty}$. It is therefore impossible to obtain exactly the optimum attenuation shape of (15), for as may be seen from (15D) the conjugate attenuation poles of this shape occur exactly on the real-frequency axis.

However, it should be realized that when the m -derived response shape is used to satisfy a selectivity requirement, the extreme attenuation produced in the region of the infinite-attenuation frequencies is often not of much practical importance for two reasons; first, the width of these infinite-attenuation cusps is usually a very small percentage of the total required width of the reject band; and second, it is usually the points where the attenuation in the reject band is a minimum (the hill points) that present the greatest difficulty in meeting the attenuation specifications.

If with finite- Q resonators it is still possible to preserve the pass-band shape and the reject-band minimum-attenuation points, the rounding off of the infinite-attenuation points is usually of negligible importance.

In most practical cases, it is possible to adjust the dissipative network so that the numerator roots of (25) coincide with the

attenuation zeros of the desired-shape equation (15) and the denominator roots of (25) have the same real-frequency coordinates as the attenuation poles of (15). Even though these poles are unfortunately displaced to the left by an amount d , the resulting response shape will differ from the optimum shape mainly by having the infinite-attenuation points round off to some finite attenuation that is almost always greater than the required hill attenuation. The attenuation at the hill points will in most practical cases be negligibly reduced from the value given by (15).

This, then, is the approximation made in calculating the minimum unloaded-resonator Q 's that can be used in m -derived band-pass configurations designed to produce the optimum shape of (15); that is, only the network poles are placed in exactly the correct position and the network zeros are allowed to be displaced a distance $1/Q_0$ to the left of their correct position.

Section 3.2 shows how to make the zero positions of a uniformly dissipative network coincide with the zero positions of a desired attenuation shape. As is evident, the limiting value of unloaded Q for which it is possible to obtain the desired zero positions is given by the horizontal distance r_1 between the jF axis and the zero that is closest to this axis. Thus given a desired attenuation shape, a solution must be found for its zeros in order to find the location of that zero nearest the jF axis. This is done in the next section for the optimum attenuation shape of (15).

4.2.1 Lowest Unloaded-Resonator Q 's for Attenuation Shapes of Section 2.1

Setting the desired optimum-attenuation-shape equation (15A) equal to zero and solving, the real r and imaginary i coordinates of the attenuation zeros are given by (26).

$$\frac{r_m}{BW_v/f_0} = \frac{\left[\left(\frac{sn}{cn} \right)_{f'} B_c \right] \left[f'^2 \left(\frac{sn}{dn^2} \right)_f A_m^c \right]}{1 + f'^2 \left[\left(\frac{sn}{cn} \right)_{f'}^2 B_c \right] \left[\left(\frac{cn}{dn} \right)_f^2 A_m^c \right]}, \quad (26A)$$

$$\frac{i_m}{BW_v/f_0} = \frac{\left[\left(\frac{dn}{cn^2} \right)_{f'} B_c \right] \left[\left(\frac{cn}{dn} \right)_f A_m^c \right]}{1 + f'^2 \left[\left(\frac{sn}{cn} \right)_{f'}^2 B_c \right] \left[\left(\frac{cn}{dn} \right)_f^2 A_m^c \right]}, \quad (26B)$$

where the angles A_c and B_c are given by (27).

$$\left. \begin{aligned} A_c^c &= (2m - 1) \frac{K_f}{n}, \\ B_c &= \left\{ \frac{1}{n} \frac{K_f}{K_v} \left(\frac{sn}{cn} \right)^{-1} \frac{1}{[(V_p/V_v)^2 - 1]^{1/2}} \right\}. \end{aligned} \right\} \quad (27)$$

It should be realized that in most practical cases v' is close to unity and the approximation $(sn/cn)^{-1} x \doteq \sinh^{-1} x$ can be used.

In the design of the networks, it is necessary to know the required location of the infinite-attenuation points, and for the sake of completeness the real and imaginary coordinates of these poles are given by (28).

$$\frac{r_m^\infty}{BW_h/f_0} = 0, \quad (28A)$$

$$\frac{i_m^\infty}{BW_h/f_0} = \frac{1}{(cn/dn)_f A_m^c}. \quad (28B)$$

Equation (28) is obtained by simply setting the denominator of (15D) equal to zero and solving for BW_∞/f_0 .

It should be realized that $(cn/dn)_k u = sn_k(K_k - u)$, so that the values of the cn/dn can be obtained simply from the sn tables.

For the limiting case of no ripples in the pass band, solution for the zeros of (21A) produces (29).

$$\frac{r_m}{BW_h/f_0} = \frac{\sinh B_t \sin A_m^t}{\sinh^2 B_t + \cos^2 A_m^t}, \quad (29A)$$

$$\frac{i_m}{BW_h/f_0} = \frac{\cosh B_t \cos A_m^t}{\sinh^2 B_t + \cos^2 A_m^t}, \quad (29B)$$

where the angles A_t and B_t are given by (30).

$$A_m^t = (2m - 1) (90^\circ/n), \quad (30A)$$

$$B_t = \left\{ \frac{1}{n} \sinh^{-1} [(V_p/V_h)^2 - 1]^{1/2} \right\}, \quad (30B)$$

and again for the sake of completeness solving for the infinities of (21A) produces (31).

$$\frac{r_m}{BW_h/f_0} = 0, \quad (31A)$$

$$\frac{i_m}{BW_h/f_0} = \frac{1}{\cos A_m^t}. \quad (31B)$$

The general pattern formed when the zero and infinity locations are plotted on the complex-frequency plane are shown in Figure 10.

From Figure 10 and (26) and (29), it is found that setting m equal to unity gives that root closest to the jF axis. Therefore, following the principle of section 3.2, (26) and (29) with m set equal to unity will give directly the highest unloaded decrement (that is, the inverse of the lowest unloaded Q) that can be used to produce

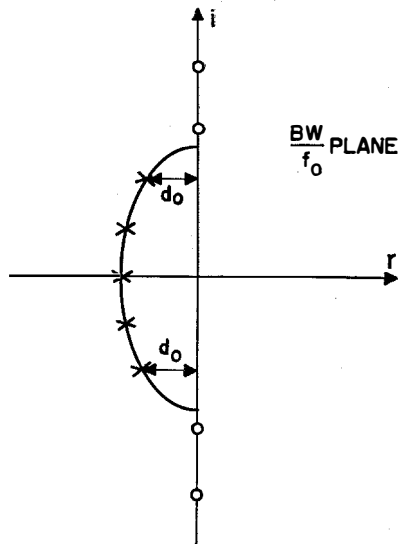


Figure 10—The networks of Figure 3 must be adjusted so that their attenuation zeros and poles are in the positions given by (26) and (28), and by (29) and (31). The perpendicular distance d_0 of that attenuation zero nearest the jF axis sets the lowest allowable Q . See sections 3.2 and 4.2.

the zero-position pattern called for by the optimum attenuation shapes of Figure 9 and (15) and (21A).

For the limiting response of Figure 3A, that is the complete Chebishev accept- and reject-band behavior, where the valley bandwidth BW_v is identical with the required accept bandwidth BW_a and the hill bandwidth BW_h is identical with the required reject bandwidth BW_r , (32) is obtained directly from (26A).

$$\frac{Q_0^{cc}}{f_0/BW_a} = \frac{1 + f^2 \left[\left(\frac{sn}{cn} \right)_{f'}^2 B_c \right] \left[\left(\frac{cn}{dn} \right)_f^2 A_1^c \right]}{\left[\left(\frac{sn}{cn} \right)_{f'} B_c \right] \left[f'^2 \left(\frac{sn}{dn^2} \right)_f A_1^c \right]}, \quad (32)$$

where the angles A_1^c and B_c are given by (27) with m set equal to unity and with n_{cc} , f , and v obtained from (22). Equation (32) is the fourth of the desired design equations for m -derived configurations and gives the lowest unloaded-resonator Q

that can be used to obtain the correct zero positions required by the complete Chebishev accept- and reject-band attenuation shape of Figure 9A.

For the other limiting case of Taylor accept-band behavior shown in Figure 9C, there is obtained directly from (29A) the next desired equation (33).

$$\frac{Q_0^{tc}}{f_0/BW_a} = \frac{\sinh^2 B_t + \cos^2 A_1^t}{\sinh B_t \sin A_1^t}, \quad (33)$$

where the angles A_1^t and B_t are given by (30) with m set equal to unity and n_{tc} is obtained from (23). This is the fifth of the desired design equations for m -derived configurations.

Finally, for the incomplete Chebishev accept-band and complete Chebishev reject-band behavior wherein the required accept bandwidth BW_a is outside the valley bandwidth BW_v (but the required reject bandwidth BW_r is still equal to the hill bandwidth BW_h), there must be substituted in (26A) the value of BW_v in terms of the specified accept bandwidth BW_a . With the understanding that this relation is given by (24), (26A) gives (34).

$$\frac{Q_0^{icc}}{f_0/BW_a} = \frac{1 + f^2 \left[\left(\frac{sn}{cn} \right)_{f'}^2 B_c \right] \left[\left(\frac{cn}{dn} \right)_f^2 A_1^c \right] \frac{1}{f} \left(\frac{BW_a}{BW_r} \right)}{\left[\left(\frac{sn}{cn} \right)_{f'} B_c \right] \left[f'^2 \left(\frac{sn}{dn^2} \right)_f A_1 \right]} \quad (34)$$

where the values of f , f' , v , v' , K_v , K_f , and n are not independent of each other but are the values obtained when (24) is solved by the method given immediately below that equation and the angles A and B are then obtained from (27). Equation (34) is the sixth and last of the desired design equations for m -derived configurations and gives the minimum unloaded-resonator Q that can be used to obtain the zero locations required by the response shape of Figure 3B.

The numerical example given previously in section 2.3 illustrates the use of these three pairs of equations.

4.3 ANOTHER OPTIMUM ATTENUATION SHAPE FOR USE WHEN n IS EVEN

As pointed out in Figure 9, when n is even the optimum relative-attenuation shape of (15) calls for finite attenuation at infinite frequency. Be-

cause of this requirement, it will be found that, when synthesizing an even- n network to produce the shape given by (15), it is necessary to include in the synthesis procedure, the following restriction:

A. If the basic node configuration of Figure 3A is to be used, then there must be a *short-circuit termination* at that end of the network at which the *series* arm occurs.

B. If the basic mesh network, which is the dual of Figure 3A, is to be used, then there must be an *open-circuit termination* at that end of the network at which the *shunt* arm occurs.

In many practical situations, the above restriction cannot be satisfied. When this is the case, the relative-attenuation shape given in (35) can be used.¹¹ Figure 11 illustrates this shape for the specific case of $n = 6$ and it will be noted that instead of n infinite-attenuation points, there are only $n - 2$ points of infinite attenuation called for with this shape. This fact means that the rate of cutoff produced by the shape is slower than that produced by (15) and Figure 9. However, because the shape calls for infinite attenuation at infinite frequency (for n even), resistive terminations can be used at both ends of a correctly synthesized network.

$$\left| \frac{V_p}{V} \right|^2 = 1 + \left[\left(\frac{V_p}{V_v} \right)^2 - 1 \right] cd_v^2 \left[n \frac{K_v}{K_f} u \right],$$

where

$$u = \left(\frac{sn}{cn} \right)_f^{-1} \left\{ \left[\left(\frac{BW_v}{BW} \right)^2 - 1 \right]^{1/2} \times \frac{dn_f(K_f/n)}{f'} \right\},$$

where the modulus v is obtained from (36).

$$v = \left[\frac{(V_p/V_v)^2 - 1}{(V_p/V_h)^2 - 1} \right]^{1/2}$$

and for a given n , the modulus f is obtained from (37).

$$\log q_f = \frac{1}{n} \log q_v.$$

After the modulus f has been obtained, solution of (35) shows that the bandwidth ratio

¹¹ The author is indebted to H. J. Orchard of the British Post Office for pointing out the closed form of (35).

between the hill bandwidth and the valley bandwidth is given by (38).

$$\frac{BW_h}{BW_v} = 1 / f \left(cd_f \frac{K_f}{n} \right).$$

The information contained in the paragraph following (18) applies also to the equations in this section.

In the cutoff region of Figure 11, that is, between BW_v and BW_h , (35) turns into (35A).

$$\left| \frac{V_p}{V} \right|^2 = 1 + \frac{(V_p/V_v)^2 - 1}{dn_v'^2 \left(n \frac{K_v}{K_f} sn_{f'}^{-1} x \right)},$$

where

$$x = \left[1 - \left(\frac{BW_v}{BW} \right)^2 \right]^{1/2} \frac{dn_f(K_f/n)}{f'},$$

where v' and f' are the complementary moduli of v and f , respectively.

Finally, in the reject band of Figure 11, that is, between BW_h and infinity, (35) turns into (35B).

$$\left| \frac{V_p}{V} \right|^2 = 1 + \frac{(V_p/V_h)^2 - 1}{cd_v'^2 \left(n \frac{K_v}{K_f} dn_{f'}^{-1} \frac{1}{x} \right)},$$

where x is given in (35A).

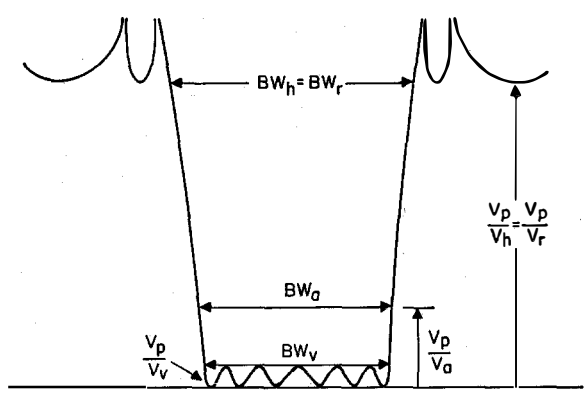


Figure 11—The optimum relative-attenuation shape of (35) for the case of $n = 6$. When n is even, the shape given by (15) and Figure 9 will demand a short-circuit (open-circuit) termination at one end of the synthesized network, whereas the above shape for n even will allow resistive terminations at both ends of the network. Note that the number of infinite-attenuation points is two less than the number of zero-decibel relative-attenuation points and infinite attenuation is produced at infinite bandwidth.

To obtain the required number of resonators and their required unloaded Q , the interested reader can perform on (35) the operations described in sections 4.1, 4.1.1, 4.1.2, and 4.2 with reference to (15).

For the limiting case of zero-decibel ripples in the pass band of the shape shown in Figure 11, it will be found that (35) approaches in the limit (39).

$$\left| \frac{V_p}{V} \right|^2 = 1 + \frac{(V_p/V_h)^2 - 1}{\cosh^2(n \cosh^{-1} y)}, \quad (39)$$

where

$$y = \left[\left(\frac{BW_h}{BW} \cos \frac{90^\circ}{n} \right)^2 + \sin^2 \frac{90^\circ}{n} \right]^{1/2}.$$

It is worth noting that the relative-attenuation shape discussed in this section is the shape that can be produced by many wide-band crystal filters. It is also worth noting that when an m -derived-configuration ladder is to be synthesized to produce this attenuation shape, it will be found that a constant- K -configuration half-section will be required at one end of the resulting network.

5. Symbols

BW_a = specified width in cycles per second of the accept band, that is, the required bandwidth between those points in the skirt where the attenuation is V_p/V_a . See Figures 7 and 9.

BW_h = bandwidth in cycles per second between those points on the skirt of the response that are the same number of decibels down as the hills in the reject band. See Figure 9.

BW_r = specified width in cycles per second of the reject band, that is, the required bandwidth between those points on the skirt where the attenuation is V_p/V_r . See Figures 7 and 9.

BW_o = bandwidth in cycles per second between those points on the skirt of the response that are the same number of decibels down as the valleys in the accept band. See Figures 7 and 9.

$BW/f_0 = F$ = fractional bandwidth.

$f = BW_o/BW_h$ = specific modulus of the elliptic functions to which it is attached as a subscript.

f_0 = midfrequency of the attenuation shape in cycles per second.

$F_\infty = BW_\infty/f_0$ = fractional bandwidth between infinite-attenuation points of the response shown in Figure 9.

K_f, K_v = complete elliptic integrals of the first kind evaluated for the modulus value given by the subscript. See for example Dwight's "Mathematical Tables," pages 199-203.

$\log q_k$ = log to the base 10 of the so-called modular constant of that modulus given by the subscript. See for example Jahnke and Emde, pages 49-51.

$m = 1, 2, 3, \dots, n$.

n = number of arms in the basic networks of Figures 2A and 3A. It also equals the number of attenuation zeros produced by these networks.

n_b = number of arms required in the network of Figure 2A to satisfy an attenuation specification when the Butterworth behavior of Figure 7C is used. See (7).

n_c = number of arms required in the network of Figure 2A to satisfy an attenuation specification when the complete Chebishev behavior of Figure 7A is used. See (6).

n_{cc} = number of arms required in the network of Figure 3A to satisfy an attenuation specification when the complete Chebishev accept- and reject-band behavior of Figure 9A is used. See (22).

n_{ic} = number of arms required in the network of Figure 2A to satisfy an attenuation specification when the incomplete Chebishev behavior of Figure 7B is used. See (8).

n_{icc} = number of arms required in the network of Figure 3A to satisfy an attenuation specification when the incomplete Chebishev accept and complete Chebishev reject-band behavior of Figure 9B is used. See (24).

n_{ic} = number of arms required in the network of Figure 3A to satisfy an attenuation specification when the Taylor accept and complete Chebishev reject-band behavior of Figure 9B is used. See (23).

Q_0 = Q of the unloaded resonators used in the arms of Figures 2A and 3A.

$Q_{0\min}^c$

$Q_{0\min}^b$

$Q_{0\min}^{ic}$ = smallest unloaded Q that can be allowed in the resonators of Figure 2 if n_c , n_b , n_{ic} arms are to satisfy the shape-factor specifications. See (11) (12), and (13).

$Q_{0\min}^{cc}$

$Q_{0\min}^{ic}$

$Q_{0\min}^{ic_e}$ = the smallest unloaded Q that can be allowed in the resonators of Figure 9 if n_{cc} , n_{ic} , or n_{icc} arms, respectively, are to satisfy the shape-factor specification. See (32), (33), and (34).

r, i = real and imaginary coordinates on the complex fractional-bandwidth plane of the attenuation zeros of a desired attenuation shape and the attenuation poles of a desired response shape.

$v = \{[(V_p/V_v)^2 - 1]/[(V_p/V_h)^2 - 1]\}^{1/2}$
= specific modulus of the elliptic functions to which it is attached as a subscript.

v', f' = complementary moduli of v and f , respectively.

V_p/V = attenuation ratio at some fractional bandwidth BW/f_0 .

V_p/V_a ,

V_p/V_r = the attenuation given in a specification as defining the accept bandwidth and thereject bandwidth, respectively. See Figures 7 and 9.

V_p/V_h = peak-to-hill ratio occurring in the reject band. See Figure 9.

V_p/V_v = peak-to-valley ratio allowed in the accept band. See Figures 7 and 9.

Attenuation and Power-Handling Capability of Helical Radio-Frequency Lines*

By J. H. BRYANT and E. J. WHITE

Federal Telecommunication Laboratories, a division of International Telephone and Telegraph Corporation; Nutley, New Jersey

A METHOD is described for computing cold insertion loss as well as power-handling capabilities of a helical radio-frequency line. The helically-conducting-cylinder model in free space is considered first. Computations are then extended to account for the presence of an outer, coaxial, uniformly conducting cylinder.

• • •

1. Attenuation

An expression for the loss due to imperfect conductivity will be derived by applying the helically-conducting-sheet model, which is shown surrounded by a coaxial cylinder in Figure 1, to

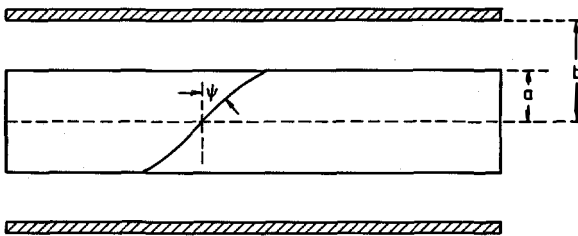


Figure 1—Model helix. a is the mean radius of the helically conducting cylindrical surface, b is the inner radius of the uniformly conducting, coaxial, cylindrical sheet surrounding the helix, and ψ is the angle defining the direction of conduction along the helix.

a helix. The power flow along the helix is given by

$$P_T = P_0 \exp[-2\alpha z],$$

where P_T is the transmitted power, P_0 is the initial input power, α is the attenuation in nepers per unit length, and z is the axial distance from the input of the helix. This can be expressed as

$$\alpha = -\frac{1}{2P_T} \frac{dP_T}{dz}. \quad (1)$$

* Reprinted from *Transactions of the IRE Professional Group on Microwave Theory and Techniques*, volume MTT-1, pages 33-38; November, 1953.

The quantity P_T is given by Pierce¹ as

$$P_T = B^2 \frac{k\beta}{\gamma^4} \frac{1}{F^3(\gamma a)}. \quad (2)$$

The only factor remaining to be evaluated is dP_T/dz , which may be obtained by considering a cylindrical element of the helically conducting sheet. The area of such an element of length dz is $2\pi a dz$, where a is the radius of the cylinder. If P_L is the power loss per unit area, then the total loss over the element is

$$dP_T = 2\pi a P_L dz. \quad (3)$$

The power loss per unit area P_L is found by using the customary method of computing attenuation of radio-frequency lines as follows. If E and H are the electric and magnetic fields, respectively, n is a unit vector normal to the surface of the sheet, and R_s is the skin-effect resistance, $E = R_s(n \times H)$. Hence, $E_z = R_s H_\theta$; $E_\theta = -R_s H_z$. The power flow, given by the Poynting vector, becomes

$$P_L \equiv \frac{1}{2}(\mathbf{E} \times \mathbf{H}) = \frac{1}{2}R_s(|H_\theta|^2 + |H_z|^2) \quad (4)$$

where R_s is the skin-effect resistance. The skin-effect resistance is given by $R_s = (\pi\mu_0 f \rho)^{1/2}$ where μ_0 is the permeability of free space and ρ is the resistivity of the helix material (see Figure 2 for specific values). The field solutions from Pierce² for the helically conducting sheet in free space are used to evaluate (4) by analysis of the fields both inside and outside the helix structure. Inside the helix,

$$H_\theta = j \frac{B}{(\mu/\epsilon)^{1/2}} \frac{k}{\gamma} I_1(\gamma r),$$

$$H_z = -j \frac{B}{(\mu/\epsilon)^{1/2}} \frac{\gamma I_0(\gamma a)}{k I_1(\gamma a)} \frac{1}{\cot \psi} I_0(\gamma r).$$

¹ J. R. Pierce, "Traveling-Wave Tubes," D. Van Nostrand Company, New York, New York; 1950: Appendix 2.

² Page 231 of footnote reference 1.

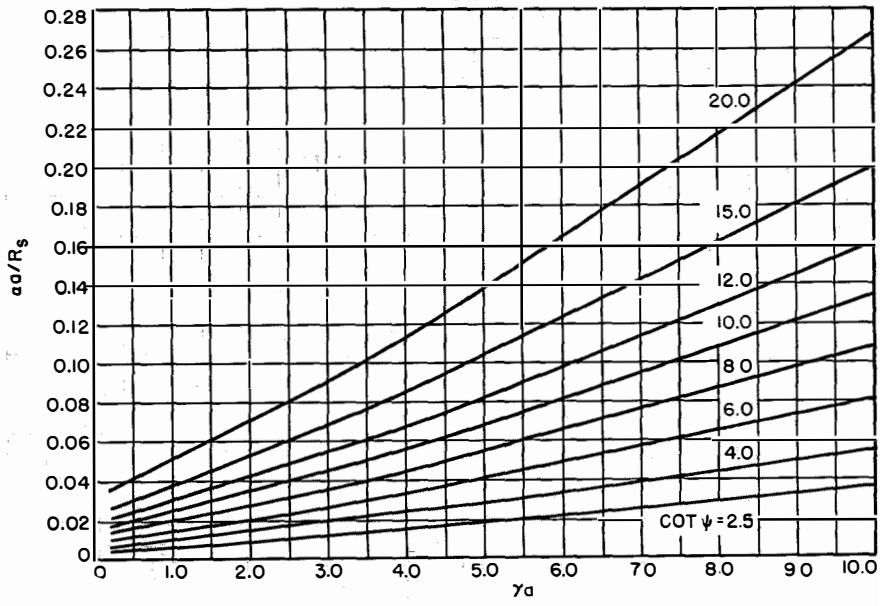
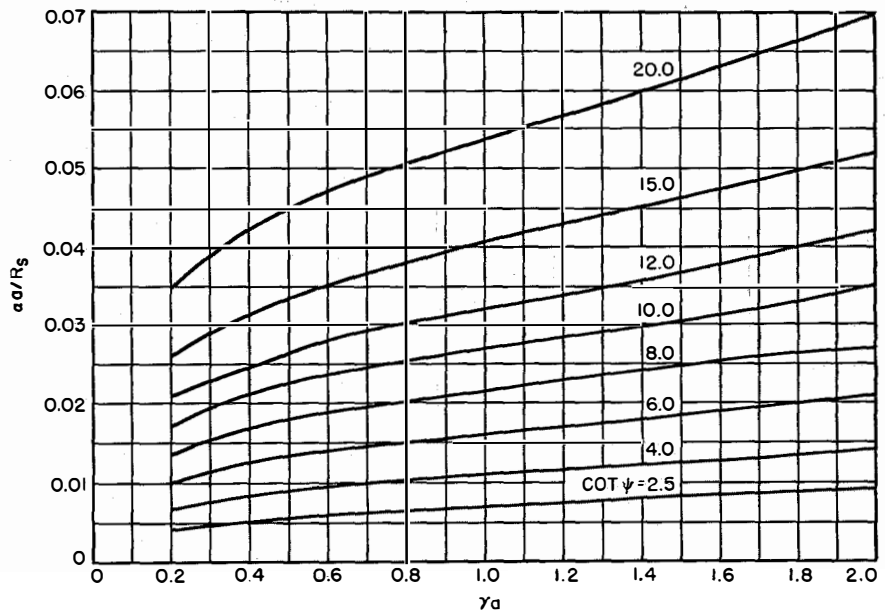
Outside the helix,

$$H_{\theta} = -j \frac{B}{(\mu/\epsilon)^{1/2}} \frac{k}{\gamma} \frac{I_0(\gamma a)}{K_0(\gamma a)} K_1(\gamma r), \quad H_z = j \frac{B}{(\mu/\epsilon)^{1/2}} \frac{\gamma}{k} \frac{I_0(\gamma a)}{K_1(\gamma a)} \frac{1}{\cot \psi} K_0(\gamma r).$$

The total loss per unit area, the sum of the inside and outside losses, becomes

$$P_L = \frac{B^2 R_s}{2.88 \times 10^4 \pi^2} (I_1^2 K_0^2 + I_0^2 K_1^2) \left[\left(\frac{k}{\gamma} \right)^2 \frac{1}{K_0^2 \cot^2 \psi} \left(\frac{\gamma}{k} \right)^2 \frac{I_0^2}{I_1^2 K_1^2} \right], \quad (5)$$

Figure 2—Helix attenuation due to conductor losses $\alpha a/R_s$, where α = attenuation in nepers per unit length of radius, a = helix mean radius, and $R_s = 2.61 \times 10^{-7} f^{1/2}$ ohms for copper, $4.706 \times 10^{-7} f^{1/2}$ ohms for tungsten, and $4.741 \times 10^{-7} f^{1/2}$ ohms for molybdenum.



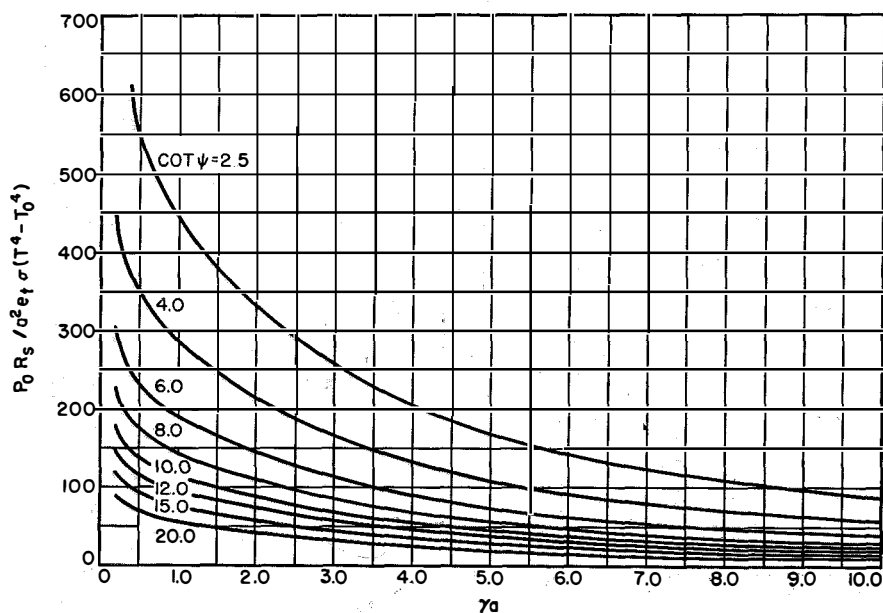
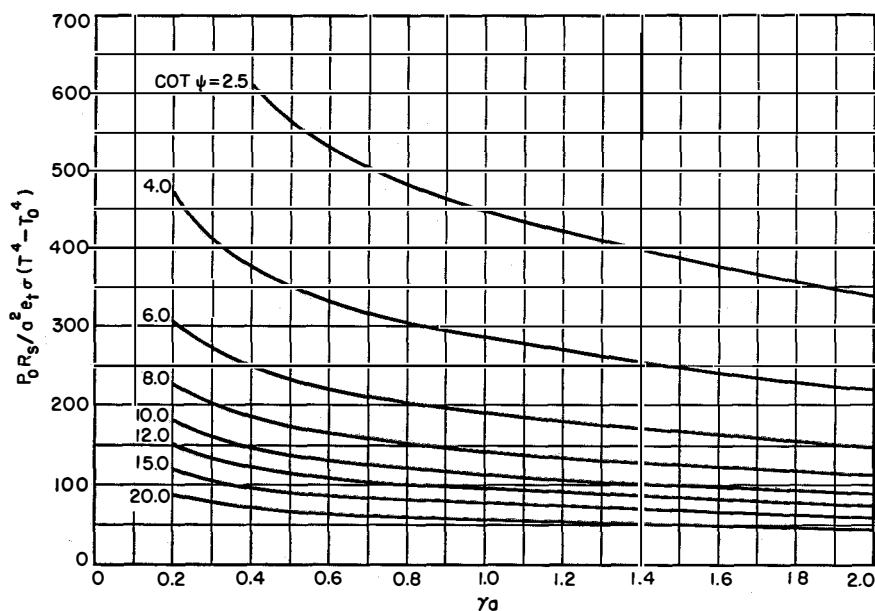
where the argument of all the Bessel functions is γa . Solving for α , we obtain

$$\alpha = -\frac{\pi (\gamma a)^4 F^3(\gamma a)}{a B^2(ka) (\beta a)} P_L \quad (6)$$

Combining (5) and (6),

$$\frac{\alpha a}{R_s} = \frac{(\gamma a)^4 F^3(\gamma a)}{2\pi(120)^2 (ka) (\beta a)} [I_1^2(\gamma a) K_0^2(\gamma a) + I_0^2(\gamma a) K_1^2(\gamma a)] \times \left[\left(\frac{k}{\gamma} \right)^2 \frac{1}{K_0^2(\gamma a)} + \frac{\gamma}{k \cot^2 \psi} \frac{1}{I_1^2(\gamma a) K_1^2(\gamma a)} \right] \quad (7)$$

In Figure 2 are plotted the graphs of $\alpha a/R_s$ versus γa , with $\cot \psi$ as parameter.



2. Power Handling

With a satisfactory method of computing the attenuation of a helix having been given, the remaining problem of power-handling capabilities will be solved.

For a helix structure operating as a radio-frequency transmission line in a vacuum, where conduction losses are insignificant, the initial input power P_0 is

$$P_0 = P_T + P_R, \quad (8)$$

where P_T is the total transmitted power and P_R is the total power radiated from the structure.

Figure 3—Power-handling capability.

$$P_0 R_s / a^2 e_t \sigma (T^4 - T_0^4)$$

plotted against γa . P_0 = input power in watts, R_s = skin-effect resistance in ohms, a = helix mean radius in centimeters, e_t = total emissivity, T = helix temperature in Kelvin scale, T_0 = ambient temperature in Kelvin scale, and $\sigma = 5.67 \times 10^{-12}$ watts per square centimeter per degree⁻⁴ Kelvin.

The total power radiated from a helix structure can be written as

$$P_R = 2\pi azW, \quad (9)$$

where a is the helix radius, z is the axial length, and W is the power radiated per unit area, which is a function of temperature and the helix material as well as of surface conditions. From (1) and Figure 2, it can be shown that for any given helix structure

$$\alpha = kR_s/a, \quad (10)$$

where k is a function of γa and $\cot \psi$. Substituting (10) in (1), the total transmitted power is

$$P_T = P_0 \exp[-2kR_s z/a], \quad (11)$$

and substituting (9) and (11) in (8), we obtain

$$P_0 = \frac{2\pi azW}{1 - \exp[-2kR_s z/a]} \quad (12A)$$

Now assuming that $2kR_s z/a$ is small compared to unity as is true for all structures considered here, the input power P_0 can be expressed as

$$P_0 = \frac{\pi a^2 W}{kR_s}. \quad (12B)$$

The power radiated per unit area W is given by

$$W = e_t \sigma (T^4 - T_0^4) \text{ watts per square centimeter,} \quad (13)$$

where e_t is the total emissivity of the helix material, σ is the Stefan-Boltzmann constant, T is the helix temperature in degrees Kelvin, and T_0 is the ambient temperature.

A graph of $P_0 R_s / a^2 e_t \sigma (T^4 - T_0^4)$ versus γa is plotted for various values of $\cot \psi$ in Figure 3.

3. Effect of Outer, Coaxial, Conducting Cylinder

In practice, the occasion may arise for the use of a helix inside a coaxial, uniformly conducting cylinder as a radio-frequency transmission line (see Figure 1). Since the presence of the outer cylinder will modify the field components with respect to those of a helix in free space, it is to be expected that the degree of attenuation and the power-handling capability would also be altered. Expressions for the field components have been given elsewhere^{3,4}. When these are substituted into (4), the attenuation factor, corresponding to (7), for the case where the helically conducting

³J. H. Bryant, "Some Wave Properties of Helical Conductors," *Electrical Communication*, volume 31, pages 50-56; March, 1954.

⁴H. W. Cole, "Attenuation and Power-Handling Capability of Helix Structures." Paper presented at the Tenth Annual Conference on Electron-Tube Research, Stanford University, California; June, 1953.

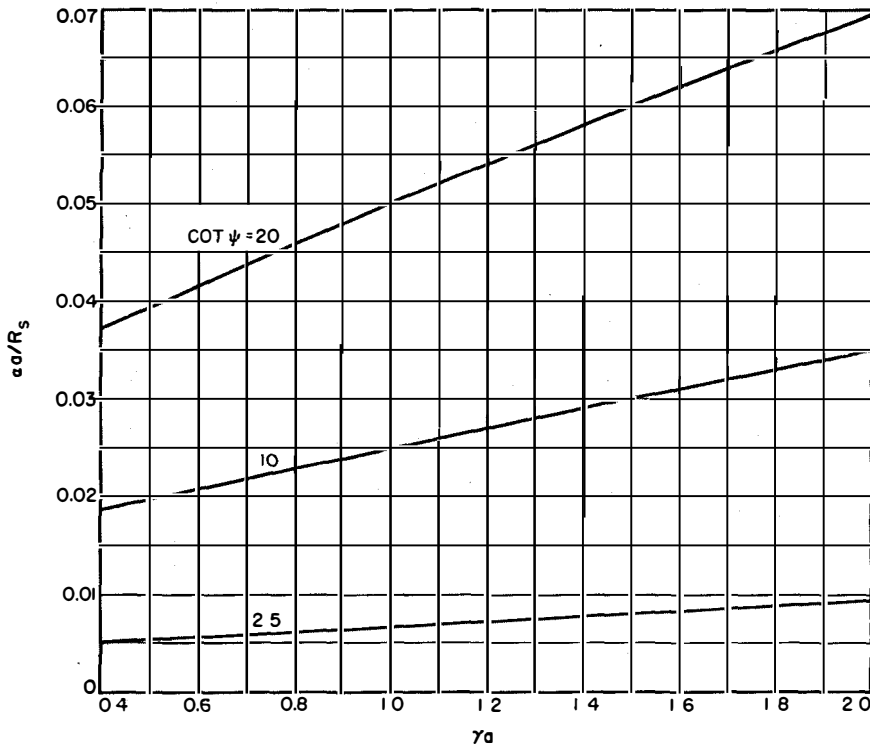


Figure 4—Helix attenuation due to conductor losses for the case where the helically conducting sheet is surrounded by an outer, uniformly conducting, coaxial cylinder of the same material with a diameter twice that of the sheet and at the same temperature.

sheet and surrounding cylinder are of the same material and at the same temperature, becomes

$$\frac{\alpha a}{R_s} = \frac{(\gamma a)^4 F^3(\gamma a, \gamma b)}{2(120)^2 (ka)(\beta a)} \left\{ I_0^2(\gamma a) \left(\frac{k}{\gamma} \right)^2 \left\{ \frac{I_1^2(\gamma a)}{I_0^2(\gamma a)} + \left[\frac{I_1(\gamma a)K_0(\gamma b) + K_1(\gamma a)I_0(\gamma b)}{I_0(\gamma a)K_0(\gamma b) - K_0(\gamma a)I_0(\gamma b)} \right]^2 \right. \right. \\ \left. \left. + \left[\frac{I_1(\gamma b)K_0(\gamma b) + I_0(\gamma b)K_1(\gamma b)}{I_0(\gamma a)K_0(\gamma b) - K_0(\gamma a)I_0(\gamma b)} \right]^2 \right\} + \left(\frac{\gamma}{k} \right)^2 \frac{I_0^2(\gamma a)}{\cot^2 \psi} \left\{ \frac{I_0^2(\gamma a)}{I_1^2(\gamma a)} \right. \right. \\ \left. \left. + \left[\frac{I_0(\gamma a)K_1(\gamma b) + K_0(\gamma a)I_1(\gamma b)}{I_1(\gamma a)K_1(\gamma b) - K_1(\gamma a)I_1(\gamma b)} \right]^2 + \left[\frac{I_1(\gamma b)K_0(\gamma b) + I_0(\gamma b)K_1(\gamma b)}{I_1(\gamma a)K_1(\gamma b) - K_1(\gamma a)I_1(\gamma b)} \right]^2 \right\} \right\}, \quad (14)$$

where b is the inside radius of the cylinder. A graph of this function for a ratio of cylinder-to-helix radius b/a equal to 2 is shown in Figure 4. A corresponding graph for power handling is shown in Figure 5.

By comparing Figure 3 with Figure 5, it may be noted that the effect of the outer, uniformly conducting cylinder of diameter twice the helix diameter seems to be to increase the power-handling capability slightly.

The above computations of power-handling capability were made for a helix without dielectric supports. This approximation has some justification, since although dielectric support material may give added loss, the dielectric supports will give more surface area for heat radiation.

4. Conclusions

A method has been described for calculating the cold insertion loss as well as the power-handling capabilities of a helix structure with or without an outer, uniformly conducting, coaxial cylinder.

5. Glossary of Symbols

- a = radius of the helically conducting cylinder
- b = radius of the outer conducting cylinder
- c = velocity of light

- $F(\gamma a)$ = impedance function. See footnote references 1 and 3
- $F(\gamma a, \gamma b)$ = impedance function. See footnote reference 3
- I_0 = modified Bessel function of first kind and zero order
- I_1 = modified Bessel function of first kind and first order
- $k = \omega/c$
- K_0 = modified Bessel function of second kind and zero order
- K_1 = modified Bessel function of second kind and first order
- v = axial phase velocity
- $\beta = \omega/v$
- $\gamma^2 = \beta^2 - k^2$
- ψ = angle made by the helical direction with a circumference
- ω = radian frequency.

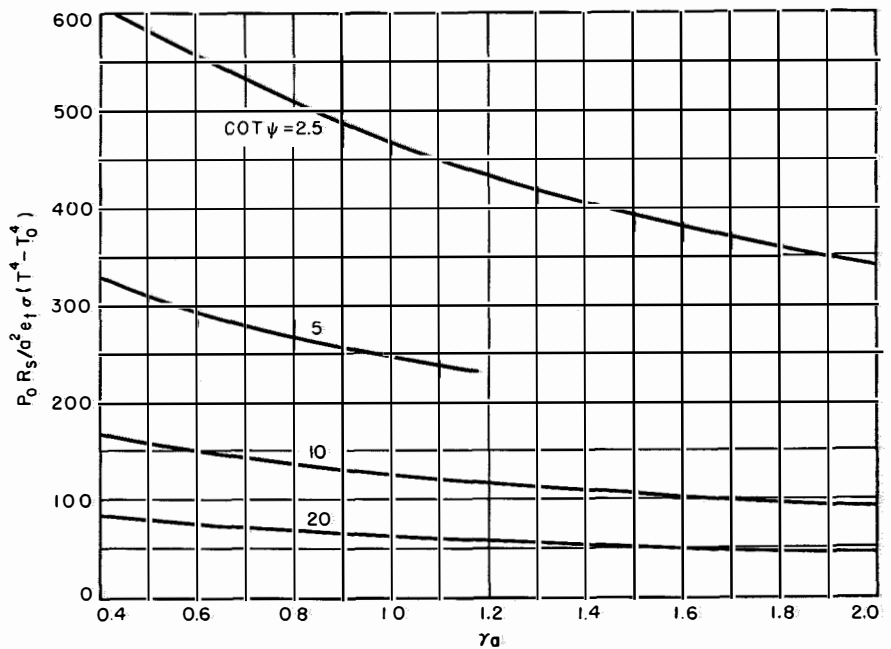


Figure 5—Power-handling capability as limited by the conductor losses and radiation from the helically conducting sheet.

Average Spectrum of a Periodic Series of Identical Pulses Randomly Displaced and Distorted

By R. M. FORTET

Faculté des Sciences de Paris and Laboratoire Central de Télécommunications; Paris, France

PULSE TECHNIQUE has naturally led to the study of the following problem: A signal $S(t)$ consists of a series of pulses that are in principle periodic and identical. In fact, however, the periodicity of the series and the shape of the pulses are distorted either systematically in the case of modulation or in an aleatory manner due to random causes. The problem is to calculate the average spectrum of $S(t)$.

Assuming random causes, general equations are given that are easily derived and readily useable for each particular application. Also, they provide a basis for discussing in particular the influence of the characteristics of the disturbance on the spectrum.

It appears that the spectrum consists of two parts.

A. A discrete spectrum (see (8)), the elements of which coincide with the various harmonics of the theoretical pulse-repetition frequency. The amplitude of these elements depends in a rather intricate manner on the characteristics of the disturbances affecting the shape and the timing of the pulses. A substantial simplification occurs when the shape and timing disturbances are independent (see (11)).

B. A continuous spectrum depending on both distortion and shift (see (6)). If the pulse series were not disturbed, the continuous spectrum would vanish while the discrete spectrum would remain. Consequently, the ratio of the energy contained in the continuous spectrum to the energy present in the discrete spectrum has the same meaning as a noise-to-signal ratio.

Section 2 gives the derivation of both spectrums under as general conditions as possible. Section 3 shows the application of these equations to the specific problem of a periodic pulse series, and section 4 deals with typical particular

cases; approximations are considered that allow mathematical simplifications.

1. Statement of Problem

Let I be a pulse sent at time τ and represented by a (real) function $J(t)$ of the time t , where $-\infty < t < +\infty$. The time function $\mathcal{T}(t) = J(\tau + t)$ will be called the *shape* of the pulse (sending instant referred to zero); it may be noted that for an actual pulse, the shape $\mathcal{T}(t)$ should satisfy

$$\mathcal{T}(t) \equiv 0, \quad \text{for } t < 0 \quad (1)$$

if the instant of emission is defined as the beginning of the pulse. The restriction (1), however, does not play any essential part in the following calculations and, except when otherwise specified, it will not be taken into account. Then let $S(t)$ be a signal consisting of an indefinite series of pulses I_n (with $n = 0, \pm 1, \pm 2, \dots$) of the shape $\mathcal{T}_n(t)$, being emitted at instant τ_n so that I_n is represented by

$$\mathcal{I}_n = \mathcal{T}_n(t - \tau_n)$$

and

$$S(t) = \sum_n \mathcal{I}_n(t - \tau_n).$$

If the τ_n 's are definite numbers and if the $\mathcal{T}_n(t)$ are definite shapes, $S(t)$ is not random, but it becomes random if the τ_n 's and functions $\mathcal{T}_n(t)$ are random. This is what occurs if the emission, periodic with a repetition period T of pulses that are all of the same form $\mathcal{T}(t)$, happens to be randomly perturbed.

Without being restricted immediately to this important case, but in preparation for its examination, let

$$\tau_n = nT + T_n,$$

where T is a positive constant of arbitrary value,

T_n is a random variable, and it is assumed that the random elements

$$X_n = [T_n, \mathcal{T}_n(t)],$$

($n = 0, \pm 1, \pm 2 \dots$) are mutually independent and follow the same law of probability.

The aleatory causes of the disturbance at a time t and at a time $(t + h)$ offer between them a correlation that in general decreases very rapidly when $|h|$ increases and is negligible above a value α of $|h|$. The hypothesis that when $n' \neq n''$, the aleatory elements $X_{n'} = [T_{n'}, \mathcal{T}_{n'}(t)]$ and $X_{n''} = [T_{n''}, \mathcal{T}_{n''}(t)]$ are independent, that is without any correlation, thus means that T is at least equal to α .

It should be noted that with other hypotheses, the mathematical procedures might differ from those given herein. If, for instance, as assumed by Oswald¹ during part of his lecture, the τ_n 's have a Poisson distribution, the problem then pertains to the theory of "aleatory functions derived from a Poisson process," a theory that is now a classical part of the probability theory.²

2. Mean Energy Spectrum of $S(t)$

The mean energy spectrum of $S(t)$ will now be determined. Let $\mathcal{F}_n(\omega)$ be the Fourier transform of $\mathcal{T}_n(t)$; $\mathcal{F}_n(\omega)$ is aleatory as is $\mathcal{T}_n(t)$. Let

$$\left. \begin{aligned} V_n &= \exp [i\omega T_n] \mathcal{F}_n(\omega) \\ G(\omega) &= E(|V_n|^2) \\ &= E(|\mathcal{F}_n(\omega)|^2) \end{aligned} \right\} (2)^3$$

$$\left. \begin{aligned} H(\omega) &= E(V_n) \\ &= E\{\exp [i\omega T_n] \mathcal{F}_n(\omega)\} \end{aligned} \right\} (3)$$

The aleatory variables V_n obeying the same law of probability, $G(\omega)$ and $H(\omega)$ are independent of n .

The Fourier transform of $J_n(t)$ is

$$\exp [i\omega n T] V_n,$$

so that the Fourier transform of the sum of the

¹J. Oswald, Communication at the Symposium on Pulse Theory and Techniques; Paris, France: October, 1953.

²A. Blanc-Lapierre and R. Fortet, "Theorie des Fonctions Aléatoires," Masson Edition; Paris, France: 1953.

³The symbol $E(x)$ represents the mathematical expectation of the random variable x .

($2N + 1$) pulses $I_{-N}, I_{-N+1}, I_{-N+2}, \dots, I_0, I_1, \dots, I_{N-1}, I_N$ is

$$\phi_n(\omega) = \sum_{n=-N}^N \exp [in\omega T] V_n.$$

It follows that for this same sum, the mean energy spectrum, per pulse and in the sense of the law of probabilities, has a distribution density of

$$f_n(\omega) = \frac{E[|\phi_n(\omega)|^2]}{2N + 1}. \quad (4)$$

A rather elementary derivation, which shall not be detailed here, gives

$$f_N(\omega) = G(\omega) - |H(\omega)|^2 + \frac{|H(\omega)|^2}{2N + 1} \left\{ \frac{\sin [(N + \frac{1}{2})\omega T]}{\sin (\omega/2)T} \right\}^2. \quad (5)$$

Let $F_N(\omega)$ be the distribution function of density $f_N(\omega)$, that is

$$dF_N(\omega) = f_N(\omega) d\omega.$$

Let

$$f(\omega) = G(\omega) - |H(\omega)|^2 = E[|V_N - E(V_N)|^2] \quad (6)$$

and let $F_c(\omega)$ be the distribution function of density $f(\omega)$, that is

$$dF_c(\omega) = f(\omega) d\omega.$$

It will be recalled that

$$\int_{-\infty}^{+\infty} \frac{\sin^2 x}{x^2} dx = \pi. \quad (7)$$

K being any integer ($K = 0, \pm 1, \pm 2 \dots$), taking (7) into account, and provided $H(\omega)$ is continuous, it is evident that

$$\lim_{\Delta\omega \rightarrow 0} \lim_{N \rightarrow +\infty} \int_{(2K\pi/T) - \Delta\omega}^{(2K\pi/T) + \Delta\omega} f_N(\omega) d\omega = \frac{2\pi}{T} \left| H\left(\frac{2K\pi}{T}\right) \right|^2. \quad (8)$$

Now let $F_d(\omega)$ be the totally discontinuous distribution function that varies in steps located at abscissas $2K\pi/T$ (with $K = 0, \pm 1, \pm 2 \dots$), the step at abscissa $(2K\pi)/T$ having an amplitude

$$\frac{2\pi}{T} \left| H\left(\frac{2K\pi}{T}\right) \right|^2.$$

It will be seen that the distribution function $F_N(\omega)$, when $N \rightarrow +\infty$, approaches the limiting

distribution function defined by $F(\omega)$.

$$F(\omega) = F_c(\omega) + F_d(\omega). \quad (9)$$

$F(\omega)$ thus constitutes the mean energy spectrum of the signal $S(t)$: this spectrum comprises a continuous spectrum with a density $f(\omega)$ defined by (6) and a discrete spectrum defined by $F_d(\omega)$ or by (8).

It is noteworthy that the (mean) spectrum (9) was obtained by taking a "mean per-pulse" value. A "time-interval mean value" might be preferred considering the time interval $(-NT, +NT)$ and the truncated signal

$$\begin{aligned} S_N(t) &= S(t), \quad \text{for } |t| \leq NT, \\ S_N(t) &= 0, \quad \text{for } |t| > NT. \end{aligned}$$

Instead of starting from $f_N(\omega)$, start from $f'_N(\omega)$ defined by

$$f'_N(\omega) = \frac{1}{2NT} E[|\phi'_N(\omega)|^2],$$

$\phi'_N(\omega)$ designating the Fourier transform of $S_N(t)$ and the sequence of operations being the same as above. It may be shown without any difficulty that within a factor $1/T$, the same spectrum $F(\omega)$ is obtained; at least under certain conditions that, however, will always be satisfied.

2.1 DERIVATION OF $G(\omega)$ AND $H(\omega)$

If

$$\begin{aligned} \mathfrak{F}^o(\omega) &= E[\mathfrak{F}_n(\omega)] \\ K(\omega) &= E[|\Delta_n(\omega)|^2] \\ \mathfrak{F}_n(\omega) &= \mathfrak{F}^o(\omega) + \Delta_n(\omega), \end{aligned}$$

then

$$G(\omega) = |\mathfrak{F}^o(\omega)|^2 + K(\omega). \quad (10)$$

If there is any correlation whatsoever between T_n and $\Delta_n(\omega)$, the evaluation of $H(\omega)$ may be complicated; but if T_n and $\Delta_n(\omega)$ are independent, setting

$$\varphi(\omega) = E\{\exp[i\omega T_n]\}$$

so that $\varphi(\omega)$ is the characteristic function of the variable T_n ,

$$H(\omega) = \varphi(\omega)\mathfrak{F}^o(\omega) \quad (11)$$

is obtained and

$$f(\omega) = [1 - |\varphi(\omega)|^2]|\mathfrak{F}^o(\omega)|^2 + K(\omega). \quad (12)$$

If $T_n = 0$ (no displacement of the instant of emission), $\varphi(\omega) = 1$ and gives merely

$$f(\omega) = K(\omega). \quad (13)$$

3. Periodically Transmitted Pulses of the Same Shape That Are Aleatorily Displaced and Distorted, Noise-to-Signal Ratio

Henceforth, consider more particularly the case mentioned in section 1, where the T_n 's are due to a sequence of pulses theoretically emitted periodically at the instants nT and of the same shape $\mathcal{T}(t)$ but aleatorily distorted and displaced. Let ρ be the ratio of the total energy of the continuous spectrum to the total energy of the discontinuous spectrum.

$$\rho = \frac{\int_{-\infty}^{+\infty} [G(\omega) - |H(\omega)|^2] d\omega}{\frac{2\pi}{T} \sum_K \left| H\left(\frac{2K\pi}{T}\right) \right|^2}. \quad (14)$$

This ratio is interesting in the general case, but from the present standpoint it becomes still more interesting as it assumes very nearly the meaning of the noise-to-signal ratio. In fact, in the absence of any aleatory disturbance in the transmission, then

$$\begin{aligned} T_n &\equiv 0, \\ \mathfrak{F}_n(\omega) &\equiv \mathfrak{F}(\omega), \end{aligned}$$

designating by $\mathfrak{F}(\omega)$ the Fourier transform of $\mathcal{T}(t)$; under such conditions the continuous spectrum would vanish and ρ would be zero.

Regarding the derivation of ρ , the following general remarks may be made: $V_n - E(V_n)$ is the Fourier transform of

$$\mathcal{T}_n(t - T_n) - E[\mathcal{T}_n(t - T_n)].$$

Set

$$\left. \begin{aligned} \mathcal{E} &= E \left[\int_{-\infty}^{+\infty} |\mathcal{T}_n(t - T_n)|^2 dt \right] \\ &= E \left[\int_{-\infty}^{+\infty} |\mathcal{T}_n(t)|^2 dt \right], \end{aligned} \right\} (15)$$

so that \mathcal{E} is the mean energy of one pulse, it will be noted that \mathcal{E} does not depend on the law of probability of T_n . By virtue of the properties of the Fourier transform, the numerator of ρ may be written

$$\mathcal{E} - \int_{-\infty}^{+\infty} |E[\mathcal{T}_n(t - T_n)]|^2 dt. \quad (16)$$

On the other hand, and always by virtue of the properties of the Fourier transform,

$$\int_{-\infty}^{+\infty} f_n(\omega) d\omega = \frac{1}{2N+1} E \left[\int_{-\infty}^{+\infty} \left| \sum_{n=-N}^N \mathcal{F}_n(t - nT - T_n) \right|^2 dt \right].$$

Suppose there is a zero probability of overlapping for two pulses I_n, I_m with differing indices n and m , that is, there is a zero probability for the product

$$\mathcal{F}_n(t - nT - T_n) \times \mathcal{F}_m(t - mT - T_m)$$

to differ from zero. This condition will often be met in practice or at least very approximately obtained. Then

$$\left. \begin{aligned} \int_{-\infty}^{+\infty} dF(\omega) &= \int_{-\infty}^{+\infty} f(\omega) d\omega + \int_{-\infty}^{+\infty} dF_d(\omega) \\ &= \lim_{N \rightarrow \infty} \int_{-\infty}^{+\infty} f_n(\omega) d\omega = \mathcal{E}. \end{aligned} \right\} (17)$$

Now $\int_{-\infty}^{+\infty} dF_d(\omega)$ is the denominator of ρ and from (16),

$$\rho = \frac{\mathcal{E} - \int_{-\infty}^{+\infty} |E[\mathcal{F}_n(t - T_n)]|^2 dt}{\int_{-\infty}^{+\infty} |E[\mathcal{F}_n(t - T_n)]|^2 dt}. \quad (18)$$

On the other hand, in case (12) applies,

$$\rho = \frac{\int_{-\infty}^{+\infty} \{ [1 - |\varphi(\omega)|^2] |\mathcal{F}^*(\omega)|^2 + K(\omega) \} d\omega}{\frac{2\pi}{T} \sum_K \left| \varphi \left(\frac{2K\pi}{T} \right) \right|^2 \left| \mathcal{F}^* \left(\frac{2K\pi}{T} \right) \right|^2}. \quad (19)$$

In general, the deformations will be small so that if not strictly at least approximately

$$\mathcal{F}^o(\omega) \approx \mathcal{F}(\omega).$$

If in addition $T_n \equiv 0$ (no displacement of the time of emission), the result will be that

$$\rho = \frac{\int_{-\infty}^{+\infty} K(\omega) d\omega}{\frac{2\pi}{T} \sum_K \left| \mathcal{F} \left(\frac{2K\pi}{T} \right) \right|^2}. \quad (20)$$

Note that the numerator of ρ is generally small and approximations in its evaluation must be made cautiously.

4. Periodically Emitted Pulses of the Same Shape That Are Randomly Displaced and Distorted

A good practical representation, at least approximate, of the distortion may be had by assuming it to be caused by only two variations.

A. Amplitude variations such that $\mathcal{F}_n(\omega)$ instead of being equal to $\mathcal{F}(\omega)$ is equal to

$$(1 + A_n)\mathcal{F}_n(\omega),$$

where A_n is a real random variable, arbitrary in general except of course that the condition

$$A_n \geq -1 \quad (21)$$

should be satisfied.

B. Spread variations such that $\mathcal{F}_n(\omega)$ instead of being equal to $\mathcal{F}(\omega)$ is equal to

$$(1 + U_n)\mathcal{F}[(1 + U_n)\omega],$$

where U_n is an arbitrary random variable satisfying the condition.

$$U_n \geq -1. \quad (22)$$

The *simultaneous* actions of causes A and B will thus give

$$\mathcal{F}_n(\omega) = (1 + A_n)(1 + U_n)\mathcal{F}[(1 + U_n)\omega]. \quad (23)$$

$T_n, A_n,$ and U_n may be correlated in any manner; in fact, normally A_n and U_n admit 0 as a central value and T_n also; this does not necessarily imply that $E(A_n) = E(U_n) = E(T_n) = 0$, but these equalities will hold approximately. In addition, $A_n, U_n,$ and T_n will be but slightly dispersed about the value 0 so that the representation

$$\mathcal{F}_n(\omega) \approx (1 + A_n + U_n)\mathcal{F}[(1 + U_n)\omega] \quad (24)$$

may be substituted for (19) and even for values of ω not too large

$$\mathcal{F}_n(\omega) \approx \mathcal{F}(\omega) + \mathcal{F}(\omega)A_n + [\mathcal{F}(\omega) + \omega\mathcal{F}'(\omega)]U_n,$$

where $\mathcal{F}'(\omega) = (d/d\omega)\mathcal{F}(\omega)$ so that for values of ω not too large, it will be sufficient to know $\mathcal{F}(\omega), E(A_n^2), E(U_n^2), E(A_n U_n),$ and $\varphi(\omega)$ to determine the continuous and discontinuous spectrums.

It was in this manner (representation of deformations by means of A_n and U_n) that the prob-

lem was attacked by MacFarlane⁴, who for lack of a general theory treated successively and with increasing precision the cases:

- A. $T_n \equiv U_n \equiv 0$
- B. $A_n \equiv U_n \equiv 0$
- C. $A_n \equiv T_n \equiv 0$.

4.1 EXAMPLE IN WHICH THE DISTURBANCE AFFECTS ONLY THE SPREAD OF THE PULSES

Resuming case C for which McFarlane only outlined the solution and taking precisely the example he considered in which:

A. The pulse $\mathcal{T}(t)$ is rectangular. Referring it to its middle instant rather than to the instant of its emission, this amounts to assuming

$$\left. \begin{aligned} \mathcal{T}(t) &= h, \quad \text{for } (t) \leq \tau \\ \mathcal{T}(t) &= 0, \quad \text{for } (t) > \tau, \end{aligned} \right\} (25)$$

in which $h > 0$ for the height of the pulse and $2\tau > 0$ for the width of the pulse.

B. The factor U_n follows a Laplacian law of zero mathematical expectation with a quadratic mean deviation σ (where $\sigma > 0$). Although (22) is not strictly fulfilled, it is approximately and sufficiently fulfilled if σ is small compared with unity. Then

$$\begin{aligned} \mathcal{F}_n(\omega) &= 2h \frac{\sin[\omega\tau(1+U_n)]}{\omega} \\ \mathcal{F}^o(\omega) &= \frac{2h}{\omega} \exp[-\sigma^2\tau^2\omega^2] \sin \tau\omega \end{aligned}$$

so that the discontinuous spectrum is given by the values

$$\begin{aligned} \frac{2\pi}{T} \left| \mathcal{F}^o\left(\frac{2K\pi}{T}\right) \right|^2 &= \frac{2h^2T}{T} \cdot \frac{1}{K^2} \\ &\times \exp\left[-8\sigma^2\pi^2\left(\frac{\tau}{T}\right)^2 K^2\right] \sin^2\left(2K\pi\frac{\tau}{T}\right). \end{aligned} \quad (26)$$

⁴G. G. MacFarlane, "On the Energy-Spectrum of an Almost Periodic Succession of Pulses," *Proceedings of the IRE*, volume 37, pages 1139-1143; October, 1949.

On the other hand

$$\begin{aligned} K(\omega) &= \frac{2h^2}{\omega^2} \{1 - \exp[-2\sigma^2\tau^2\omega^2]\} \\ &\times \{1 + \exp[2\sigma^2\tau^2\omega^2] \cos 2\tau\omega\}. \end{aligned} \quad (27)$$

Equation (27) gives the value of $f(\omega)$ of the continuous-spectrum density. To evaluate ρ , first determine its numerator as in (16). Then

$$\left. \begin{aligned} \mathcal{T}_n(t) &= \mathcal{T} \frac{t}{1+U_n} \\ \int_{-\infty}^{+\infty} |\mathcal{T}_n(t)|^2 dt & \\ &= (1+U_n) \int_{-\infty}^{+\infty} |\mathcal{T}(t)|^2 dt \end{aligned} \right\} (28)$$

$$\mathcal{E} = \int_{-\infty}^{+\infty} |\mathcal{T}(t)|^2 dt. \quad (29)$$

Note that (28) is always valid and the (29) holds only under the condition that $E(U_n) = 0$; in the present case where $\mathcal{T}(t)$ is given by (25).

$$\mathcal{E} = 2\tau h^2. \quad (30)$$

On the other hand, $\mathcal{T}[t/(1+U_n)]$ is equal to 0 or h . If it is assumed that $\sigma \ll 1$, which justifies certain approximations and makes it possible in particular to neglect cases where $(1+U_n) < 0$, then

$$\int_{-\infty}^{+\infty} |E[\mathcal{T}_n(t)]|^2 dt \approx 2\tau h^2(1 - \sigma/\pi^{1/2}), \quad (31)$$

which gives for the numerator of ρ

$$\frac{2}{\pi^{1/2}} \tau\sigma h^2.$$

If τ is small compared to T , the approximate expression (18) for ρ may be accepted and

$$\rho \approx \sigma/\pi^{1/2}, \quad (32)$$

which may be expressed as follows: *the noise-to-signal ratio is proportional to the relative variation in spread.*

Telephone Statistics of the World*

MORE THAN 84 million telephones were in service throughout the world on January 1, 1953, representing a gain of 5 million or about 6 percent over the previous year's total. The number of telephones in use has doubled since the beginning of 1940.

For the purpose of this compilation, only those telephones that can be connected to a commercial public system are counted. Ten countries reported more than 1 million telephones in service on January 1, 1953: United States, United Kingdom, Canada, Western Germany, France, Japan, Sweden, Italy, Australia, and Switzerland. Of the world's principal countries, 8 had more than 15 telephones per 100 of the population: United States (30.3), Sweden (26.4), Canada (22.9), Switzerland (20.9), New Zealand (20.9), Denmark (18.1), Australia (15.3), and Norway (15.1).

Statistics reported for 20 large countries show that the over-all average number of calls per

capita for those countries increased from 136 in 1948 to 153 in 1952. Comparable figures for the United States are 343 and 382.

A subdivision in certain of the tables shows the number of telephones operated under private and government ownership, respectively. The latter category has reference to municipal and state, as well as national, ownership. Although the American Telephone and Telegraph Company and its subsidiaries operated about 80 percent of this country's 48,056,308 telephones on January 1, 1953, there were nearly 5300 other privately owned companies that furnished service in the United States.

The purpose of this compilation is to present telephone statistics as of January 1, 1953. However, it is worthy of mention that in November 1953 the United States attained its 50-millionth telephone, which was presented to President Eisenhower by representatives of this nation's telephone industry.

TELEPHONES IN CONTINENTAL AREAS

Partly estimated; statistics reported as of other dates have been adjusted to January 1, 1953

Continental Area	Total Telephones			Privately Owned		Automatic (Dial)	
	Number	Percent of Total World	Per 100 Population	Number	Percent of Total	Number	Percent of Total
North America	51,430,400	61.1	29.7	50,960,300	99.1	37,743,300	73.4
Middle America	627,400	0.7	1.2	568,800	90.7	445,300	71.0
South America	2,094,800	2.5	1.8	1,021,500	48.8	1,614,400	77.1
Europe	23,785,100	28.2	4.0	3,762,600	15.8	17,184,000	72.2
Africa	1,084,300	1.3	0.5	20,000	1.8	741,900	68.4
Asia	3,268,000	3.9	0.2	209,100	6.4	752,100	23.0
Oceania	1,910,000	2.3	12.2	134,500	7.0	1,252,800	65.6
World	84,200,000	100.0	3.4	56,676,800	67.3	59,733,800	70.9
United States	48,056,308	57.1	30.3	48,056,308	100.0	35,500,000	73.9

* Abridgement from a booklet issued by the American Telephone and Telegraph Company; New York, New York.

TELEPHONES IN COUNTRIES OF THE WORLD AS OF JANUARY 1, 1953

Country	Total Telephones	Per 100 Population	Percent Automatic (Dial)	Ownership	
				Private	Government
NORTH AMERICA					
Alaska	21,932	13.7	60.7	21,789	143
Canada (1)	3,352,000	22.9	66.5	2,882,200	469,800
Greenland	0	—	—	—	—
Saint Pierre and Miquelon	154	3.3	0	0	154
United States	48,056,308	30.3	73.9	48,056,308	0
MIDDLE AMERICA					
Bahamas	5,159	6.1	99.2	0	5,159
Barbados	4,984	2.3	97.3	4,984	0
Bermuda	7,100	18.1	100	7,100	0
British Honduras	783	1.1	0	0	783
Canal Zone (2) (3)	6,614	22.0	100	0	6,614
Costa Rica	11,179	1.3	0	10,179	262
Cuba (1)	139,646	2.4	86.1	139,146	500
Dominican Republic	8,004	0.4	70	7,854	150
El Salvador	8,502	0.4	71.2	0	8,502
Guadeloupe	1,191	0.4	0	0	1,191
Guatemala	6,348	0.2	83.4	0	6,348
Haiti (1)	4,132	0.1	90.9	0	4,132
Honduras	2,500	0.2	55	0	2,500
Jamaica	16,132	1.1	97.4	16,132	0
Leeward Islands	893	0.8	0	0	893
Martinique	2,961	1.1	0	0	2,961
Mexico	312,225	1.2	66.5	310,615	1,610
Netherlands Antilles	6,594	3.7	96.9	0	6,594
Nicaragua	3,497	0.3	0	0	3,497
Panama	14,553	1.8	82	14,553	0
Puerto Rico	42,954	1.9	52.6	39,947	3,007
Trinidad and Tobago	17,585	2.6	85.9	17,585	0
Virgin Islands (U. S.)	1,685	6.2	0	0	1,685
Windward Islands					
Dominica	307	0.5	0	0	307
Grenada	850	1.2	0	0	850
Saint Lucia	372	0.5	0	0	372
Saint Vincent	410	0.6	0	0	410
Total	1,939	0.7	0	0	1,939
SOUTH AMERICA					
Argentina	928,724	5.1	79.2	73,382	855,342
Bolivia	10,885	0.4	95.1	10,885	0
Brazil	636,317	1.2	79.2	634,817	1,500
British Guiana	3,536	0.8	8	0	3,536
Chile	140,769	2.3	67	140,769	0
Colombia	114,542	1.0	50.6	20,781	93,761
Ecuador	11,500	0.3	60.9	1,500	10,000
Falkland Islands	312	13.6	0	0	312
French Guiana	304	1.0	0	0	304
Paraguay	5,627	0.4	85.4	0	5,627
Peru	56,576	0.6	82.4	56,576	0
Surinam	2,259	1.0	91.6	0	2,259
Uruguay	101,806	4.1	73	1,085	100,721
Venezuela	81,690	1.5	94	81,690	0
EUROPE					
Albania (1)	1,700	0.1	0	0	1,700
Andorra	100	2.0	0	0	100
Austria	448,936	6.5	78.9	0	448,936
Belgium	743,988	8.5	76.5	0	743,988
Bulgaria (1)	61,000	0.8	43	0	61,000
Channel Islands (5)					
Guernsey and Dependencies	9,238	20.1	0	0	9,238
Jersey	11,575	20.2	0	0	11,575
Total	20,813	20.2	0	0	20,813
Czechoslovakia (4)	350,708	2.9	59.4	0	350,708
Denmark	791,096	18.1	35.5	751,881	39,215
Finland	383,985	9.3	60.4	331,979	52,006
France	2,644,910	6.2	67.3	0	2,644,910
Germany, Democratic Republic (1)	240,000	1.3	60	0	240,000
Germany, Federal Republic (5)	2,976,953	6.1	87.3	0	2,976,953
Gibraltar	1,381	6.0	89.4	0	1,381
Greece	95,500	1.2	94	95,500	0
Hungary (1)	120,000	1.3	74	0	120,000

(1) Data partly estimated.

(2) Excluding telephone systems of the military forces.

(3) June 30, 1952.

(4) January 1, 1948 (latest official statistics).

(5) March 31, 1953.

(6) January 1, 1936 (latest official statistics).

(7) Includes the Isle of Man, but not the Channel Islands.

(8) Exclusive of Formosa.

+ Less than 0.1.

TELEPHONES IN COUNTRIES OF THE WORLD AS OF JANUARY 1, 1953—Continued

Country	Total Telephones	Per 100 Population	Percent Automatic (Dial)	Ownership	
				Private	Government
EUROPE—Continued					
Iceland	22,163	14.8	64.4	0	22,163
Ireland	97,388	3.3	65.2	0	97,388
Italy	1,540,909	3.3	93.3	1,540,909	0
Liechtenstein	2,143	15.3	100	0	2,143
Luxemburg	25,912	8.6	70.8	0	25,912
Malta and Gozo	7,617	2.4	0	0	7,617
Monaco	5,874	29.1	100	0	5,874
Netherlands	896,294	8.6	91.4	0	896,294
Norway	503,223	15.1	60.4	84,220	419,003
Poland	235,000	0.9	67.2	0	235,000
Portugal	186,154	2.2	56.9	118,578	67,576
Rumania	140,000	0.9	75	0	140,000
Russia	861,181	0.5	19.9	0	861,181
Saar	40,067	4.2	97.8	0	40,067
San Marino	280	2.2	0	0	280
Spain	819,553	2.9	77.8	805,346	14,207
Sweden	1,889,353	26.4	68.6	861	1,888,492
Switzerland	1,012,590	20.9	97.8	0	1,012,590
Trieste	31,948	8.7	98.9	31,281	667
United Kingdom	5,915,972	11.7	73.7	0	5,915,972
Yugoslavia	144,508	0.9	67.6	0	144,508
AFRICA					
Algeria	109,220	1.2	73.3	0	109,220
Anglo-Egyptian Sudan	9,658	0.1	76.3	0	9,658
Basutoland	452	+	0	0	452
Bechuanaland Protectorate	123	+	0	0	123
Belgian Congo	9,415	+	57	0	9,415
British East Africa					
Kenya	17,009	0.3	71.3	0	17,009
Tanganyika	6,855	+	57.6	0	6,855
Uganda	5,155	0.1	78.4	0	5,155
Total	29,019	0.2	69.3	0	29,019
British West Africa					
Gambia	324	0.1	100	0	324
Gold Coast	8,519	0.2	36.6	0	8,519
Nigeria	13,279	+	3	0	13,279
Sierra Leone	1,382	+	66.9	0	1,382
Total	23,504	+	20.3	0	23,504
Comoro Archipelago	0	—	—	—	—
Egypt	133,315	0.6	76.7	0	133,315
Ethiopia	4,939	+	73.7	0	4,939
French Cameroon	1,582	+	0	0	1,582
French Equatorial Africa	1,668	+	47.2	0	1,668
French Somaliland	531	1.1	0	0	531
French Togo	600	+	0	0	600
French West Africa	17,072	0.1	37	0	17,072
Liberia	417	+	100	0	417
Libya	5,214	0.4	77.5	0	5,214
Madagascar	6,800	0.2	44.1	0	6,800
Mauritius	5,524	1.1	5.6	0	5,524
Morocco					
French Zone	70,725	0.7	78.5	0	70,725
Spanish Zone	11,519	1.1	57.9	11,519	0
Tangier Zone	8,273	8.3	96.9	8,017	256
Total	90,517	0.8	77.6	19,536	70,981
Nyasaland Protectorate	1,595	+	84.1	0	1,595
Portuguese Africa					
Angola	2,189	+	74	0	2,189
Cape Verde Islands	126	+	0	0	126
Mozambique	5,573	0.1	72.2	0	5,573
Portuguese Guinea	193	+	80.3	0	193
South Tome and Principe	248	0.4	0	0	248
Total	8,329	+	69.6	0	8,329
Rhodesia, Northern	4,577	0.2	87.2	0	4,577
Rhodesia, Southern	31,666	1.4	76.7	0	31,666
Réunion	3,379	1.3	0	0	3,379
Saint Helena	89	1.8	0	0	89
Seychelles and Dependencies					
Somalia	831	+	0	0	831
Somaliland Protectorate	215	+	0	0	215
South West Africa	5,772	1.3	48.8	0	5,772
Spanish Guinea	465	0.2	68.4	465	0
Spanish West Africa					
Ifni	105	0.3	0	0	105
Spanish Sahara	52	0.1	0	0	52
Total	157	0.2	0	0	157

(1)-(7), +, see page 289.

TELEPHONES IN COUNTRIES OF THE WORLD AS OF JANUARY 1, 1953—Continued

Country	Total Telephones	Per 100 Population	Percent Automatic (Dial)	Ownership	
				Private	Government
AFRICA—Continued					
Swaziland	504	0.2	1.4	0	504
Tunisia	29,085	0.8	57.7	0	29,085
Union of South Africa	557,772	4.3	69.1	0	557,772
Zanzibar and Pemba	1,000	0.4	0	0	1,000
ASIA					
Aden, Colony of	1,496	1.5	100	0	1,496
Afghanistan	5,612	+	29.4	0	5,612
Bahrain	920	0.8	100	920	0
British Borneo					
Brunei	105	0.2	0	0	105
North Borneo	743	0.2	53.6	0	743
Sarawak	720	0.1	0	0	720
Total	1,568	0.2	25.4	0	1,568
Burma	4,651	+	0	0	4,651
Cambodia	2,000	+	0	0	2,000
Ceylon	20,420	0.3	94.3	0	20,420
China	264,000	+	70	100,000	164,000
Cyprus	7,314	1.5	73.2	7,314	0
Formosa	30,757	0.4	44.5	0	30,757
French India	76	+	100	0	76
Hong Kong	37,025	1.7	100	37,025	0
India	199,768	+	50.7	1,966	197,802
Indonesia	63,360	0.2	2	0	63,360
Iran	31,000	0.2	56.5	0	31,000
Iraq	25,257	0.5	64.1	0	25,257
Israel	40,761	2.5	89.2	0	40,761
Japan	2,250,000	2.6	40.1	0	2,250,000
Jordan	5,152	0.4	85.8	0	5,152
Korea, South	16,529	+	21.7	0	16,529
Kuwait	739	0.4	70.4	739	0
Laos	208	+	0	0	208
Lebanon	22,362	1.7	82.8	0	22,362
Malaya	33,487	0.6	45.1	1,135	32,352
Muscat and Oman	124	+	100	124	0
Pakistan	23,472	+	50.5	0	23,472
Philippine Republic	34,616	0.2	66.6	32,045	2,571
Portuguese Asia					
Macao	1,666	0.6	99.4	0	1,666
Portuguese India	224	+	0	0	224
Total	1,890	0.2	87.6	0	1,890
Saudi Arabia	7,083	0.1	0	0	7,083
Singapore	25,281	2.3	100	25,281	0
Syria	25,000	0.7	66	0	25,000
Thailand	7,181	+	100	0	7,181
Turkey	97,176	0.4	88.8	0	97,176
Viet-Nam	12,553	+	41.1	0	12,553
Yemen	0	—	—	—	—
Other Places	30,000	0.1	25	0	30,000
OCEANIA					
American Samoa	292	1.5	100	0	292
Australia	1,342,961	15.3	65.3	0	1,342,961
Fiji	2,750	0.9	0	0	2,750
French Oceania					
French Settlements	678	1.1	0	0	678
New Caledonia	1,789	2.9	0	0	1,789
Total	2,467	2.0	0	0	2,467
Hawaii	134,449	25.6	94.2	134,449	0
Netherlands New Guinea	667	+	0	0	667
New Zealand	425,186	20.9	59.1	0	425,186
Pacific Islands (British)					
Gilbert and Ellice Islands	64	0.2	0	0	64
New Hebrides Condominium	87	0.2	0	0	87
Pitcairn Islands	0	—	—	—	—
Solomon Islands Protectorate	0	—	—	—	—
Tonga (Friendly) Islands	241	0.5	0	0	241
Total	392	0.2	0	0	392
Papua-New Guinea	2,344	0.2	0	0	2,344
Portuguese Timor	299	+	0	0	299
South Seas Mandate (United States)					
Caroline Islands	105	0.3	0	0	105
Guam	4,407	5.8	61.4	0	4,407
Mariana Islands (Less Guam)	770	11.0	0	0	770
Marshall Islands	150	1.4	0	0	150
Total	5,432	4.1	49.8	0	5,432
Western Samoa	425	0.5	0	0	425

(1)-(8), +, see page 289.

TELEPHONE CONVERSATIONS FOR THE YEAR 1952

Conversation data were not available for all countries

Country	Number of Conversations in Thousands			Conversations Per Capita
	Local	Toll	Total	
Algeria	54,500	18,800*	73,300	8.0
Argentina	3,017,700	36,700	3,054,400	169.2
Australia	973,100	71,500	1,044,600	120.8
Belgium	433,800	65,500	499,300	57.2
Brazil	1,893,900	36,400	1,930,300	35.3
Canada (Preliminary)	5,482,800	126,700	5,609,500	388.7
Ceylon	43,000	3,300	46,300	5.8
Chile	371,000	20,800	391,800	66.6
Colombia	413,400	3,400	416,800	36.7
Cuba	775,000	5,000	780,000	139.5
Denmark	950,100	162,700	1,112,800	255.8
Egypt	444,800	10,600	455,400	21.3
Finland	551,900	75,200	627,100	153.3
France	1,312,700	452,900	1,765,600	41.5
Germany, Federal Republic (1)	1,952,400	407,000	2,359,400	48.7
Iceland	52,000	1,300	53,300	360.1
Ireland	77,400	11,500	88,900	30.2
Israel	74,800	3,400	78,200	48.8
Italy	2,420,000	153,500*	2,573,500	54.9
Jamaica	43,900	700	44,600	30.9
Japan (1)	9,480,500	490,200	9,970,700	116.5
Luxemburg	9,900	8,200*	18,100	60.3
Malaya	93,500	11,100	104,600	19.1
Mexico	723,400	9,100	732,500	28.0
Netherlands	607,400	188,600	796,000	76.7
Norway (2)	488,000	51,500	539,500	162.9
Paraguay	20,500	200	20,700	14.5
Peru	185,900	2,300	188,200	21.6
Philippine Republic	242,500	500	243,000	11.8
Portugal	174,300	47,400	221,700	25.9
Puerto Rico	92,800	2,900	95,700	42.7
Saar	45,000	2,300	47,400	49.4
Spain	1,698,000	70,000	1,768,000	62.5
Sweden (3)	2,072,200	119,200	2,191,400	306.4
Switzerland	420,000	337,100*	757,100	156.9
Tunisia	15,500	6,900	22,400	6.4
Turkey	102,100	14,700	116,800	5.3
Union of South Africa (1)	670,000	44,400	714,400	55.9
United Kingdom (1) (4)	3,198,200	265,300	3,463,500	68.7
United States	57,875,000	2,130,000	60,005,000	382.1
Uruguay	298,500	4,400	302,800	123.8
Venezuela	319,100	1,400	320,500	61.5

(1) Year ended March 31, 1953.

(2) Year ended June 30, 1952.

(3) Year ended June 30, 1953.

(4) Includes the Isle of Man, but not the Channel Islands.

* Three-minute units.

United States Patents Issued to International Telephone and Telegraph System; May-July, 1954

UNITED STATES patents numbering 26 were issued between May 1 and July 31, 1954 to companies in the International System. The inventors, titles, and numbers of these patents are given below; summaries of several that are of more-than-usual interest are included. In cases where corresponding Canadian patents have already issued, their numbers are given in parentheses.

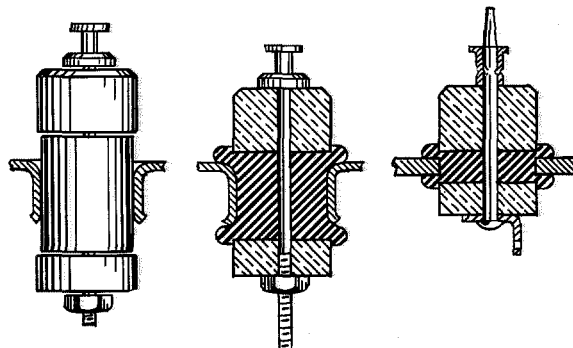
- H. H. Abelew, Electronic Timing Relay, 2,678,390
- E. S. L. Beale, Circuits for Cathode-Ray Oscilloscopes, 2,678,406 (616,752)
- J. C. Beveridge, Manufacture of Coaxial-Conductor Electric Cables, 2,677,879
- R. P. Boyer, Capacitor-Timed Relay Interrupter, 2,685,052
- E. M. Bradburd, Neutralizing Circuit for Grounded-Grid Amplifiers, 2,681,953 (624,998)
- E. M. Bradburd and R. S. Alter, Electrical Wave Filter, 2,677,809 (604,564)
- W. M. Chambers, Welding Machine, 2,680,182
- R. Compare, Polarized Alternating-Current Ringer or Buzzer for Telephone Subsets and Similar Apparatus, 2,678,436
- J. H. G. Critch, Coil-Winding Machine, 2,678,171 (627,320)
- T. W. Cunniff, Squelching System, 2,681,989 (642,355)
- M. den Hertog, Automatic Telecommunication Exchange System, 2,678,354 (609,995)
- V. J. de Santis, F. L. Hunter, and C. P. Majkrzak Refractory-Coated Article, 2,681,876
- C. C. Eaglesfield, Electrical Pulse-Code System of Communication, 2,678,350 (593,008)
- C. W. Earp, Radio Diversity Receiving System, 2,683,213 (611,277)
- R. E. Garraway, Electrical Terminal, 2,678,346
- E. H. Grover, Amplifier Employing Semiconductors, 2,680,159 (612,331)
- A. J. Henquet and O. J. Salvador, Potential-Comparing System, 2,683,214

- R. W. Hutton, Discriminating Circuits for Dual-Purpose Trunks, 2,682,577
- D. E. C. Lambert, Frequency-Modulated Generator, 2,680,229 (580,839)
- E. Mathzeit, A. Ziegler, and W. Schroder, Carrier-Separating Device Scanning the Destination Markings of Pneumatic Carriers, 2,679,990
- C. K. Mitchell, Perforation of Cable-Code Tape from Wheatstone Signals, 2,683,190
- T. R. Philips, Wrap-Around Assembly for Electrical Components, 2,682,018
- G. T. Royden, Crystal-Controlled Oscillator, 2,680,197 (628,403)
- W. Sichak, Omnidirectional Antenna, 2,677,767
- A. T. Starr, C. DeB. White, N. S. Cinderey, K. A. Matthews, and R. B. W. Cooke, Crystal Diode and Triode, 2,680,220 (615,755)
- R. Urtel, Angularly Modulated Wave Demodulator, 2,683,215

Electrical Terminal

R. E. Garraway
2,678,346—May 11, 1954

An insulated electrical terminal for connecting terminal wires through a metallic sheet. The terminal comprises a bushing of insulating



deformable elastic material having a normal diameter just small enough to slip through the opening in the metal, a conductive pin extending through a hole in the center of the grommet, and

a pair of insulating bushings on opposite sides of the grommet.

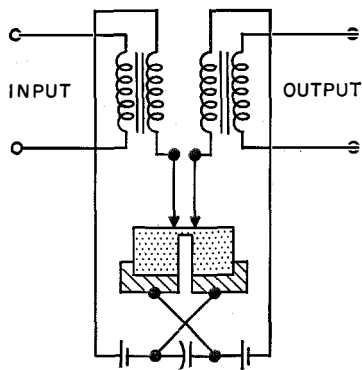
The pin is provided with means for tightening the bushings against the grommet and forcing it completely to fill the openings and to deform over the walls thereof.

Amplifier Employing Semiconductors

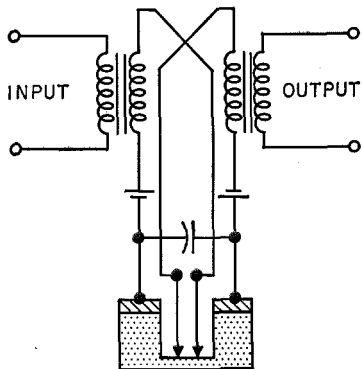
E. H. Grover

2,680,159—June 1, 1954

A transistor amplifier arrangement in which the semiconductor is partially divided to provide



two main portions and an intermediate portion interconnecting these main portions, the thickness of the intermediate portion being much less than the thickness of the main portions.



The collector and emitter electrodes are positioned for point contact on the intermediate portion and two base electrodes are positioned in surface contact with the main portions of the surface so that the emitter and collector currents are constrained to flow together in the intermediate portion in order to reach the base electrode.

Refractory-Coated Article

V. J. de Santis, F. L. Hunter, and C. P. Majkrzak 2,681,876—June 22, 1954

A refractory-coated article designed to retain high tensile strength despite extreme heat exceeding 750 degrees centigrade, comprising a refractory-metal base of tantalum, columbium, molybdenum, tungsten, or alloys of these metals and a hard crystalline barrier layer on this base composed of a refractory carbide consisting essentially of zirconium carbide and a carbide of tantalum, columbium, molybdenum, or tungsten.

Manufacture of Coaxial-Conductor Electric Cables

J. C. Beveridge

2,677,879—May 11, 1954

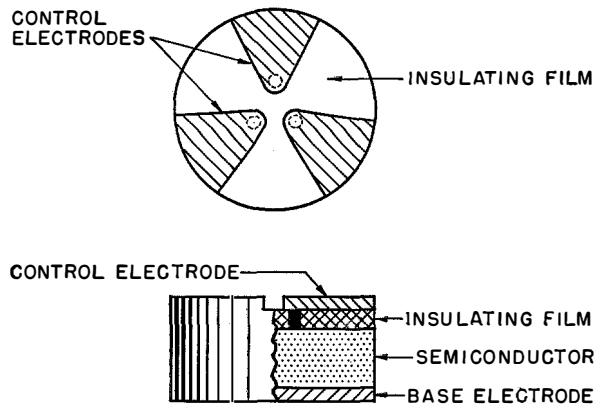
A device for applying insulating disks to a wire of a coaxial cable in which the disks are sliced and spread open immediately prior to application to the wire. This apparatus is different from a similar type of machine already known in that a single applicator wheel is used to carry the disks around for fitting onto the wire.

Crystal Diode and Triode

A. T. Starr, C. DeB. White, N. S. Cinderey, K. A. Matthews, and R. B. W. Cooke

2,680,220—June 1, 1954

A point-contact-type transistor amplifier device comprising a disk of semiconductor material with a conducting material deposited on one face in the form of a film to serve as a base electrode.



An insulating film is deposited on the other face, the insulating film having one or more holes filled with metallic film electrodes of an area between one square millimeter and 10^{-4} square millimeter to serve as emitters or collectors for transistor operation.

Electronic Timing Relay

H. H. Abelew
2,678,390—May 11, 1954

This invention covers a timing circuit in the form of a counting chain actuated by timing pulses so as to accept pulses of a predetermined range of lengths but reject pulses that are shorter or longer than this predetermined length. The device is particularly useful in automatic marine distress-call receivers.

Coil-Winding Machine

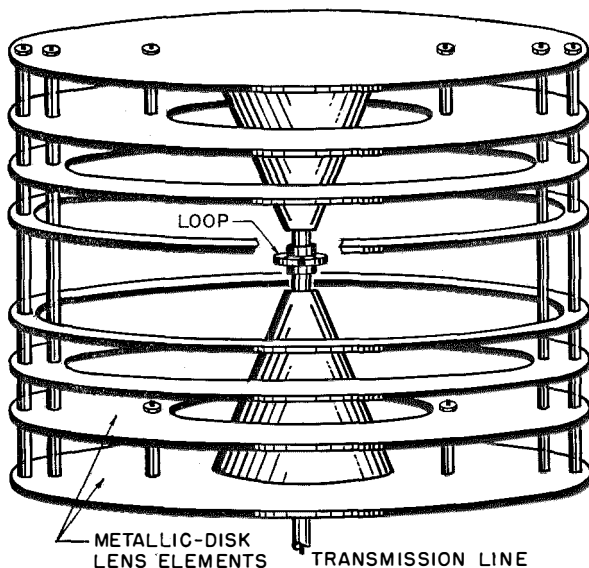
J. H. G. Critch
2,678,171—May 11, 1954

This invention covers part of a machine for winding toroidal coils on circular cores using a revolving shuttle in the form of a unitary ring provided with a cavity that carries a bobbin. The ring is unique in that it has a single break and is made of resilient material in order to be spread at the break to enable slipping the core onto the ring and to enable the bobbin to be inserted into and withdrawn from the cavity. The ring is sufficiently resilient to spring back into its proper shape after such distortion.

Omnidirectional Antenna

W. Sichak
2,677,767—May 4, 1954

An omnidirectional high-gain antenna employing a single radiator with associated reflectors and focusing elements, which can be readily



matched to a transmission line for operation over a predetermined frequency band.

The structure features a single radiator preferably in the form of a loop located between a pair of opposed conductive cones serving as reflectors and surrounded by a series of metallic disks that act as a lens to focus the radiated waves in a desired omnidirectional field pattern.

In Memoriam



JEAN E. F. ROUSSEL

JEAN E. F. ROUSSEL, a director of Le Matériel Téléphonique, La Compagnie Générale de Constructions Téléphoniques, Le Laboratoire Central de Télécommunications, and Les Télémprimeurs of Paris died on July 24, 1954, after a short illness. He was 53 years old.

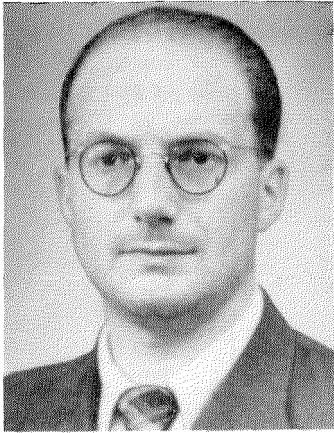
A graduate of Ecole Polytechnique and an Ingénieur Civil des Mines, he joined the engineering staff of Le Matériel Téléphonique at the age of 28. For 15 years, including the difficult period of the second world war, he was general manager of that company.

In 1950, Mr. Roussel was appointed a vice president of International Standard Electric

Corporation. He also served as a director of the Compagnie de Fives Lille, becoming general manager in 1954; he continued as a member of the board and technical consultant to the International System companies in France.

Mr. Roussel became a member of the Legion of Honor in 1952. He was known among his colleagues and friends for his forwardness of character and his ability to devote himself to the broader aspects of management. He was considerate of his associates and developed the most friendly of relations with them. He was held in high esteem in the industrial circle of France.

Contributors to This Issue



ROBERT M. FORTET

Mr. Fortet studied at the Ecole Normale Supérieure de Paris from 1931 to 1935 and, after receiving the "agregation," obtained his doctorate in mathematics. His first teaching post was that of professor of mechanics in the University of Caen (France). Since 1952, he has been professor of mathematical methods in physics and of the law of probabilities in the University of Paris (Sorbonne).

His published works bear mainly on the law of probabilities and on the various applications of mathematics to problems relating to electromagnetic propagation, background noise, et cetera. He is author of the paper in this issue on the average spectrum of a pulse series.

Since 1947, he has been a consultant engineer in mathematics to the Laboratoire Central de Télécommunications.

• • •

JOHN H. BRYANT. A photograph and biography of Dr. Bryant, coauthor of the paper on helical radio-frequency lines, will be found on page 71 of the March, 1954 issue. He has recently become a division head in the electron-tube laboratory of Federal Telecommunication Laboratories.

• • •

MILTON DISHAL. A photograph and biography of Mr. Dishal, who reports here on the design of filters, will be found on page 222 of the September, 1954 issue.

• • •

ROBERT M. FORTET was born in Périgueux, France, on May 1, 1912.



HERVÉ TANTER

G. J. LEHMANN. A photograph and biography of Mr. Lehmann, author of the paper on electric servomechanisms, will be found on page 72 of the March, 1954 issue.

• • •

HERVÉ TANTER was born in Trouville, France, on December 18, 1919. In 1939, he became a student at the Ecole Polytechnique in Paris and later was graduated as an engineer from Ecole Supérieure d'Electricité.]

In 1943, he joined the staff of Laboratoire Central de Télécommunications. From 1943 to 1946, he worked on automatic direction finders. Since 1947, Mr. Tanter has been active in radar development and is now head of the radar department at the laboratories. He reports in this issue on a special type of radar receiver.

• • •



HAROLD P. WESTMAN

HAROLD P. WESTMAN was born on May 29, 1904, in Springfield, Massachusetts. He received elementary schooling in New York City.

From 1926 to 1929, he was on the editorial staff of *QST*. From 1930 to 1942, he served as secretary of the Institute of Radio Engineers. During 1943, he was secretary of the War Committee on Radio of the American Standards Association. He joined the headquarters staff of the Institute of the Aeronautical Sciences in 1944.

He became associate editor of *Electrical Communication* in 1945 and editor in 1948.



ELIZABETH J. WHITE

Mr. Westman is a Senior Member of the Institute of Radio Engineers, a Member of the American Institute of Electrical Engineers and of the Institute of the Aeronautical Sciences. He is very active in the work of the American Standards Association and reports in this issue on a new standard on electrical graphical symbols. He is the United States delegate on graphical symbols to the International Electrotechnical Commission.

• • •

ELIZABETH JONES WHITE was born in Hackensack, New Jersey, on January 23, 1930. She received the A. B. degree

in physics from Middlebury College in 1951.

From the time of her graduation until October 1953 she was with the electron-tube department of Federal Telecommunication Laboratories, working on microwave tubes and electromagnetic-wave propagation. Mrs. White is coauthor of the paper in this issue on helical radio-frequency lines.

INTERNATIONAL TELEPHONE AND TELEGRAPH CORPORATION

MANUFACTURE AND SALES

North America

UNITED STATES OF AMERICA —

Divisions of International Telephone and Telegraph Corporation

Capehart-Farnsworth Company; Fort Wayne, Indiana
Coolerator Company; Duluth, Minnesota
Farnsworth Electronics Company; Fort Wayne, Indiana
Federal Telephone and Radio Company; Clifton, New Jersey
Kellogg Switchboard and Supply Company; Chicago, Illinois

Federal Electric Corporation; Clifton, New Jersey
International Standard Electric Corporation; New York, New York
International Standard Trading Corporation; New York, New York
Kellogg Credit Corporation; Chicago, Illinois
Thomasville Furniture Corporation; Thomasville, North Carolina

CANADA — (See *British Commonwealth of Nations*)

British Commonwealth of Nations

ENGLAND —

Standard Telephones and Cables, Limited, London
Creed and Company, Limited, Croydon
International Marine Radio Company Limited, Croydon
Kolster-Brandes Limited, Sidcup

CANADA — Standard Telephones and Cables Manufacturing Company, Limited, Montreal

AUSTRALIA —

Standard Telephones and Cables Pty. Limited, Sydney
Silovac Electrical Products Pty. Limited, Sydney
Austral Standard Cables Pty. Limited, Melbourne

NEW ZEALAND — New Zealand Electric Totalisators Limited, Wellington

Latin America and West Indies

ARGENTINA — Compañía Standard Electric Argentina, S.A.I.C., Buenos Aires

BRAZIL — Standard Eléctrica, S.A., Rio de Janeiro

CHILE — Compañía Standard Electric, S.A.C., Santiago

CUBA — Compañía Distribuidora de Productos Standard S. A., Havana

MEXICO — Standard Eléctrica de México, S.A., Mexico City

PUERTO RICO — Standard Eléctrica de Puerto Rico, Inc., San Juan

Europe

AUSTRIA — Vereinigte Telephon- und Telegraphenfabriks A. G., Czeija, Nissi & Co., Vienna

BELGIUM — Bell Telephone Manufacturing Company, Antwerp

DENMARK — Standard Electric Aktieselskab, Copenhagen

FINLAND — Oy Suomen Standard Electric AB, Helsinki

FRANCE —

Compagnie Générale de Constructions Téléphoniques, Paris
Le Matériel Téléphonique, Paris
Les Téléimprimeurs, Paris

GERMANY —

Standard Elektrizitäts-Gesellschaft A.G., Stuttgart
Divisions
Mix & Genest, Stuttgart
Süddeutsche Apparatefabrik, Nürnberg
C. Lorenz, A.G., Stuttgart
G. Schaub Apparatebau G.m.b.H., Pforzheim

ITALY — Fabbrica Apparecchiature per Comunicazioni Elettriche, Milan

NETHERLANDS — Nederlandsche Standard Electric Maatschappij N.V., The Hague

NORWAY — Standard Telefon og Kabelfabrik A/S, Oslo

PORTUGAL — Standard Eléctrica, S.A.R.L., Lisbon

SPAIN —

Compañía Radio Aérea Marítima Española, Madrid
Standard Eléctrica, S.A., Madrid

SWEDEN — Aktiebolaget Standard Radiofabrik, Stockholm

SWITZERLAND — Standard Telephone et Radio S.A., Zurich

TELEPHONE OPERATIONS

BRAZIL — Companhia Telefônica Nacional, Rio de Janeiro

CHILE — Compañía de Teléfonos de Chile, Santiago

CUBA — Cuban American Telephone and Telegraph Company, Havana

CUBA — Cuban Telephone Company, Havana

PERU — Compañía Peruana de Teléfonos Limitada, Lima

PUERTO RICO — Porto Rico Telephone Company, San Juan

CABLE AND RADIO OPERATIONS

UNITED STATES OF AMERICA —

American Cable & Radio Corporation; New York, New York
All America Cables and Radio, Inc.; New York, New York
The Commercial Cable Company; New York, New York
Mackay Radio and Telegraph Company; New York, New York

ARGENTINA —

Compañía Internacional de Radio, Buenos Aires
Sociedad Anónima Radio Argentina, Buenos Aires (Subsidiary of American Cable and Radio Corporation)

UNITED STATES OF AMERICA —

Federal Telecommunication Laboratories; Nutley, New Jersey; a division of International Telephone and Telegraph Corporation
International Telecommunication Laboratories, Inc.; New York, New York

BOLIVIA — Compañía Internacional de Radio Boliviana, La Paz

BRAZIL — Companhia Radio Internacional do Brasil, Rio de Janeiro

CHILE — Compañía Internacional de Radio, S.A., Santiago

CUBA — Radio Corporation of Cuba, Havana

PUERTO RICO — Radio Corporation of Porto Rico, San Juan

RESEARCH

ENGLAND — Standard Telecommunication Laboratories, Limited, London

FRANCE — Laboratoire Central de Télécommunications, Paris

ASSOCIATE LICENSEES FOR MANUFACTURE AND SALES IN JAPAN

Nippon Electric Company, Limited, Tokyo

Sumitomo Electric Industries, Limited, Osaka